LUND UNIVERSITY

Particle Interferometry in e+e- Annihilation

Muresan, Raluca

2000

Link to publication

Citation for published version (APA):
Muresan, R. (2000). *Particle Interferometry in e+e- Annihilation*. [Doctoral Thesis (compilation), Particle and nuclear physics]. Lund University, Elementary Particle Physics Department, Box 118, S-22100, Lund, Sweden.

Total number of authors:
1

General rights
Unless other specific re-use rights are stated the following general rights apply:
Copyright and moral rights for the publications made accessible in the public portal are retained by the authors and/or other copyright owners and it is a condition of accessing publications that users recognise and abide by the legal requirements associated with these rights.
• Users may download and print one copy of any publication from the public portal for the purpose of private study or research.
• You may not further distribute the material or use it for any profit-making activity or commercial gain
• You may freely distribute the URL identifying the publication in the public portal

Read more about Creative commons licenses: https://creativecommons.org/licenses/

Take down policy
If you believe that this document breaches copyright please contact us providing details, and we will remove access to the work immediately and investigate your claim.

LUND UNIVERSITY

PO Box 117
221 00 Lund
+46 46-222 00 00

Particle Interferometry in e^+e^- Annihilation

Raluca Mureşan
Department of Physics
Lund University, 2000

LUND
UNIVERSITY

ISBN 91-628-4084-3
LUNFD6/(NFFL-7183)2000

Particle Interferometry in e^+e^- Annihilation

By due permission of the faculty of mathematics and natural science at the University of Lund, to be publicly discussed at the lecture hall B of the Department of Physics, May 5, 2000, at 10.00 a.m., for the degree of Doctor of Philosophy

by

Raluca Mureşan

Department of Physics
Lund University
Professorsgatan 1
Box 118
SE-221 00 Lund
Sweden

LUND
UNIVERSITY

To Ana

This thesis is based on following papers, included as Appendices A to D:

A. R. Mureşan, O. Smirnova, B. Lörstad, **"Appearance of an artificial length scale in Jetset Bose-Einstein simulation"**, reprinted from *European Physical Journal C* 6, 629-635 (1999), with the permission of Springer-Verlag.

B. O. Smirnova, B. Lörstad, Mureşan R., **"Tests of the Jetset Bose-Einstein correlation model in the e^+e^- annihilation process"**, reprinted from *8th International Workshop on Multiparticle Production: Correlations and Fluctuations '98*, Mátraháza, Hungary, 14 - 21 Jun 1998, *Proceedings World Sci.*, Singapore, 1998, with the permission of World Scientific.

C. DELPHI Coll., P. Abreu et. al., **"Two-dimensional Analysis of Bose-Einstein Correlations in e^+e^- Annihilation at the Z^0 peak"**, reprinted from *Physics Letters B*, 471 (2000) 460, with the permission of Elsevier Science.

D. B. Lörstad, R. Mureşan, O. Smirnova, **"Multidimensional analysis of the Bose-Einstein correlations at DELPHI"**, reprinted from *ISMD99 XXIX International Symposium on Multiparticle Dynamics QCD and Multiparticle Production*, Brown University, Providence, RI, USA., *Proceedings World Sci.*, Singapore, with the permission of World Scientific.

Abstract

This thesis is the result of three years of work in Lund University, as a member of DELPHI group, at the Elementary Particle Physics Department.

The work concerns the study of Bose-Einstein correlations in electron-positron collisions at LEP. Since the JETSET event generator and its implementation of the Bose-Einstein correlation effect, LUBOEI, is the most used tool in the particle physics community, a study of this simulator, its performances and some limitations of its applicability area are presented in the first part of the thesis.

In the second part, using DELPHI experiment data, the multidimensional analysis of the two-particle Bose-Einstein correlations is performed, testing the string model prediction that the transverse correlation length is considerably smaller than the longitudinal one.

The dependence of the Bose-Einstein correlation function parameters on the average transverse mass of the boson pair is discussed for both JETSET hadronic events and DELPHI data.

Contents

1 Introduction **3**

2 DELPHI experiment at LEP **8**

2.1 LEP collider 8

2.2 DELPHI detector 12

2.2.1 Tracking detectors 14

2.2.2 Electromagnetic calorimeters and scintillator counters 17

2.2.3 The hadron calorimeter 18

2.2.4 Charged hadron identification 18

2.2.5 Detectors used in luminosity measurement 19

3 Bose-Einstein correlations **21**

3.1 The BEC correlation function 24

3.2 BEC in the frame of the string model 26

3.3 Monte Carlo models of BEC 30

3.4 Reference sample 33

3.5 Correction procedure 37

3.6 Longitudinal Center of Mass System 37

3.7 m_t dependence of BEC function parameters 42

4 Study of BEC in JETSET **45**

4.1 Event and track selection 46

4.2 Dependence on particle origin 47

4.2.1 λ dependence on m_t 47

4.2.2 Radius components dependence on m_t 49

4.3 The dependence on input radius 52

4.4 Discussion 63

5 BEC at DELPHI **65**
5.1 Data selection 65
5.2 Correction procedure 67
5.3 Two-dimensional BEC – systematic errors 69
5.4 Three-dimensional analysis 76
5.5 LEP1 results comparison 77
5.6 Discussion 79

Summary **80**

Acknowledgements **83**

Appendix A **89**

Appendix B **99**

Appendix C **109**

Appendix D **123**

Chapter 1

Introduction

People were from antiquity wondering about the origin of the relative diversity and unity of nature, explained always in the same way: everything is just a combination of few "fundamental" elements. The concept of fundamental elements evolved from considering earth, fire, air, water, metal, wood as fundamental substances to the constituents based on experimental discoveries which are used to describe the world nowadays (see Figure 1.1): a world made of leptons, quarks and force carriers [1].

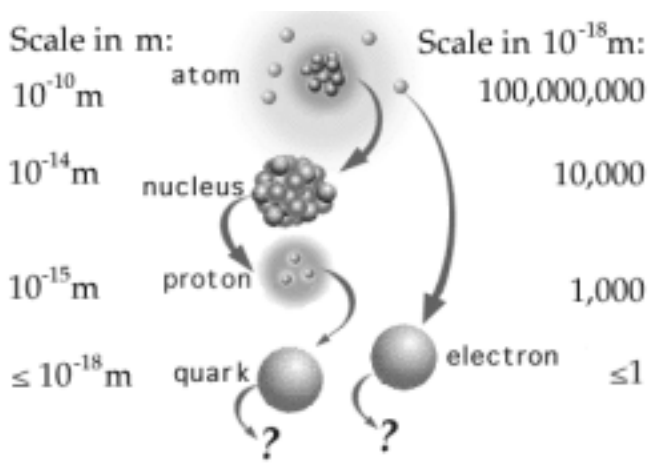

Figure 1.1: *A view inside the matter*

But, did we discover the ultimate building blocks of the matter? This is still an open question.

We use the information carried by light waves to perceive the shapes. Other animals, like dolphins and bats, emit and detect sound waves. In fact, any kind of wave can be used to provide information about the surroundings. Using waves to detect the physical world, the dimension of the objects you can "see" is limited by their wavelength. How and where can we find detectable waves with wavelength small enough to allow us to look deep inside the matter?

In 1925, Louis de Broglie, starting from the theory of Einstein and Planck according to which, radiation, wave-like, can act as an staccato of particles, introduced the hypothesis that particles of matter can exhibit wave-like characteristics and the associated wavelength is given by:

$$\lambda \sim \frac{1}{p}$$

where p denotes the particle momentum, ($p = mv$, v being particle velocity). This strange marriage between classical ideas and wave ingredients gave rise

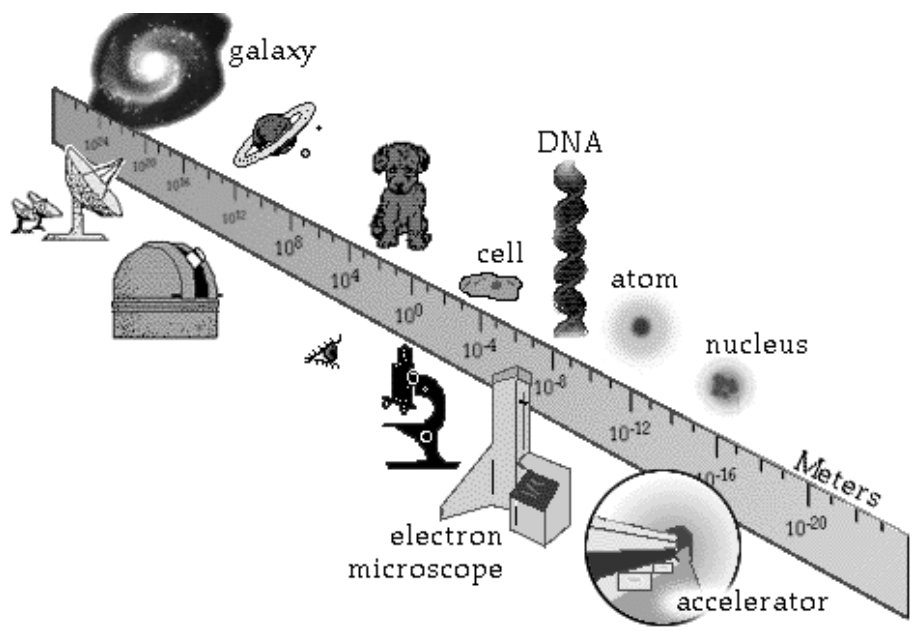

Figure 1.2: *How do we see different size objects?*

to the modern quantum mechanics and provided physicists with a great variety of waves that could be used to look inside the matter (Figure 1.2).

As it was known since long time, energy can be converted from one form, such as mechanic energy, chemical energy, heat energy, to another. Einstein proved that a different form of energy conversion can take place: energy can be converted to mass and vice-versa. The amount of energy that is produced as result of the conversion of a mass m is given by Einstein's famous equation $E = mc^2$, where c denotes the speed of light, and, vice-versa, the energy necessary to create, at rest, a particle having the mass, m, is given by the same equation. De Broglie principle together with the Einstein equation of creation and annihilation of particles opened the door to many physics experiments.

Using these tools, in the last half of the 20-th century, a dramatic progress of our understanding of the fundamental constituents of the matter and the forces that are acting between them took place. This resulted in what is called the Standard Model (SM) [1] of particle physics that provides the microscopic base for almost all the known physics phenomena, except gravity, explaining particle physics in terms of properties and interactions of a small number of particles. According to the SM, our world is created by a combination of three classes of particles: leptons, quarks and gauge bosons (force carriers). There are six known leptons, that occur in pairs, called families, which are written generally as doublets:

$$\begin{pmatrix} \nu_e \\ e^- \end{pmatrix} \begin{pmatrix} \nu_\mu \\ \mu^- \end{pmatrix} \begin{pmatrix} \nu_\tau \\ \tau^- \end{pmatrix} .$$

The three charged leptons are the well known electron and two other particles: muon and tauon. Associated with them there are three neutral leptons, or neutrinos (ν_e, ν_μ, ν_τ), which have very small masses, if any.

In addition to leptons there are six quarks. They also occur in pairs, or families, denoted:

$$\begin{pmatrix} u \\ d \end{pmatrix} \begin{pmatrix} c \\ s \end{pmatrix} \begin{pmatrix} t \\ b \end{pmatrix} .$$

Each family consists of a quark with electric charge $\frac{2}{3}e$ (u, c or t called "up", "charm" or "top") together with a quark with an electric charge $-\frac{1}{3}e$ (d, s or b called "down", "strange" or "bottom"). Here e is denoting the charge of the electron.

The quarks and the leptons can interact by four fundamental interactions

by exchanging the gauge bosons mentioned below:

force	acts on	carrier
gravity	all particles	graviton(proposed)[1]
weak	quarks and leptons	$W^{\pm}$, Z^0
electromagnetic	electric charge	photon
strong	quarks and gluons	gluons

Each particle has a corresponding antiparticle. A particle and its antiparticle have identical mass and spin but opposite quantum numbers[2]. The antiparticle of an electron is a positron, that has exactly the same mass as an electron but positive charge.

Whenever sufficient energy is available to provide the rest masses, a particle and its matching antiparticle can be produced together. All the conservation laws apply in these processes. When a particle collides with a matching antiparticle, they may annihilate – which means they both disappear. The energy of the annihilated particles appears in the form of fundamental bosons. The bosons decay afterwards producing other particles and antiparticles.

In particle physics, high energies are needed both to create new and unstable particles and to explore the structure of the subatomic particles. Until the early 1950-ies the only sources of such high energy particles were cosmic rays and studies of cosmic radiation led to notable discoveries. Today, cosmic rays are used only for specific studies and the great majority of experiments are conducted using beams of particles produced by machines called accelerators.

Accelerators solve two problems for physicists. First physicists use accelerators to increase the particle momentum, thus decreasing its wavelength enough to "look" inside atoms. Second, the energy of speedy particles is used to create the massive particles that physicists want to study. The beam, produced in an accelerator can be directed on a target at rest so that particles in the beam are interacting with particles from the target (fixed target experiment). The target can also be another beam of moving particles (colliding beam experiment). The advantage of the latter arrangement is that both beams have significant kinetic energy, therefore, a collision between produces a much higher energy and a higher mass particle than a

[1] The study of gravity is not object of SM.

[2] E.g. electric charge, color charge, flavour, electron, muon, tau-lepton and baryon numbers.

fixed target interaction would do at the same beam energy.

When an electron and its antiparticle, the positron, annihilate in a collider, in our case at the Large Electron Positron collider (LEP)[3], a big amount of energy is released. The energy is converted, via virtual photon or Z^0 e.g. into quarks and gluons. During strong interaction processes, called fragmentation, the quarks and gluons are converted into the particles that we can actually observe, mainly hadrons[4]. The rules of fragmentation are not fully understood and the size of the region in which this process is taking place is not clearly determined. The particle interferometry studies, as the one presented in this thesis, are interesting since they can contribute to the understanding of these phenomena for which we still have no appropriate theory. The detailed studies of the two-particle interferometry allow to determine the shape of the region in which the detected particles are produced and to analyse its spatial and temporal characteristics.

[3]For extended information about LEP see next chapter.
[4]Particles made of two or three quarks.

Chapter 2

DELPHI experiment at LEP

2.1 LEP collider

The particle accelerators are nowadays the most important research tools in nuclear and high-energy physics, providing physicists with multiple possibilities of studying the structure and properties of atomic nuclei and the interactions of subatomic particles.

An e^+e^- collider is a type of particle accelerator that stores and then accelerates counter rotating beams of electrons and positrons before bringing them to collision. Since the total momentum of oppositely directed beams is zero, the products can be created at rest, all the energy of the collision being converted into the mass of the produced particles.

The basic element of such a collider is a synchrotron ring [2] that can accommodate the two beams of particles travelling in opposite directions. Bunches of each type of particles are injected into the synchrotron ring until a sufficiently large intensity has been accumulated in each beam and then the two beams are accelerated simultaneously. The accelerating system causes the particles to circulate in bunches so that the collisions take place in only few places in the ring, where the particle detectors are located. This small number of intersections simplifies the operation by minimising the disruption of each beam caused by interactions with the other, allowing more intense beams to be collected and used in the ring. Actual interactions between particles are relatively rare and the beams can typically circulate for several hours before they are "dumped" and the machine is "filled" once again.

LEP (Large Electron Positron collider) is the largest accelerator yet built with a circumference of 26.67 km. It is located at CERN on the border between Switzerland and France. Since the energy density released in the

annihilation of electrons and positrons is comparable with the one that existed in universe a fraction of a second after its creation, the studies that can be done at LEP are a synthesis between cosmology and particle physics.

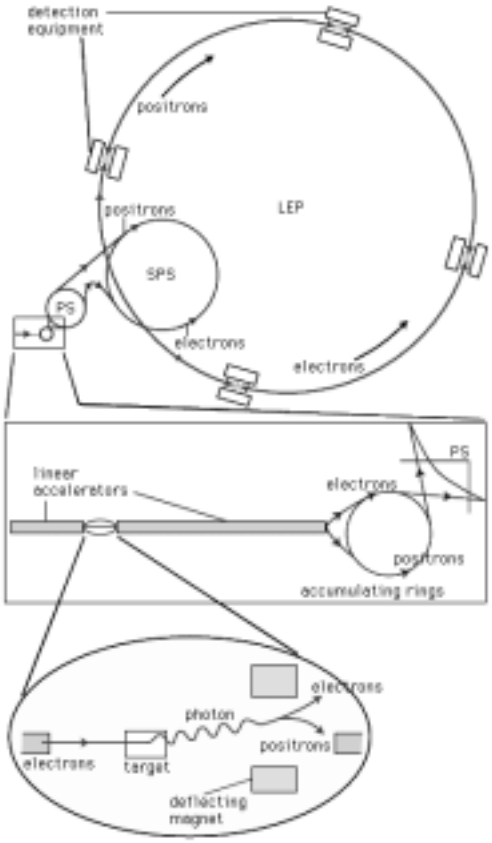

Figure 2.1: *The scheme of LEP collider*

Studies of the design of the LEP machine [3] started in 1976 at CERN and the first practical design was published in 1978. LEP was projected to be a large circular tunnel in which the machine was installed in stages corresponding to new physics events that were predicted by the unified theory of the weak and electromagnetic interactions [4].

In LEP there are four interaction regions surrounded by particle detectors (ALEPH, DELPHI, L3, OPAL) that measure the properties of the

secondary particles coming from the collisions. Each detector is optimised differently to study various physics aspects of the interaction.

Other accelerators built earlier at CERN act as injectors to LEP in a complex interlinked system [3] (see Figure 2.1). A purpose-built linear accelerator produces bunches of electrons and positrons at 600 MeV and feeds them into the 28 GeV Proton Synchrotron (PS) to be accelerated to 3.5 GeV and further transfered to the Super Proton Synchrotron (SPS). In SPS they are accelerated to 20 GeV before injection into LEP. In the final stage, LEP accelerates the counterrotating beams of electrons and positrons to a maximum energy of 100 GeV.

The two important parameters that decide what kind of physics can be performed at a particular collider are the beam energy, to allow the observation of the required physics, and the integrated luminosity (that will be defined further in this section), to allow such an observation at a reasonable rate.

At LEP the energy was defined for the generation of Z^0 and $W^{\pm}$ pair of particles and resulted in a range of $40 - 100$ GeV per beam.

Once the energy was decided, the next problem was to optimise the physical size of the collider in order to minimise the construction and running costs. An important point in the definition of circumference is the influence of synchrotron radiation. When the trajectories of the charged particles are bent, as in the case of storage rings, they radiate a fraction of their energy by emission of photons. The energy loss is proportional to $(E/p)^4$, a large value for high energy electrons. If this energy is not replenished, the particles would rapidly decelerate in a spiral being lost inside of the vacuum chamber's wall. The radio-frequency acceleration system (RF) replenishes the energy lost by particles during each revolution. The RF voltage in the accelerating gaps oscillates at high frequency and is synchronised to the harmonic of the revolution frequency of the particles. Consequently, the bunches cross the accelerating gaps at a constant phase relative to the voltage. In this way all the particles gain energy crossing the accelerating cavities. The energy gain per turn must compensate the energy loss per turn due to synchrotron radiation

As was already mentioned, the second important parameter in the design of colliders is the luminosity, L, defined for any physical process as:

$$L = \sigma \frac{dN}{dt} \tag{2.1}$$

with σ being the cross section of the process and $\frac{dN}{dt}$ the rate at which the events are produced. The luminosity at LEP is limited by the interplay

between beam-beam effects, background in the detectors, and the aperture, as set by the collimator system [3]. To achieve high luminosity it is not only important to store a large number of electrons but also to squeeze the transverse beam size at the interaction point as much as possible.

During LEP first running period (LEP1), 1989 - 1995, the operation has been a mixture of physics data taking around the Z^0 energy (91 GeV) and machine studies aiming at performance improvement, beam energy calibration and future upgrades.

Z bosons were produced copiously and it made possible to challenge the validity of the Standard Model (SM) with an unprecedent degree of precision. LEP has turned out to be a superb laboratory for the study of quantum chromodynamics (QCD)[5] and ElectroWeak theory (EW)[4].

Very high precision measurements of the electroweak parameters of the SM at the level of few per mill [6], including Z mass and width from the very precise measurement of the beam energy, were performed. These studies severely constrainted the number of the light neutrino families excluding any further fermion family beyond the three already known ones. Other studies predicted the mass of the top quark and explored the lower mass sector of whatever may exist beyond the Standard Model. The clean conditions at LEP with almost no background favoured the studies of the the fragmentation mechanism of quarks and gluons providing a splendid test of QCD [6].

Examples of results from this first running period are: accurate and consistent measurements of the strong coupling constant using several independent methods, providing clear evidence for its energy dependence; searches for new particles including Higgs bosons and supersymmetric partners of the particles which are known today (so far none of these searches were successful); studies of short-lived particles, tau-lepton and B hadrons, with an important contribution to the knowledge of their life-times and decay modes. The exploration of the B sector has been particularly successful leading to the observation of the individual B_S decays and the evidence for $B^0 - \bar{B}^0$ oscillation at a confidence level of 99 % [6].

Measurements done at the Z peak provided information on the axial (g_A) and vector (g_V) coupling constants of the weak neutral current. Determination of the partial width for decay in a lepton-antilepton pair, Γ_{ll}, forward-backward asymmetries A_{FB} and τ polarisation gives high precision measurements for g_A and g_V and deep understanding of the SM. The SM prediction for the value of the weak mixing angle, $sin^2\theta_W$, could agree with the experimental data only if the top mass was very large, 175 GeV, an energy at which CDF and D0 experiments actually discovered it [7].

In the second running period, LEP2, higher and higher energy ranges were explored with the aim of searching for new particles up to the masses of the order of 100 GeV, testing the SM, studying the W^+W^- and Z^0Z^0 pairs and searching for new particles: Higgs boson and suppersymmetric particles. If these searches fail, lower limits will be set for the mass of each of them.

Despite the increase in energy and the consequent decrease of the cross-section outside Z peak, LEP2 continues to contribute to the precision measurements of the SM parameters through an accurate determination of the mass of W's which are produced in pairs at energies above 160 GeV. Both semileptonic events $e^+e^- \rightarrow W^+W^- \longrightarrow e\nu J_1 J_2$ and hadronic ones $e^+e^- \rightarrow W^+W^- \longrightarrow J_1 J_2 J_3 J_4$ are used to estimate W's mass (here J_i stands for jet). The four-jet events must be handled with care since hadrons, contained in the two jets coming from the decay of different W's, are subject to Bose-Einstein correlations [8, 9], due to the fact that, at LEP2, the average space-time separation between the two W's decay points is less than 0.1 fm while the hadronization scale is 1 fm. A certain interest in the study of the BEC in e^+e^- appeared following the issue of a theoretical result[10], which suggested a significant influence of BEC on the W mass determination. The estimated values of this W mass shift are however strongly varying from approach to approach [10, 11, 12] being dependent on the model used for simulation. Also the study of Bose-Einstein correlation in W^+W^- is depending on the tuning of the model parameters to the corresponding values obtained at the Z peak and on the theoretical model used for comparison. All these reasons enhanced the interests for studies of particle generators and their BEC simulation. At the Z^0 peak, detailed studies of BEC using e^+e^- data can be performed with confidence, due to the big amount of data available. Such studies are presented here.

2.2 DELPHI detector

DELPHI (DEtector with Lepton, Photon and Hadron Identification) [13, 14], is a general purpose detector for e^+e^- physics, with special emphasis on powerful particle identification (leptons and hadrons) over most of the solid angle, even in complex events. It offers three-dimensional information on curvature and energy dissipation; high granularity over a 4π solid angle and precise vertex determination. DELPHI has been operating at LEP since 1989.

The detector consists of a cylindrical part, covering the central region,

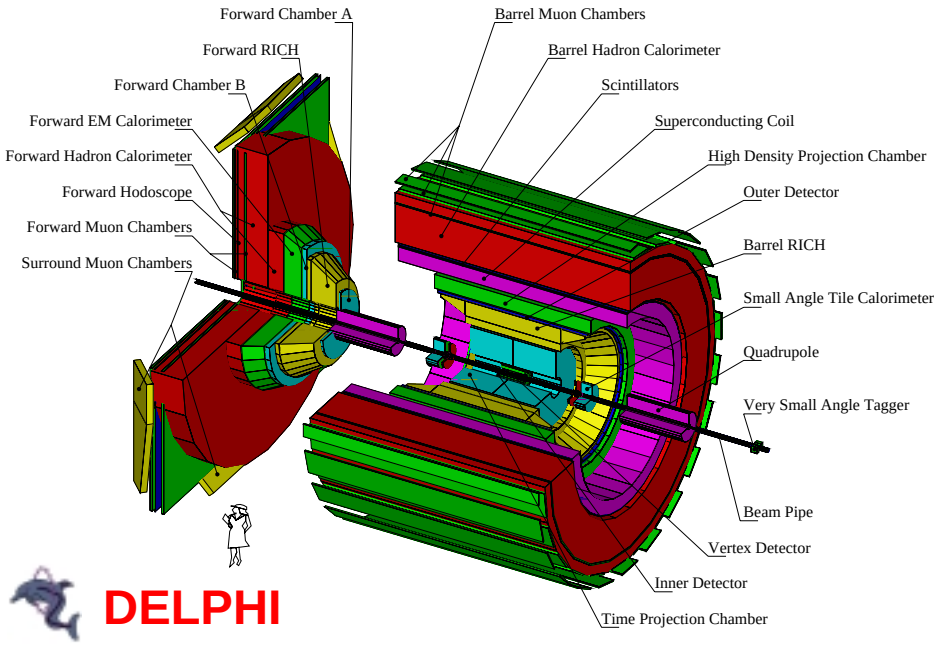

Figure 2.2: *DELPHI detector*

and two end-caps, covering the forward regions (see Figure 2.2). The end-caps can be moved to allow access at the subdetectors. The overall length and diameter are over 10 m each and the total weight is 3500 tons.

The superconducting solenoid, the largest so far built (7.4 m length and 5.2 m inner diameter), provides a highly uniform magnetic field of 1.23 T, parallel to the beam pipe, throughout the central tracking volume, containing the barrel tracking detectors: the Vertex Detector (VD), the Inner detector (ID), the Time Projection Chamber (TPC) and the Outer Detector (OD) and also the forward tracking chambers (Forward Chambers A and B).

Electron and photon identification is provided primarily by the High density Projection Chamber (HPC), in the barrel region, and by the Forward Electromagnetic Calorimeter (FEMC), in the end-caps. The smaller polar angles, essential for detecting e^+ and e^- from $\gamma\gamma$ processes[1] and for luminosity measurement from $e^+e^- \to e^+e^-$ events, are covered by the Small angle

[1] When electrons and positrons interact in LEP they radiate photons at small angles relative to the beam axis. This is the source of two-photon collisions, producing a hadronic state X . While for a given beam energy the kinematics of an annihilation process is fixed, the continuous spectra of the photons will allow simultaneous measurements at different invariant masses and for different momentum transfers

Tile Calorimeter (STIC) (which replaced the Small Angle Tagger (SAT) in April 1994), and the Very Small Angle Tagger (VSAT). In order to achieve complete hermeticity for high energy photon detection, additional scintillators have been installed in the cable duct regions between the barrel and each end-cap and in the small gaps between the HPC modules, not adequately covered for this purpose by the Time Of Flight (TOF) scintillators. The iron return yoke of the magnet is instrumented with limited streamer mode detector to create a sampling gas calorimeter, the Hadron Calorimeter (HAC). Muon identification is achieved by comparing the extrapolation of the reconstructed tracks with the hits in the Barrel (MUB) and Forward (MUF) muon drift chambers. A layer of Surrounding Muon Chamber (SMC) based on limited streamer tubes, was installed to fill the gap inbetween the barrel and forward regions. The Ring Imaging Cherenkov (RICH) detectors provide charged particle identification in both the barrel (BRICH) and forward (FRICH) regions.

In the standard DELPHI coordinates system, z axis is considered along the electron direction, x axis points towards the centre of LEP, and y axis points upwards. The polar angle to the z axis is called θ and the azimuthal angle around the z axis is called ϕ, the radial coordinate is defined as $R = \sqrt{x^2 + y^2}$.

2.2.1 Tracking detectors

The tracking detectors are devoted to precise measurement of tracks, and hence to the precise determination of the directions and momenta of the charged particles. I shall present the tracking detectors starting from the closest to the interaction point to the farthest one.

Vertex Detector is an advanced silicon detector providing very precise tracking, in order to detect short-lived particles by extrapolating the tracks back, towards the interaction point. It consists of three coaxial cylindrical layers of silicon strip detectors at average radii of 6.3, 9.0 and 10.9 cm. Each layer covers the full azimuthal angle and is composed of 24 sectors, with overlaps between adjacent sectors. For polar angles of $44^\circ \leq \phi \leq 136^\circ$, a particle crosses all the three layers of the VD.

The VD was initially designed as a two-layer silicon strip detector measuring $R\phi$ coordinates in the barrel region. In 1991, VD was upgraded by adding the third layer of silicon strips and in 1994 was further upgraded by adding a z readout to the external and closer layers. The polar angle cover-

age of the closer layer was extended into the forward region down to 25°.

Inner Detector provides high redundancy for vertex reconstruction and trigger information. Initially it was composed of an inner drift chamber with jet chamber geometry, giving 24 $R\phi$ points per track, and five cylindrical MultiWire Proportional Chamber(MWPC) layers. The MWPC layers had sense wires spaced by about 8 mm, providing fast trigger information and solving the left-right ambiguities inherent to the jet chamber, and a circular cathode strips giving Rz information.

Since the beginning of 1995 a new, longer, ID has been operational. The inner drift chamber has exactly the same wire configuration as the previous one. The polar angle acceptance for tracks, giving a hit to the innermost anode wires, is $15° \leq \phi \leq 165°$. Surrounding the jet chamber there are five cylindrical layers of straw tube detectors measuring $R\phi$ and having the same functionality as the old MWPC trigger layers. There is no longer any z measurement.

Time Projection Chamber is the principal tracking device of DELPHI. Pattern recognition starts from its information. The size of TPC being limited (R = 120 cm, L = 2 x 150 cm), by the inclusion of RICH-es, other track chambers were added (OD, FCA and FCB) to improve momentum resolution. Both end-plates of the TPC are divided into 6 azimuthal sectors, each with 192 sense wires and 16 circular pad rows with constant spacing. At least three such pad-rows are crossed down by a particle to polar angles $20° \leq \phi \leq 160°$. The dead space between the pads of adjacent end-plate sectors corresponds to 4% of the $R\phi$ plane. Short cathode pads (in R), totally 1680 pads per sectors, were chosen for better two-track separation. The detector provides up to 16 points per particle tracks at radii between 40 and 110 and polar angles of $39° \leq \phi \leq 141°$. Laser beams are used to monitor the drift velocity continuously during data taking.

The identification of charged hadrons in DELPHI relies on the specific ionisation energy loss per unit length (dE/dX) in the TPC and on the information provided by RICH-es.

Outer Detector consists of five layers of drift tubes located between radii 197 cm and 206 cm. The active length of the detector corresponds to polar angles from 42° to 138°. It provides a final, precise direction measurement after the Barrel Ring Imaging Cherenkov detector, giving fast trigger information in both $R\phi$ and z and improving the momentum resolution by a large factor. It is composed of 24 modules mounted on the BRICH, each consisting of 145 drift tubes in five layers. The layers are staggered, the

adjacent modules overlap, providing full azimuthal coverage. All layers provide $R\phi$ information. Three layers provide, in addition, fast z information by relative timing of signals from both ends.

Forward Chamber A provides powerful tracking and triggering information. It is mounted on both ends of the TPC at an average $z = 160$ cm from the interaction point. Each side consists of three chambers, each of them with two staggered layers of drift tubes. The layers are split into half-discs, with an outer radius of 103 cm. There is a rotation of 120° between the wire orientation of the modules. The chamber covers polar angles from 11° to 32° and from 148° to 169°.

Forward Chamber B is a drift chamber situated at an average distance of $z = 275$ cm from the interaction point. The sensitive area of the chamber corresponds to polar angles from 11° to 36° and from 144° to 169°.

FCB provides a precise information for tracking, triggering, pattern recognition and substantially improves momentum resolution in the forward direction. The chamber consists of 12 read-out planes. Coordinates in each of three directions, rotated by 120°, are defined by four planes. The high redundancy provided by the 12 read-out planes offers the possibility to analyse track elements in a high multiplicity and background environment

The FCA and FCB are supported independently on the yoke, between the forward RICH and FEMC.

Very Forward Tracker, the very forward part of the Silicon Tracker, is located on both ends of the barrel. It covers the polar angle from 10° to 25° and from 155° to 170°. The detector was added to LEP2 since, increasing the energy, many of the interesting physics channels, with large cross section, peak in the forward region of the apparatus. The obtained information is used to provide stand-alone tracking and pattern recognition. The inner two layers are made of pixels and the outer two layers are made of strips. The ministrip detector is made of four planes two on either ends of the barrel. Each plane consists of twelve detector modules measuring two orthogonal coordinates. The modules are mounted at an angle of 50° with respect to the beam.

The Muon Chambers are the farthest from the collision point, since muons are the only charged particles that can traverse the lead and iron of both calorimeters essentially unaffected. Most muons of momenta above 2 GeV/c are expected to penetrate to the muon chambers. Muon identification is achieved by comparing the extrapolations of the reconstructed tracks

with the hits in the MUB that covers polar angles from 53.0° to 88.50° and from 91.5° to 127.0° and MUF that covers polar angles from 20° to 42° and from 138° to 160°. In 1994 a layer of SMC based on limited streamer tubes was installed outside the end-caps to fill the gap between the barrel and forward regions.

In the barrel part of the detector, precise measurement of the tracks varies from $5 - 10$ μm in the Vertex Detector, to a fraction of a millimeter in the TPC and to $1 - 3$ mm in the Barrel Muon Chambers, after traversing 5 m of the detector.

2.2.2 Electromagnetic calorimeters and scintillator counters

High density Projection Chamber, barrel electromagnetic calorimeter, is situated outside OD, inside the solenoid. The polar angle coverage is 43° to 137°. It has the aim to measure the three-dimensional charge distribution induced by electromagnetic showers and by hadrons, with very big granularity, in all the coordinates, having an acceptable number of read-out channels. It allows to detect electromagnetic showers and to separate them from hadrons even in the complex topologies encountered at LEP. It consists of 144 modules, arranged in 6 rings inside the magnetic field. Each ring consists of 24 modules, coaxially arranged around the beam axis and has an inner radius of 208 cm and an outer radius of 260 cm. Each HPC module is a small TPC with layers of high density material (lead wires) in the gas volume.

Forward ElectroMagnetic Calorimeter consists of two 5 m diameter disks. The front faces are placed at $|z| = 284$ cm covering the polar angles $8° \leq \theta \leq 35°$ and $145° \leq \theta \leq 172°$. Good energy resolution and granularity are the principal aims. The detector disks consist of arrays of 4532 Cherenkov lead glass blocks. The blocks are truncated pyramids with inner (outer) face dimensions of 5x5 cm^2 and depth of 40 cm, corresponding to 20 radiation length. Each block is pointing to the interaction region. The Cherenkov signal induced by the charged particles in the shower is read out by a single stage photomultiplier.

In order to achieve complete hermeticity for high energy photon detection and to be sensitive to the possible new physics, whose experimental signatures are based on missing energy and momentum of the event, scintillators have been installed additionally between the barrel and each end-cap and between the HPC modules, the **Hermeticity detectors**. In addition

DELPHI has in the barrel part **TOF** and in the forward part the Horizontal Flight tagger, **HOF**. The TOF counters are also used to provide information about those particles (mainly photons) that go in the dead regions of the innermost detector layers of DELPHI. The scintillator counters are fast trigger for beam events and cosmic radiation. TOF are trigger and time of flight information providers.

2.2.3 The hadron calorimeter

Hadron CALorimeter provides energy measurements of charged and neutral hadrons. It gives a detailed picture of the hadronic showers, thus good distinction between showers caused by neutral and charged hadrons and correct muon identification. The barrel part covers polar angles between 42.6° and 137.4° and the end-caps, polar angles in ranges 11.2° - 48.5° and 131.5° - 168.8°. The barrel is constructed of 24 sectors, with 20 layers of limited streamer mode detectors inserted in 2 cm slots, between the 5 cm iron plates, in each sector. The modularity of the end-caps is similar to the barrel, 12 sectors each with a sample depth of 19 layers. The whole Hadron Calorimeter covers almost the full solid angle $11° \leq \theta \leq 169°$.

2.2.4 Charged hadron identification

Charged particle identification is provided mainly by liquid and gas Ring Imaging Cherenkov Counters (RICH), both in barrel and forward region. DELPHI RICH-es contain two radiators of different refractive indices. The liquid radiator is used for particle identification in the momentum range from 0.7 to 9 GeV/c and the gas radiator for the range 2.5 to 25 GeV/c. The full solid angle coverage is provided by two independent detectors, one in the end-cap regions (FRICH), and one in the the barrel regions (BRICH).

Barrel RICH is located between the Time Projection Chamber and the Outer Detector. It is a 350 cm long cylinder with inner radius 123 cm and outer 197 cm, divided into two halves by a central support wall, 6.4 cm thick. Liquid radiator boxes with quartz windows on the outer surface are mounted near the inner surface of the cylinder. UV photons are detected in the drift tubes constructed entirely from quartz plates, which act as TPC-s with readout chambers at the outer end. Cherenkov photons produced in the outer gas volume are reflected by parabolic mirrors and focused into ring images in the same drift tubes. Each half contains 24 drift tubes and liquid

radiators containers, in azimuth, grouped in pairs. C_6 F_{14} is used as liquid radiator and C_5 F_{12} as gas radiator. BRICH covers polar angles between 40° and 140°.

Forward RICH is located between 1.7 m $\leq |z| \leq$ 2.7 m and covers polar angles between 15° and 35°. Each end-cap consists of two truncated half-cones and is divided in azimuth in 12 modular sectors. Each such sector contains one driftbox, two MWPC, three liquid radiator containers and five mirrors. The vessel is built from carbon-epoxy laminate and contains heating elements on the inside and cooling pipes on the outside. The two vessels of one end-cap are supported by the iron yoke on a carbon-epoxy cylinder. C_6 F_{14}, C_5 F_{12} are used as liquid respective gas radiators.

2.2.5 Detectors used in luminosity measurement

Small Angle Tagger, a two arms detector, was optimised for luminosity measurements by counting Bhabha events[2]. Each arm consisted of a calorimeter and a tracker in front. The calorimeter covering polar angles from 2.46° to 7.73° consisted of alternating layers of lead sheets and plastic scintillating fibres aligned parallel to the beam.

STIC (that replaced the SAT detector) is a sampling lead-scintillator calorimeter formed by two cylindrical detectors, placed on either side of the DELPHI interaction region, at a distance of 220 cm, and covers a wider angular region between 1.66 ° and 10.60° in polar angle (from 6.5 to 42 cm in radius).

Very Small Angle Tagger consists of four calorimeter modules. The detector modules contain tungsten absorbers, interspaced with silicon planes for the energy measurement. The electromagnetic shower coordinates, in the horizontal and vertical directions, are determined by the silicon strip planes. It is located close to the beam, at 7.7 m from the interaction point, and covers the angular region 0.3° to 0.4°. The physical processes being monitored are Bhabha scattering and two photon collisions.

Most of the elements of DELPHI provide information directly in three-dimensional form, which is being read out via some 200,000 electronic channels by 72 dedicated microprocessors. The data are then merged to form an "event" (event building) and shipped to a central set of computers where

[2]Elastic scattering of electrons on positrons

they are logged onto mass storage for subsequent analysis. A typical event contains 1 million bits of information. An optical data link sends the compressed data to the main computer and control center.

Design and construction of the DELPHI detector took 7 years. Data have been taken every year for the last 9 years, typically throughout the summer and autumn. During the data-taking periods, LEP and the detectors are operated around the clock. Winter and spring (when electric power is much more expensive) are reserved for a long shutdown, used for maintenance and modifications (including upgrading of LEP as well as of the detectors).

Chapter 3

Bose-Einstein correlations

In the beginning of 1920s, quantum statistics became an important tool to describe ensembles of identical atoms and subatomic particles, that, according to their properties, were classified in two categories. The ones that are characterised by asymmetric wave function and satisfy the exclusion principle (eg: leptons and quarks) were called fermions and the Fermi-Dirac statistics was developed to describe their behaviour. The others, with a symmetric wave function and not restricted by the exclusion principle (eg. photons, mesons, gluons, W and Z intermediate vector fields), were called bosons and described by the Bose-Einstein statistics.

During the 50-ies, in particle physics experiments and in the astronomical observations, it was discovered that bosons emitted from the same source show the tendency to have similar energy-momentum characteristics [8, 9]. This phenomenon of increasing probability for the emission of identical bosons from close regions of space and time is called Bose-Einstein correlation (BEC). The Bose-Einstein effect originates in the quantum mechanical interference of the boson wave functions being a consequence of their symmetry under particle exchange, that gives an effective clustering of the particles in the phase space (opposite to the exclusion principle), explaining their preference to occupy the same quantum states.

Presuming that only particles emitted from the same or very close sources enhance the probability to produce particles with small relative momentum, it is expected that, from the studies of BEC, one could obtain important information about the space-time extension of the sources. This method to estimate the source size proved to be a reliable tool in astronomy, where the so-called HBT (after Hanbury-Brown and Twiss, - astronomers who first reported of it [15]) effect is used to measure stellar sizes by analysing

correlations between detected photons. In particle physics, the hadron interferometry was proven to fulfil a similar task of defining the size, the shape and the evolution in time of a microscopic source of mesons.

High energy heavy ion collision experiments developed precise methods, using boson interferometry studies, to obtain information about the space-time development of the particle emitting source. This is an interesting feature out of many because of the implications in Quark Gluon Plasma (QGP) studies [1]. Positive identification of the QGP state in the relativistic heavy-ions collisions is extremely difficult, since if created, the QGP will have a very transient existence [16]. Correlations measurements, using various particles, may be particularly helpful in understanding the dynamical evolution of heavy-ions collisions. In the experimental search for QGP formation, a suggested signature is the extended emission time of mesons from a system undergoing a phase-change: this can be measured by components of the two-particle correlation function [16, 17].

Analysis performed for the three components of the four-momentum difference of two identical bosons shows a dependence of radii on the mean transverse mass of pairs, which can be described by hydrodynamical models of the particle source expansion [18, 19]. A common dependence of radius parameters on m_t can indicate collective flow as the momentum-position correlations caused by the flow increase with increasing p_t [17]. Preliminary studies of BEC between like-charged bosons in e^+e^- annihilation at the centre-of-mass energy of $M(Z^0) = 91.2$ GeV, using the DELPHI experiment data, see [20] and Appendix D, revealed also the existence of the transverse mass dependence for the correlation radius components, similar in some respects to the one found in heavy-ion experiments.

The study of BEC function for identical particles is very interesting since the process of hadron production, or fragmentation, in high energy physics is poorly comprehended. At this moment, no appropriate theory could describe it, only phenomenological models being available for the hadronization process and the Bose-Einstein phenomenon in particular. Studies of the space-time characteristics of a hadron source give important information about the hadronization process as a whole and also provide tests of fragmentation models.

Detailed studies of the two-particle interferometry in Z^0 hadronic decays in e^+e^- annihilation allow the determination of the shape of the source

[1] State of matter, in which, quarks and gluons, are not longer confined within the dimensions of the nucleon but free to move around over a volume in which high enough temperature and/or density prevails.

of bosons, which gives the possibility to analyse the spatial and temporal characteristics of the hadronization region. These studies are of considerable interest partly due to the recent predictions of possible influence of BEC on the measured value of the W boson mass in e^+e^- annihilation [10, 11]. Estimates of the strength of this effect have been made using the Monte Carlo particle generator JETSET [21], involving a simple algorithm for the two-particle BEC simulation which uses a correlation function in terms of the invariant four-momentum difference of identical particles, Q. This algorithm is known to reproduce well basic features of BEC in experimental data, like the shape of the correlation function in terms of Q [22] and the shift of the ρ^0 mass [23], but it does not describe other related effects, like the higher order correlations [24], neither does it reproduce its own input parameters in a wide range, as it will be shown later in this work. More detailed tests are necessary to establish the extent of applicability of the mentioned algorithm, the reliability of its predictions and to further improve and develop it.

The investigation of BE correlations in e^+e^- annihilation is particularly interesting since there are phenomenological models describing almost all features of hadron production except for quantum mechanical effects. Until recently, studies of the identical-boson correlations in e^+e^- annihilation process at LEP energies have concentrated on the shape of the two-particle correlation function in terms of Q [22]. At lower energies, several collaborations have studied BEC using two-dimensional distributions of components of Q [25]. Multidimensional analyses of the BEC are now being made by the LEP experiments as well.

The string model [31] describes e^+e^- annihilation data with high accuracy and provides an appropriate framework in which to consider the Bose-Einstein enhancement. In the two-jet hadronic decays $Z^0 \to q\bar{q}$, the comparison between the transverse and longitudinal radii of the BEC (with respect to the initial parton direction of motion) can test the string model prediction [26] that the transverse correlation length is considerably smaller than the longitudinal one.

Since fragmentation models are mostly of probabilistic nature, it is very difficult to incorporate the Bose-Einstein symmetrization into them. Thus effects of BEC are often absent in event generators, which apparently does not significantly affect their performance. To account for and to describe it properly in event generators, the Bose-Einstein phenomenon must be well understood, therefore more profound interferometry studies are required. The proper treatment of such effects is an interesting goal for the next generation of hadronization models.

3.1 The BEC correlation function

In order to study the enhanced probability for the emission of two identical bosons, it is useful to define a correlation function. Considering the production of two identical bosons with four-momenta p_1 and p_2, the correlation function C_2 of two identical bosons is defined as:

$$C_2(p_1, p_2) = \frac{P(p_1, p_2)}{P(p_1)P(p_2)} \ , \tag{3.1}$$

where $P(p_1, p_2)$ is the probability density of two particles to be produced, and $P(p_1)$ and $P(p_2)$ – the probability densities for a single particle to be produced with four-momentum p_1 or p_2. From the experimental point of view, $P(p_1, p_2)$ is a double differential cross section. In practice, it is difficult to construct the product $P(p_1)P(p_2)$, therefore it is often replaced by $P_0(p_1, p_2)$, which is equal to $P(p_1)P(p_2)$ in the absence of correlation. One of the major problems in this kind of studies is to build $P_0(p_1, p_2)$, usually called the "reference sample".

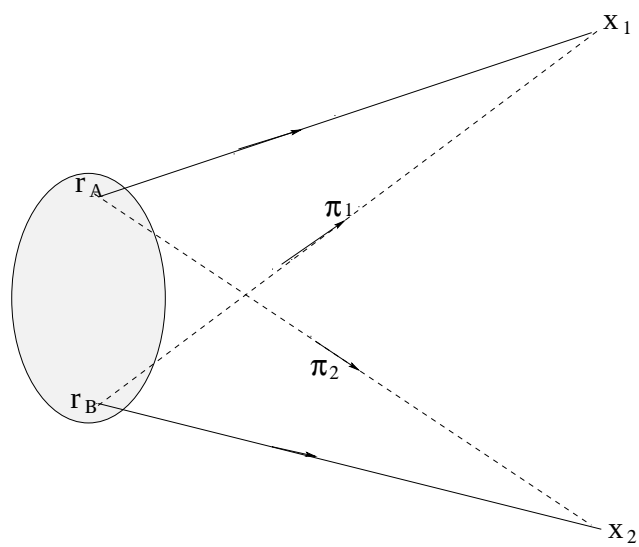

Figure 3.1: *Two particles π_1 and π_2, with four-momenta p_1 and p_2, are emitted by the same source from the points r_A, r_B. They are detected at points x_1 and x_2.*

To calculate the above probabilities, let us discuss the emission of two bosons. If a particle A is emitted from a point r_A having a four-momentum

p_1 and another identical one B is emitted from the point r_B having a four momentum p_2 and we assume that the particle with four-momentum p_1 (p_2) is detected with a detector x_1 (x_2), it will be impossible to decide if the particle originates from the point r_A or r_B (see Figure 3.1). This is reflected in the wave function of the boson pair that has a symmetric expression. For uncorrelated emission of particles we have:

$$\psi_{12} = \frac{1}{\sqrt{2}}\left(\psi_{1A}\psi_{2B} + \psi_{1B}\psi_{2A}\right), \tag{3.2}$$

where $\psi_{i\alpha}$ denotes the wave function for a boson produced at a point r_α and registered with momentum p_i.

If we assume that the source of particles has a space-time distribution given by $\rho(r,t)$, the probability to detect a particle of four-momentum p_1 at x_1 and the other one, of four-momentum p_2, at x_2 is given by the expression:

$$P(p_1,p_2) = \int |\psi_{12}^{BE}(x_1x_2;r_Ar_B)|\rho(r_A)\rho(r_B)d^4r_Ad^4r_B. \tag{3.3}$$

Here, $\psi_{12}^{BE}(x_1x_2;r_Ar_B)$ is defined as the amplitude for a pion pair produced at r_A, respective r_B, to be registered at x_1 and x_2. Assuming that bosons propagate as free particles after emission, one gets:

$$\psi_{12}^{BE}(x_1x_2;r_Ar_B) = \frac{1}{\sqrt{2}}[e^{ip_1(x_1-r_A)}e^{ip_2(x_2-r_B)} + e^{(ip_1(x_1-r_B)}e^{(ip_2(x_2-r_A)}]. \tag{3.4}$$

On the other hand, if ψ^{REF} corresponds to the case with no BEC, i.e. where one can distinguish the different particles, then the probabilities for the alternative histories are added:

$$|\psi_{12}^{REF}|^2 = \frac{1}{2}(|e^{ip_1(x_1-r_A)}e^{ip_2(x_2-r_B)}|^2 + |e^{ip_1(x_1-r_B)}e^{ip_2(x_2-r_A)}|^2). \tag{3.5}$$

The correspondent probability is:

$$P_0(p_1,p_2) = \int |\psi_{12}^{REF}(x_1x_2;r_Ar_B)|^2\rho(r_A)\rho(r_B)d^4r_Ad^4r_B. \tag{3.6}$$

Evaluating the above probabilities, one obtains for the correlation function [30]:

$$C_2(Q) = 1 + |\tilde{\rho}(Q)|^2, \tag{3.7}$$

where $Q = p_1 - p_2$ and $\tilde{\rho}(Q)$ is the Fourier transform of $\rho(r)$ with respect to Q:

$$\tilde{\rho}(Q) = \int \rho(r)e^{-iQr}dr. \tag{3.8}$$

Considering the source to be a sphere of emitters distributed according to the Gaussian probability density and having a radius R:

$$\rho(r) = \frac{1}{4\pi^2 R^2} e^{-\frac{r^2}{2R^2}}, \tag{3.9}$$

the corresponding Fourier transform will be:

$$\tilde{\rho}(Q) = e^{-\frac{Q^2 R^2}{2}}. \tag{3.10}$$

To account for all the possible effects which reduce the strength of the Bose-Einstein correlations, a parameter, denoted λ, is used as a factor in front of the enhancement term. The correlation function (3.1) can be parameterized as:

$$C_2(Q) = 1 + \lambda e^{-Q^2 R^2} \ , \tag{3.11}$$

where λ and R are free parameters. The interpretation of the λ parameter is that it is related to the fraction of identical bosons which do interfere. Parameter R is usually interpreted as the geometrical radius of the presumably spherical boson emitting source.

The customary parameterization for the correlation function in case of electron-positron annihilation is:

$$C_2(Q) = N[1 + \lambda e^{-Q^2 R^2}][1 + \delta Q] \ , \tag{3.12}$$

where N is the overall normalisation and the additional linear term $[1 + \delta Q]$ is used to describe the observed slopes in the correlation function at Q values outside the BEC region.

3.2 BEC in the frame of the string model

In the framework of the perturbative QCD it is possible to obtain many useful formulas but all the results are expressed in partonic language. In order to be able to compare the hadronic distributions which are observed in the experiments to the model, it is necessary to add a fragmentation process to the perturbative results.

The experimental results on BEC in hadronic jets from e^+e^- annihilation [22, 25] show clear evidence for a correlation effect of identical particles of roughly the same momentum. This correlation effect, that was unexpected for a supposedly coherent process, has been explained within the Lund string model [31] in the works of B. Andersson and W. Hofmann [32] and further clarified by M. Bowler [33], B. Andersson and M. Ringnér [26].

To understand the string fragmentation model, I shall refer to the simplest possible system. Consider a quark q and an antiquark $\bar{q}$ going out, back to back, in the overall center of mass frame, the typical situation in a e^+e^- annihilation. The energy stored in the colour dipole field between a charge and an anticharge increases linearly with the separation between charges, if the Coulomb term is neglected. Because of the three-gluon coupling (or vacuum pressure) [31], the color flux lines will not be spread over all space as the electromagnetic field lines do, but rather constrained in a thin tube-like region.

In the string model [31], the confining color field is approximated by a massless relativistic string. The end-points of the string are identified with q and $\bar{q}$ properties while the gluons are assumed to behave as transverse excitation of the string. The string can break-up into smaller pieces producing $q\bar{q}$ pairs, the new end-points. Such a pair will immediately start to separate because of the string tension, which, in the rest frame of a string segment corresponds to a constant energy density $\kappa \sim 1$ GeV/fm. Final states mesons are formed from a q and $\bar{q}$ from adjacent vertices (see Figure 3.2, where j is denoting a meson).

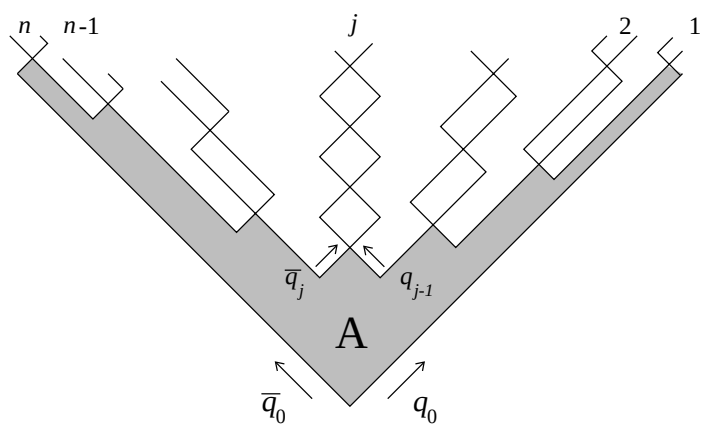

Figure 3.2: *The decay of a Lund Model string.*

The unique break-up rule results in the following probability for a string to decay in to the hadrons, $p_1, p_2, ..., p_n$, [26][2]:

$$dP(p_1, ..., p_n) = \left[\prod_i (N dp_i \delta(p_i^2 - m_i^2))\right] \delta(\sum_j p_j - P_{tot}) \exp(-bA) \quad (3.13)$$

[2]The arguments in this section are based on [26]

where A is the area of the break-up region as indicated in Figure 3.2 and n and b are parameters.

The similarity of the formula to Fermi's Golden rule for the probability of a quantum mechanical transition, size of the final state phase space multiplied by the square of the matrix element $|\mathcal{M}|^2$ (expressed by the exponential area suppression), provides a reasonable starting point to derive a quantum mechanical process. A massless $q\bar{q}$ pair without transverse momentum must be classically produced at such a distance that the string energy between q and $\bar{q}$ can be used to fulfil energy-momentum conservation. If the transverse momentum is conserved in the production process, i.e. the $q\bar{q}$, with masses m, obtain $\pm\vec{k}_\perp$, respectively, then the pair may appear, from the classical point of view, at a distance $\delta x = 2m_\perp/\kappa$, where $m_\perp$ is the transverse mass $\sqrt{m^2 + \vec{k}_\perp^2}$.

There are at least two possible mechanisms [26] to derive the corresponding matrix element, a quantum mechanical tunnelling process a la Schwinger and (or) the possible relationship to the Wilson field operators in a gauge field theory. It was proved [26] that they provide very similar answers to the problem, giving rise to a matrix element as follows:

$$\mathcal{M} = exp(i\kappa - b/2)A \tag{3.14}$$

which not only provides us with the Lund decay amplitude, but can also be used in accordance, to provide a model for BEC among identical bosons.

If one considers a final state containing (among possibly a lot of other hadrons) n identical bosons, there are $n!$ ways to describe such a state, each corresponding to a different permutation of the particles. According to quantum mechanics, the transition matrix element has to be symmetrised with respect to exchange of identical bosons. This leads to the following general expression for the production amplitude:

$$\mathcal{M} = \sum_{\mathcal{P}} \mathcal{M}_{\mathcal{P}}, \tag{3.15}$$

where the sum goes over all possible permutations $\mathcal{P}$ of the identical bosons. The cross section will then contain the square of the symmetrised amplitude $\mathcal{M}$:

$$|\mathcal{M}|^2 = \sum_{\mathcal{P}} (|\mathcal{M}_{\mathcal{P}}|^2 (1 + \sum_{\mathcal{P}' \neq \mathcal{P}} \frac{2\mathrm{Re}(\mathcal{M}_{\mathcal{P}} \mathcal{M}^*_{\mathcal{P}'})}{|\mathcal{M}_{\mathcal{P}}|^2 + |\mathcal{M}_{\mathcal{P}'}|^2})). \tag{3.16}$$

The phenomenological models used to describe the hadronization process are formulated in a probabilistic language. This implies that the interference

between different ways to produce identical bosons is not included. In this case the probability for producing this state is:

$$|\mathcal{M}|^2 = \sum_{\mathcal{P}} |\mathcal{M}_{\mathcal{P}}|^2 \tag{3.17}$$

instead of the probability from Eq (3.16). Comparing Eq (3.16) and Eq (3.17) we can see that a particular configuration leading to the final state $\mathcal{P}$ can be produced according to a probabilistic scheme and that the quantum mechanical interference that appears during the production of identical bosons can be incorporated by weighting the produced event with:

$$w = 1 + \sum_{\mathcal{P}' \neq \mathcal{P}} \frac{2\mathrm{Re}(\mathcal{M}_{\mathcal{P}} \mathcal{M}^*_{\mathcal{P}'})}{|\mathcal{M}_{\mathcal{P}}|^2 + |\mathcal{M}_{\mathcal{P}'}|^2}. \tag{3.18}$$

In order to see the main feature of symmetrizing the hadron production amplitude in the Lund Model, one can consider, see Figure 3.3, that two of the produced hadrons, denoted $(1, 2)$, are identical bosons and denote the state between them I. There are two different ways to produce the entire state corresponding to the production configurations, $(\ldots, 1, I, 2, \ldots)$ and $(\ldots, 2, I, 1, \ldots)$, i.e. exchanging the two identical bosons. The two production configurations are shown in the Figure 3.3 and the main observation is that they correspond, in general, to different areas. The area difference, ΔA, depends only on the energy momentum vectors p_1, p_2 and p_I, but can, in a dimensionless way, be written as:

$$\frac{\Delta A}{2\kappa} = \delta p \delta x = QR \tag{3.19}$$

where $\delta p = p_2 - p_1$ and $\delta x = (\delta t, 0, 0, \delta z)$ are a reasonable estimate of the space-time difference, along the surface area, between the production points of the two identical bosons. After some careful calculations [26], the weight in the Lund Model can be written as:

$$w = 1 + \sum_{\mathcal{P}' \neq \mathcal{P}} \frac{\cos \frac{\Delta A}{2\kappa}}{\cosh\left(\frac{b\Delta A}{2} + \frac{\Delta(\sum p^2_{\perp q})}{2\sigma^2_{p_\perp}}\right)} \tag{3.20}$$

where Δ denotes the difference with respect to the configurations $\mathcal{P}$ and $\mathcal{P}'$, the sum of $p^2_{\perp q}$ is performed over all vertices and $\sigma_{p_\perp}$ is the width of the transverse momenta for the generated hadrons, (i.e. $\sigma^2_{p_\perp} = 2\sigma^2$).

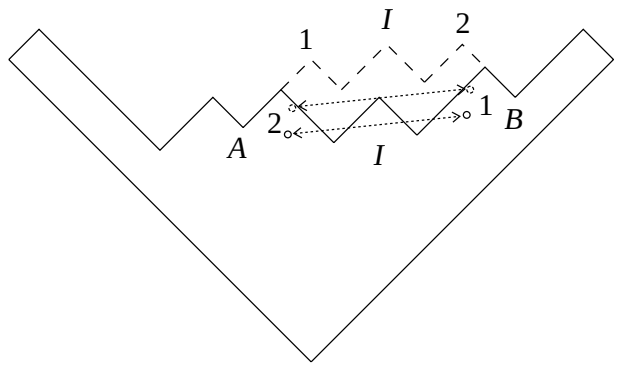

Figure 3.3: *The two possible ways to produce the entire state when two of the bosons are identical*

Using Eq (3.19) for a single pair exchange, one sees that the area difference is, for small δp, governed by the distance between the production points and that ΔA increases quickly with this distance. ΔA vanishes with the four-momentum difference and the contribution to the weight given by a configuration, $\mathcal{P}'$, vanishes fast with increasing area difference ΔA. From these considerations it is obvious that only exchanges of pairs with a small δp and a small δx will give a contribution to the weight.

In this approach [26], the BEC function Eq.(3.11), is defined as the ratio between the two-particle probability density ρ_2 with or without Bose-Einstein weights:

$$C(Q) \sim R(p_1, p_2) = \frac{\rho_{2w}(p_1, p_2)}{\rho_2(p_1, p_2)}. \tag{3.21}$$

3.3 Monte Carlo models of BEC

The Bose-Einstein effect between identical bosons produced in hadronic interaction is not easy to include in the event generator programs for high-energy physics. The event generators most frequently used for the Z^0 decay, HERWIG (based on the Marchesini-Weber parton cascades and ending by cluster fragmentation) [34] and JETSET [21] (based on the Lund string model dynamics) are built in accordance with classical stochastic processes. They produce a probability weight for an event without taking into account the quantum mechanical effects.

Torbjörn Sjöstrand introduced in JETSET a device that simulates the

Bose-Einstein effect as an attraction between identical bosons. Starting from a set of energy-momentum vectors of identical bosons, $p_1, p_2, ..., p_n$, generated without any Bose-Einstein effect, it is possible to reshuffle the set into another set where, keeping the energy-momentum conservation for the whole event, the particles of a pair are moved closer, to reproduce the correlation. Bo Andersson and Markus Ringnér developed a method to provide the Lund model with a quantum mechanical interpretation using a production matrix element with well defined phases (this model was already described in Section 3.2). BEC is implemented, in this case, by weights assigned to the events generated by JETSET. Several models [12, 35], were developed following the same pattern, but the simulations based on the weight methods are not yet usable alternatives for practical purposes, the associated calculations being too time-consuming.

Since the JETSET program is the simulation program most commonly used by the high energy experimental groups and being provided with the only working procedure to simulate BEC, its performance, drawbacks and the possible improvements have been studied often [36, 37].

JETSET is a simulation program able to generate hard processes, in particular, the electron-positron annihilation $e^+e^- \to \gamma^*/Z^0 \to q\bar{q}$ (here '*' is used to denote that the photon is off mass shell). The quark q in the reaction may have any flavour, except of top. The flavour in each event is picked at random, according to the relative couplings evaluated at the hadronic center of mass energy. JETSET is intimately connected with the string fragmentation model in the form of Lund model [31]. The JETSET program has a probabilistic and iterative nature, with the fragmentation process being described in terms of one or few simple underlying branches, as, for example, $string \to hadron + remainder\ string$ and so on. At each branching, probabilistic rules are given for production of new flavours and for sharing of the energy and momentum between the products.

The procedure used to implement the BEC is rather simple. Defining Q_{ij} value, associated to a pair i, j, as:

$$Q_{ij} = \sqrt{(p_i + p_j)^2 - 4m^2}\ , \tag{3.22}$$

where m is the common particle mass and p_i, p_j are particle momenta, a shifted smaller Q'_{ij} is then to be found, such that the ratio $C_2(Q)$ of "shifted" to the "unshifted" Q distribution is given by the requested parameterization. The shape can be chosen to be either exponential or Gaussian, as in Eq.(3.11):

$$C_2(Q) = 1 + \lambda e^{-(QR)^r}, \quad r = 1\ or\ 2\ . \tag{3.23}$$

If the inclusive distribution of the Q_{ij} values is assumed to be given just by the simple, spherical phase space, Q'_{ij} can be found as a solution of the equation:

$$\int_0^{Q_{ij}} \frac{Q^2 dQ}{\sqrt{Q^2+4m^2}} = \int_0^{Q'_{ij}} C_2(Q) \frac{Q^2 dQ}{\sqrt{Q^2+4m^2}} , \tag{3.24}$$

that gives, indeed, as a new distribution, Q'_{ij} – the product of the old distribution and $C_2(Q)$:

$$Q'_{ij} = Q_{ij} C_2(Q) . \tag{3.25}$$

The algorithm used to simulate the Bose-Einstein effect, implemented in the LUBOEI subroutine, does not represent a true model and implies very specific assumptions and choices. The fragmentation and the decays of the short-lived particles like ρ are allowed to proceed independently of the Bose-Einstein effect. Since the procedure is an imitation of the interference effect, in the case of the assumed spherical shape of the distribution in Q, it is not guaranteed that other features of the interference effect will be well described. The Bose-Einstein effect is interpreted almost as a classical force, acting on the final state particles, rather than being a quantum mechanical phenomenon affecting the production amplitude. So far, this Bose-Einstein algorithm should be used which caution and only as a first approximation to what Bose-Einstein effect can mean. The astonishing fact is that this parameterization reproduces rather well the dependence of the correlation function parameters on the average transverse mass of the pair, seen in experimental data [20, 38]. It is difficult to accept that this phenomenon is explained by traditional hydrodynamical models, used in heavy-ion physics. However, the fact that JETSET reproduces the effect quite satisfactory, implies that profound studies using this particle generator ought to be performed in order to explain the observed transverse mass dependence [20, 38].

In JETSET there are five parameters that decide the characteristics of the BEC:

- MSTJ(51): r parameter Eq. (3.23), that can take the value 0, if no Bose-Einstein symmetrization is included; 1, for an exponential form of the BEC function and 2 for the Gaussian one. In what will follow when I refer to the Eq.(3.23) and I would refer only to its Gaussian variant, $r = 2$.

- MSTJ(52): number of the particle species for which Bose-Einstein correlation are to be included, taken in order along the chain $\pi^+, \pi^-, \pi^0, K^+, K^-, K^0_L, K^0_S, \eta, \eta'$.

- PARJ(91): minimum particle width above which particle decays are assumed to take place before the stage where BE effects are introduced. The default value is 0.020 GeV. Particles with width broader than PARJ(91) are assumed to have time to decay before Bose-Einstein effects are to be considered.

- PARJ(92): nominal strength of Bose-Einstein effects λ with default value 1, λ in Eq. (3.23).

- PARJ(93): size of the BE effect region in terms of the Q variable, R^{-1} in Eq. (3.23) (default value 0.2 GeV).

3.4 Reference sample

To prove that the production of bosons with similar space-time characteristics is enhanced, it is necessary to compare the data with a reference sample, free of BEC. Such kind of reference sample must contain all the features which are present in the distributions constructed for identical pairs in data (presence of correlations due to energy-momentum conservation, presence of the correlations due to the jet structure of events) except the Bose-Einstein symmetry and must not contain additional features (absence of additional dynamical correlations).

During the years, several methods were developed to construct a reference sample for the study of BE correlations: combining pairs of tracks of opposite sign, mixing tracks from different events, generating Monte Carlo samples which describe data without containing BEC simulation.

Since pions are the most copiously produced particles in hadronic decays, the effects of the Bose-Einstein symmetry are studied traditionally among the same sign pion pairs. An obvious reference set is, in this case, the opposite-sign pions [37]. However some clear disadvantages for this kind of reference sample were observed: Q distribution of the unlike sign pion pairs includes peaks due to the neutral meson resonances and exhibits a slow rise in Q, relative to the same sign pairs, arising from the different number of pairs (the number of the charge-like pairs is smaller than the number of the different charge-pairs, see Fig 3.4), and charge conservation; it is affected by other dynamical effects including local charge ordering and additional dynamical correlations. Giving these reasons it became clear [25] that the construction of the uncorrelated reference sample by the unlike pions combination gives large systematic errors. Also recent theoretical

study of isospin symmetry implies that the unlike charge reference sample should be avoided [39].

Another type of reference set can be derived from MC generators. This relies on a correct simulation of the physics in a complete absence of any BE symmetry and a correct simulation of the apparatus effect. The disadvantage of this method is that the fragmentation process and BEC are strongly related and it is possible that by removing BEC from the model, one removes too much. In practice, it is more useful to use simulated data to correct both the same sign sample and the reference data for the imperfections given by the way in which the reference sample is constructed and for the detector acceptance effect.

A better method to construct the reference sample is the track mixing. For events with high center of mass energy, where two-jet topologies dominate, particles from different hemispheres can be combined by reflecting the particle momenta $\vec{p} \rightarrow -\vec{p}$ [37]. This approach is valid provided that the masses of pairs in the reference sample are typically much greater than those influenced by BE effect [37]. Some correlations are also lost because of the additional gluon radiation that causes jets to be non-collinear.

Particles observed in one event can be combined with particles from another event with similar topology and orientation. Here the problem is that the energy-momentum conservation is not taken into account, but, since this is a long range effect, it ought to be possible to extract the short range effect of the interference without large systematic errors. The main disadvantage of this approach is that some other kind of correlations are also removed. An advantage of the use of the mixed reference sample is that it is free of additional dynamic correlation or local energy-momentum compensation. Also if the high-energy particles close to phase-space limits are removed and if the detector efficiency is isotropic, correlations due to the jet structure of the event are also taken in to account.

Two kinds of final-state interactions may change the BEC pattern: the Coulomb force between the two pions under study and between one of the pions and the other hadrons; and the hadronic interaction. The latter is not well known.

To correct the correlation function for the Coulomb effects means to correct it for the wave function modification at infinity, when compared with the wave functions to the origin. This correction is small unless the relative velocity of those two pions in the $\pi\pi$ rest frame is small, of the order of MeV/c and can be taken into account by weighting the reference density by the appropriate Gamow factor [25].

At small Q, Coulomb repulsion (attraction) between like (unlike) charged

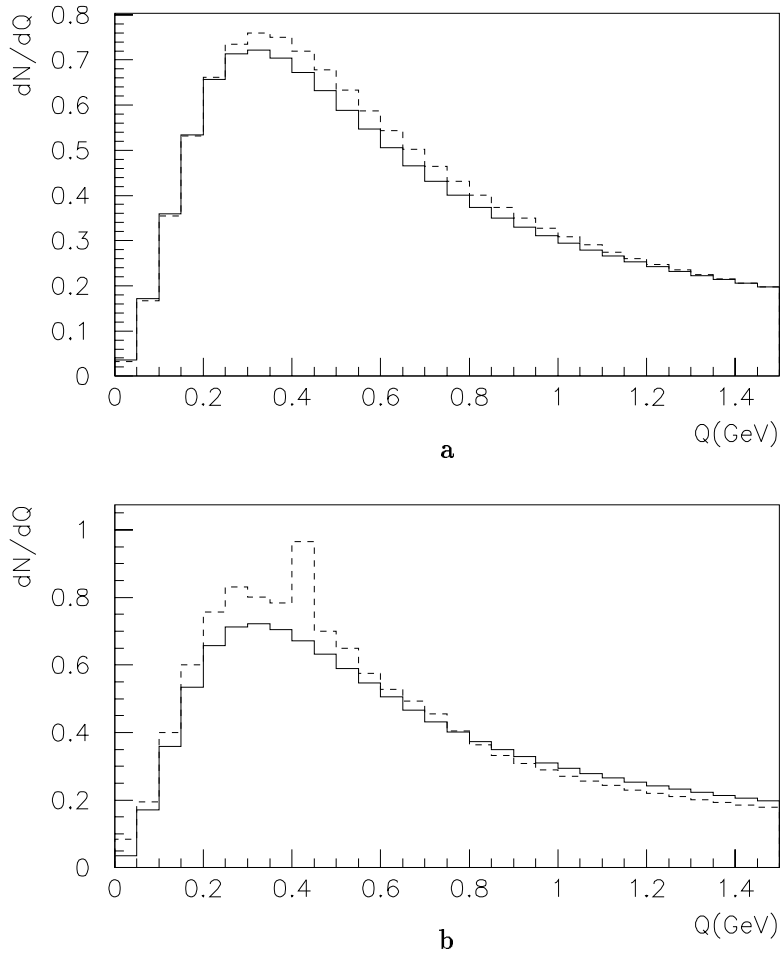

Figure 3.4: *Comparison between the Q distribution for* JETSET *simulated events without Bose Einstein phenomenon included (full line) and (a) the reference sample obtained by mixing procedure; (b) reference sample obtained by using different sign particles (dashed line). It is easy to observe that the reference sample obtained using the mixing procedure is following better the* JETSET *sample in the absence of BEC simulation. Another straightforward observation is that the number of different-sign pions pairs is bigger than the same-sign ones. A resonance peak can been easily seen on the profile associated with the unlike-charge sample.*

pions moving away from the source is expected to modify the two-pion cross section in the data by:

$$G_l(\eta) \sim \frac{\eta}{e^{\eta}-1}, \quad G_u(\eta) \sim \frac{\eta}{1-e^{\eta}}. \tag{3.26}$$

where $\eta = 2\pi\alpha m_\pi/Q$.

Since the net charge, $\pm 2e$, of the remaining system is small and the two pions of a like-sign pair are subject to similar Coulomb forces, the Coulomb correction due to the forces between a pion and the remaining hadrons is expected to be negligible [25].

Near $Q = 0$, the effect of Coulomb repulsion between two identical charged bosons will lead to the suppression of the probability of finding two like-charged particles with small relative momentum. The effect is dominant in case of pions for $Q < 10$ MeV. For $Q > 50$ MeV the Coulomb repulsion is negligible, since it has only a small effect on the studied distributions.

In our work (present thesis and the articles in appendices) we used the mixing procedure to construct the reference sample. We combined particles from kinematically similar events, assuming that the selection criteria of the two-jet events provide us with a proper set of events. The "mixing" procedure can be described by following steps:

- After the determination of the thrust axis[3], each event is rotated to a new coordinate system, which has the z axis along the thrust axis.
- Tracks from each rotated event are stored in a reference buffer. Events in the buffer are continuously updated to prevent any regularities in the particle spectra.
- The reference sample is built pairing a real track with a randomly picked track from the reference buffer. First, a random event of the stored ones is selected, then a track from this event is also randomly picked up.

The mixing procedure does not conserve energy and momentum, and destroys not only the Bose-Einstein correlation but even some other kinds of correlations, making necessary some corrections.

[3]The quantity thrust T is defined by:

$$T = \max_{|\vec{n}|=1} \frac{\sum_i |\vec{n}\cdot\vec{p_i}|}{\sum_i |\vec{p_i}|} ,$$

and the thrust axis $\vec{v}_1$ is given by the $\vec{n}$ vector for which maximum is attained. The allowed range is $1/2 \leq T \leq 1$, with a 2-jet event corresponding to $T \approx 1$ and an isotropic event to $T \approx 1/2$.

3.5 Correction procedure

To construct properly the correlation function, eliminating side effects introduced by the mixing procedure, we accumulate four kinds of charge-like pairs distribution, N, as a function of Q[4]:

- Bose-Einstein correlation effect turned on, but the mixing procedure not performed: N_{BEon}, see Figure 3.5a (closed circles).
- Bose-Einstein correlation effect turned on, and the mixing procedure performed: N_{BEon}^{MIX}, see Figure 3.5a (open circles).
- Bose-Einstein effect turned off, and the mixing procedure performed: N_{BEoff}^{MIX}, see Figure 3.5b (open circles).
- Bose-Einstein effect turned off, and the mixing procedure not performed: N_{BEoff}, see Figure 3.5b (closed circles).

The corrected correlation function is given by:

$$C_2(Q) = \frac{N_{BEon}(Q)/N_{BEon}^{MIX}(Q)}{N_{BEoff}(Q)/N_{BEoff}^{MIX}(Q)} \ , \tag{3.27}$$

The ratios $N_{BEon}(Q)/N_{BEon}^{MIX}(Q)$ and $N_{BEoff}(Q)/N_{BEoff}^{MIX}(Q)$ are very similar in shape, as Figure 3.6 a shows. Even in the $N_{BEoff}(Q)/N_{BEoff}^{MIX}(Q)$ case, a small enhancement, that has approximately the same width, appears due to the other kinds of correlation. In Figure 3.6b, the ratio $N_{BEon}^{MIX}(Q)/N_{BEoff}^{MIX}(Q)$ shows that the mixing procedure does not eliminate correlations totally. To obtain a clear Bose-Einstein effect over the $C_2(Q) = 1$ level, one has to calculate the double ratio (3.27) obtaining $C_2(Q)$ almost constant for $Q > 1$ GeV, as it is shown below (see Figure 3.7).

3.6 Longitudinal Center of Mass System

To analyse the correlation function in terms of Q components the so-called Longitudinal Centre-of-Mass System [40] (LCMS) (see Figure 3.8) is frequently used. The LCMS is defined for each pair of particles as the system in which the sum of the two particle momenta is perpendicular to

[4] In all the examples presented in this section we used only $q\bar{q}$ JETSET simulated events

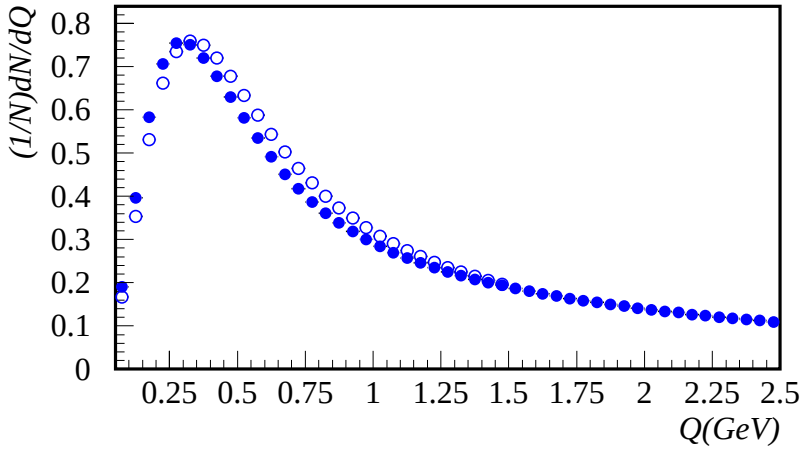

a

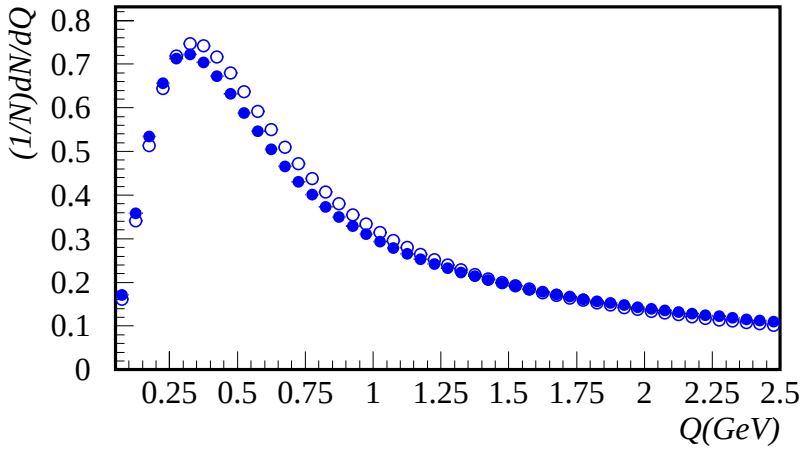

b

Figure 3.5: *The stored Q histograms (normalised to unit), for all charged particles, 2 millions* JETSET *events: a) Bose-Einstein correlation effect included b) Bose-Einstein effect not included. Closed circles: mixing procedure not performed and open circles: the mixing procedure performed.*

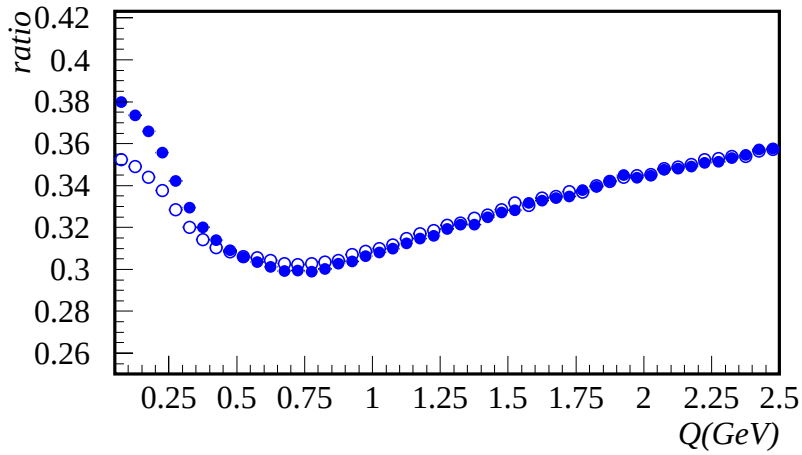

a

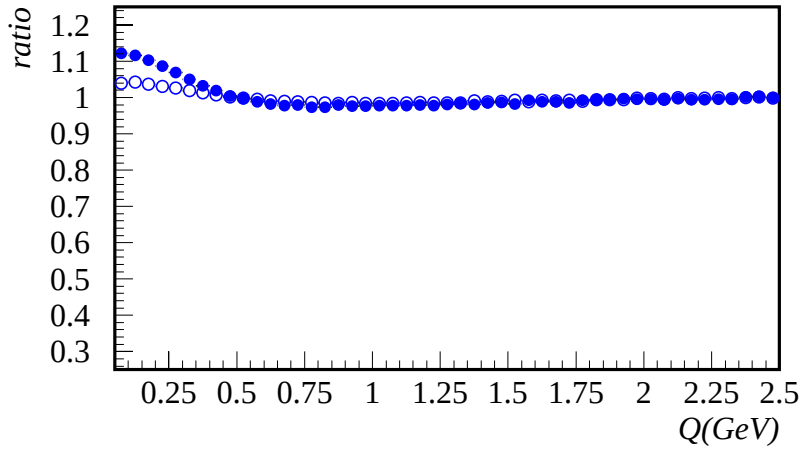

b

Figure 3.6: *a) The ratios* $N_{BEon}(Q)/N^{MIX}_{BEon}(Q)$ *(closed circles) and* $N_{BEoff}(Q)/N^{MIX}_{BEoff}(Q)$ *(open circles); b) The ratios* $N_{BEon}(Q)/N_{BEoff}(Q)$ *(closed circles) and* $N^{MIX}_{BEon}(Q)/N^{MIX}_{BEoff}(Q)$ *(open circles).*

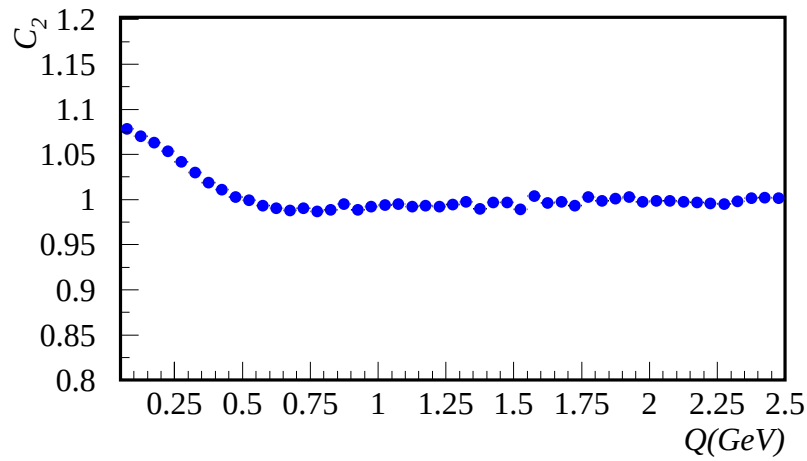

Figure 3.7: *The final corrected correlation function, as in Eq.(3.27).*

a selected reference axis. The reference axis has to be a physical axis of the process: for example, in e^+e^- annihilation it can be the direction of a primary parton, or that of the corresponding jet. In this analysis, the thrust axis was chosen as the reference. In such a system, $\vec{Q}$ is decomposed into: Q_{long}, parallel to the thrust axis; $Q_{t,out}$, collinear with the sum of the two particles' momenta, and the complementary $Q_{t,side}$, perpendicular to both Q_{long} and $Q_{t,out}$. The four-momentum difference is then:

$$Q^2 = Q^2_{t,out} + Q^2_{t,side} + Q^2_{long} - \Delta E^2 \ . \tag{3.28}$$

This system is convenient for calculations and interpretations. The projection of the momentum sum of the two particles is non-zero only in the "t, out" direction. The spatial dimensions of the source affect all components of Q. However, the energy difference and hence the temporal dimension of the source, couples only to the $Q_{t,out}$ component see Eq. (3.30). If the string model is considered, the longitudinal direction of the LCMS has to be aligned with the direction of motion of the initial partons, so that the system itself will be the local rest frame of a string. Mixing procedure is simple to apply in this kind of reference system. To calculate the particle momenta in the frame of LCMS, one must first rotate them until the z (longitudinal)

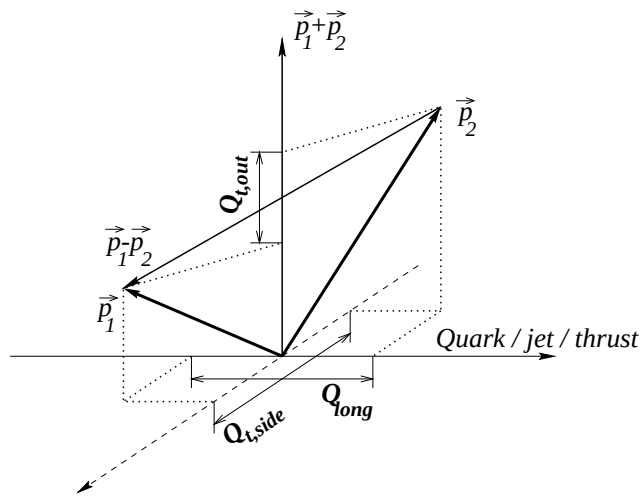

Figure 3.8: *The LCMS reference system*

axis coincides with the jet axis and next boost them with the longitudinal velocity :

$$\beta_z = \frac{p_{z,1} + p_{z,2}}{E_1 + E_2} \ , \tag{3.29}$$

where $p_{z,1}$, $p_{z,2}$ denote the z-axis projections of momenta and E_1, E_2 are energies of the two particles. The energy difference in the longitudinal center of mass system will be:

$$\Delta E = \beta_t Q_{t,out} \quad , \tag{3.30}$$

where β_t is the transverse velocity of the pair :

$$\beta_t = \frac{p_{t,1} + p_{t,2}}{E_1 + E_2} \ . \tag{3.31}$$

Here $p_{t,1}$ and $p_{t,2}$ are transverse momenta of particles.

From Eq.(3.11), Eq.(3.28), Eq.(3.30) one obtains for the correlation function the following expression:

$$C_2(Q_{t,out}, Q_{t,side}, Q_{long}) = 1 + \lambda e^{-R^2 Q^2_{t,out}(1-\beta_t^2) - R^2 Q^2_{t,side} - R^2 Q^2_{long}} \ . \tag{3.32}$$

Using the three components of the radius related to this reference system, the correlation function can be parameterized as:

$$C_2(Q_{t,out}, Q_{t,side}, Q_{long}) = 1 + \lambda e^{-R^2_{t,out} Q^2_{t,out} - R^2_{t,side} Q^2_{t,side} - R^2_{long} Q^2_{long}} \ , \tag{3.33}$$

where $R_{t,out}$, $R_{t,side}$, R_{long} are the corresponding components of the radii, with the following relations:

$$R_{t,side} \sim R_{long} \sim R_{t,out}\gamma \sim R \ , \tag{3.34}$$

where $\gamma = 1/\sqrt{1-\beta_t^2}$.

The two-dimensional projection of the LCMS is often used in analysis, with longitudinal component $Q_{||} \equiv Q_{long}$ and perpendicular component $Q_{\perp} = \sqrt{Q_{t,out}^2 + Q_{t,side}^2}$. The parameterization of C_2 in the two-dimensional case is chosen here as:

$$C_2(Q_{\perp}, Q_{||}) = 1 + \lambda e^{-Q_{\perp}^2 R_{\perp}^2 - Q_{||}^2 R_{||}^2} \ . \tag{3.35}$$

In what will follow the two- and three-dimensional correlation functions are obtained using normalised double, respective triple differential cross section (following the same procedure as for the one-dimensional distributions).

3.7 m_t dependence of BEC function parameters

Analysis of experimental data in the e^+e^- annihilation, at the center-of-mass energy 91.2 GeV, using DELPHI data [20], Appendix D, showed a dependence of the three-dimensional BEC parameters, Eq.(3.33), on the average transverse mass of the boson pair:

$$m_t = \frac{m_{t,1} + m_{t,2}}{2} = \frac{\sqrt{m_1^2 + p_{t,1}^2} + \sqrt{m_2^2 + p_{t,2}^2}}{2} \tag{3.36}$$

A qualitative similar dependence was observed for JETSET generated events with the DELPHI JETSET tuning[5] [41], in particular: λ=1, R=0.394 GeV (see Figure 3.9).

The three-dimensional correlation function $C_2 \equiv C_2(Q_{t,out}, Q_{t,side}, Q_{long})$ was constructed in four m_t intervals:

- 0.25 GeV $\leq m_t <$ 0.35 GeV,
- 0.35 GeV $\leq m_t <$ 0.45 GeV,
- 0.45 GeV $\leq m_t <$ 0.60 GeV,

[5] When referring here to DELPHI tuning for JETSET parameters, I refer to the tuning of the main JETSET parameters including the BEC ones (if not specified otherwise).

- 0.6 GeV $\leq m_t <$ 1.5 GeV.

Fit of these distributions to Eq: (3.33) was used to show the dependence of the correlation function parameters on m_t.

In Figure 3.9 we present the results obtained using DELPHI data corrected for detector effects and effects introduced by mixing and JETSET generated events with DELPHI tuning. The λ parameter grows with increasing transverse mass, while $R_{t,out}$, $R_{t,side}$ and R_{long} exhibit a tendency to decrease with different slopes.

In heavy ion interactions at high energy, a m_t dependence of the radii has also been found, but the behaviour is in some respects different to that found here [17, 42]. In these reactions all the radii show a similar dependence being proportional to $1/\sqrt{m_t}$. The λ parameter does not depend on m_t in heavy ion experiments.

The increase of the λ parameter with m_t in e^+e^- annihilation is usually explained by the disappearance of the resonance decay products with increasing m_t. In the clean sample of the two-jet events, the λ dependence is considered a purely kinematic effect given by the resonance decays. A popular explanation of the observed m_t dependence of the radius is that it is also due to the resonance decays. Resonances are propagating out of the primary pion source and the pions produced in their decay have comparatively low momenta. The effective size of the source increases towards small m_t values. Final state interaction and resonance production can affect the shape of the correlation function. The above explanation cannot possibly be valid in case of JETSET since the resonance propagation is not included in the generator.

The fact that this effect is reproduced qualitatively quite satisfactory without any explicit input of the transverse mass dependence, opens the interest for studies of the origin of this effect in JETSET generated events.

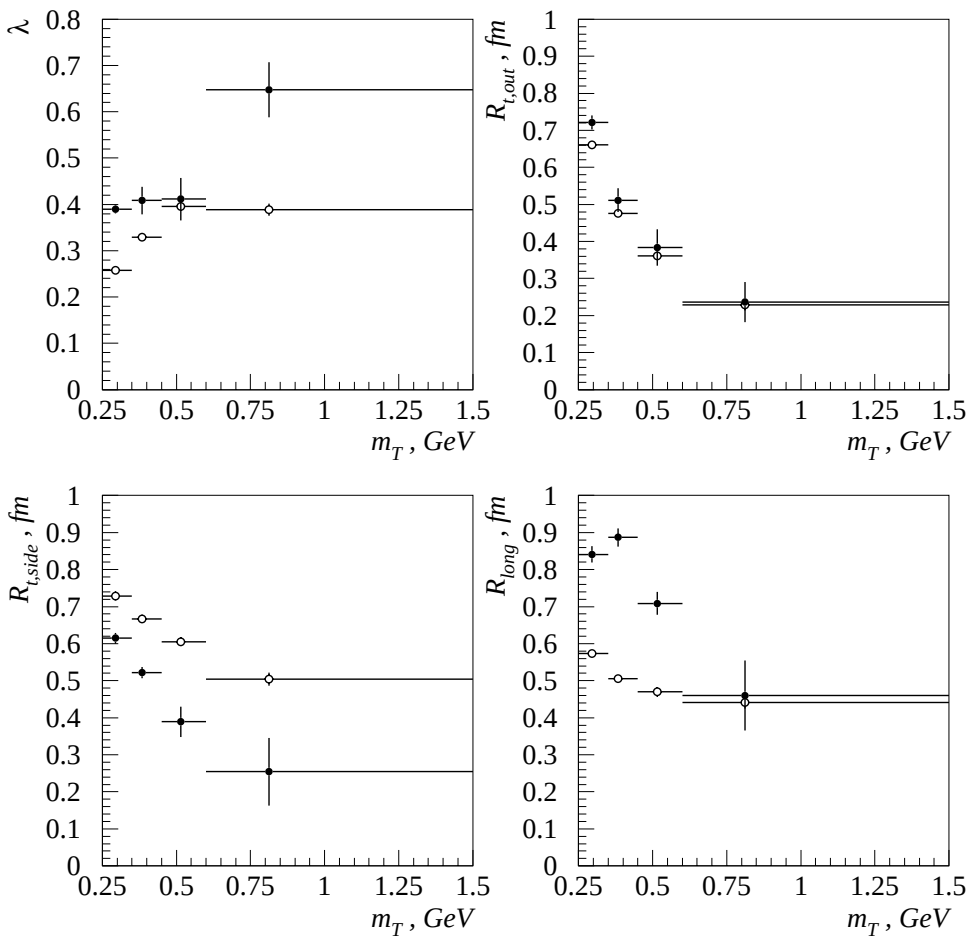

Figure 3.9: *Transverse mass dependence for the fit parameters of the correlation function $C_2(Q_{t,out}, Q_{t,side}, Q_{long})$ using Eq.(3.33). Closed circles represent the DELPHI data corrected for detector effects, while open circles –* JETSET *with DELPHI tuning.*

Chapter 4

Study of BEC in JETSET

The string model provides an appropriate framework, in which the Bose-Einstein enhancement can be studied [31, 32, 33]. The associated calculations are quite complex and time-consuming, especially when more than two particles are considered to be affected by Bose-Einstein symmetrization [26]. For this reason, it is convenient to use the simple semiclassical model that is implemented in the JETSET generator [21]. In the current standard algorithm, identical particles are pulled closer together to enhance the two-particle correlation at small Q values (see Section 3.3). Several shapes of the enhancement can be simulated. In particular, for the analysis discussed here, the Gaussian shape of the correlation function was chosen, ($r = 2$) (3.23), with the input values for the parameters λ and R tuned to the DELPHI data: λ =1 and R = 0.394 GeV^{-1}=0.5 fm [41] (for the other parameters of JETSET we used the default ones).

We used JETSET in order to generate events at the center of mass energy of 91.2 GeV. The study of the Bose-Einstein effect was performed here only for charged particles since the low efficiency of the neutral particle reconstruction in DELPHI experiment makes the comparison of simulated data with the experimental results very difficult, if neutral particles are also included. To see how the BEC function parameters depend on the origin of particles involved in the analysis, we studied samples that include all charged particles, subsamples of charged pions, pions that were produced directly from the hadronization of quarks and gluons (direct pions), pions coming from resonance decays and separately pions that appeared in decays of ρ mesons which were, in turn, produced in the hadronization of the string (direct ρ's). To study how the radius parameter provided as input is affecting the shape of the output correlation function, different values of the

JETSET input radius, R, were used for our studies.

4.1 Event and track selection

In this study $q\bar{q}$ events were generate using JETSET. To compare the results with previous experimental results, the thrust value was required to be bigger than 0.95 and the following cuts were introduced:

- The correlation function was constructed for particles having momentum below 5 GeV/c to avoid the limits of phase space where dynamical correlations are non-negligible.

- To reduce correlations due to the local transverse momentum compensation, the pairs were rejected if their opening angle in transverse plane exceeded 120°. This cut was introduced for the compatibility with experimental data and reduces slightly the background at high Q values.

Since the number of pairs of particles that accomplished all the cuts is small (especially in the case of mixed samples for pions from resonances and direct pions, where the multiplicity is low) it was necessary to analyse large samples (see Table 4.1).

	Number of events	Average multiplicity
Charged particles	2 000 000	14
Pions	2 000 000	12
Direct pions	5 000 000	2
Pions from resonances[1]	5 000 000	6
Pions from direct ρ	50 000 000	3

Table 4.1: *Number of events analysed. Samples of pions coming from direct ρ were generated for five different values of input radii in the* JETSET *simulation.*

[1] Resonances with width larger than 20 MeV

4.2 Dependence on particle origin

Since the tentative explanations of the m_t dependence of the three-dimensional BEC parameters are related to the different origin of the particles that are involved in BEC, the study of the dependence of the BEC parameters on particle origin, using JETSET simulated events, seemed to be useful for a better understanding of the phenomenon.

The results of the fit of the three-dimensional correlation functions (see Section 3.6, constructed as it is described in the previous chapter using Eq. (3.33), in different m_t intervals) for particles having different origin are presented in this section.

4.2.1 λ dependence on m_t

λ represents a measure of the fraction of particles sensitive to the BEC effect. Figure 4.1 and Table 4.2 show that λ has a similar behaviour in case of all the charged particles and all the pions (the vast majority of charged particles in our case are pions). The values are lower if all the particles are taken into account than in case only pions are analysed, since hadrons of different kind, that are not subject to Bose-Einstein symmetrization, can be paired. In case of direct pions and pions from resonances, λ is almost

$< m_t >$ (GeV)	a)	b)	c)	d)	e)
0.19	0.055±0.003	0.072±0.003	1.349±0.090	0.724±0.012	1.147±0.019
0.30	0.194±0.006	0.241±0.007	1.175±0.052	0.736±0.014	1.241±0.016
0.38	0.269±0.010	0.348±0.011	1.303±0.066	0.754±0.030	1.197±0.022
0.52	0.299±0.018	0.441±0.034	1.141±0.079	0.725±0.049	1.207±0.034

Table 4.2: *Values of λ for : a) all particles, b) all pions, c) direct pions, d) pions from all resonances and e) pions from direct ρ.*

constant as a function of m_t, as one should expect, with a ~20 % overshoot that can be connected with the input-output discrepancy that will be discussed later on in this chapter. Studying the sample of pions coming from the decay of all the resonances, one can observe that λ is ~40 % smaller than in case of the pions coming from direct ρ's, although it manifests a similar behaviour. This could be explained by the fact that in the first case one includes also pions coming from the decay of other resonances which cannot interfere with the pions coming from direct ρ's.

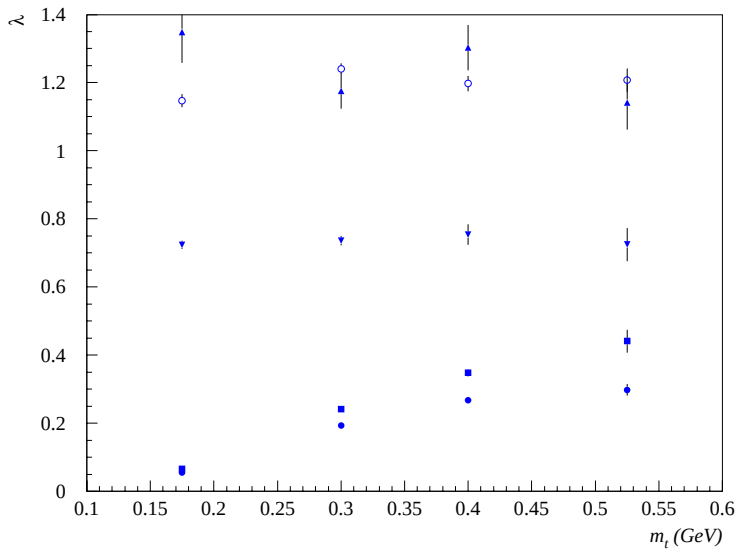

Figure 4.1: *Dependence of* λ. *One represents with* • *the results for all charged particles, with* ■ *the ones for all pions, for direct pions using* ▲, *for pions coming from all the resonances decay with* ▼ *and for pions coming from the decays of direct* ρ *with* ○.

Since the direct pions and the pions coming from direct ρ are all subject to Bose-Einstein correlation, as originating from the same source, λ values are almost constant for these samples. We can conclude that λ's dependence on m_t is given by that mixture of particles of different origin that are subject of BEC. This can be understood starting from the fact that λ is assumed to be related to the fraction of particles, that are subject of BEC. When we restrict our study to particles that are coming from the string, or to particles that appear in the decay of directρ's, the percentage of the particles that will be correlated will be close to 100%. In the case of mixture of particles, we pair not only particles that are coming from the same source, but also particles coming from different sources that are not subject to BEC. LUBOEI is introducing BEC for each pair of pions according with their momenta irrespective if they have the same origin or not. The fact that λ is behaving different for mixtures of particles and particles coming from the same source is mainly the result of the fragmentation process.

4.2.2 Radius components dependence on m_t

In Eq. (3.33), the three radius components are defined in the LCMS reference system (see Section 3.6). $R_{t,out}$ value, obtained as the result of the fit of the three-dimensional correlation function to Eq. (3.33), behaves similarly for all the samples, decreasing with increasing m_t, although the values change somewhat from sample to sample (see Figure 4.2 and Table 4.3). This behaviour was expected since $R_{t,out} \sim R/\gamma$ (see Eq. 3.34).

$< m_t >$ (GeV)	a)	b)	c)	d)	e)
0.19	0.803±0.051	0.717±0.046	0.621±0.048	0.664±0.017	0.720±0.015
0.30	0.788±0.021	0.775±0.020	0.544±0.025	0.659±0.012	0.670±0.008
0.38	0.562±0.023	0.554±0.018	0.476±0.029	0.545±0.021	0.560±0.011
0.52	0.415±0.038	0.423±0.039	0.288±0.057	0.365±0.050	0.463±0.011

Table 4.3: *Values of $R_{t,out}$ for : a) all particles, b) all pions, c) direct pions, d) pions from all resonances and e) pions from direct ρ*

$R_{t,side}$ is decreasing with m_t for mixtures of particles (if we ignore the first bin of the histogram, where, the values obtained for the radius components are less reliable due to the small values of λ, obtained from the fit procedure) and it is varying around a constant value for the pure samples see Figure 4.3 and Table 4.4.

$< m_t >$ (GeV)	a)	b)	c)	d)	e)
0.19	0.381±0.066	0.095±0.198	0.649±0.047	0.642±0.015	0.607±0.015
0.30	0.730±0.021	0.734±0.019	0.605±0.025	0.731±0.012	0.674±0.007
0.38	0.668±0.023	0.655±0.022	0.606±0.022	0.665±0.023	0.701±0.009
0.52	0.603±0.032	0.654±0.048	0.524±0.028	0.681±0.045	0.673±0.013

Table 4.4: *Values of $R_{t,side}$ for : a) all particles, b) all pions, c) direct pions, d) pions from all resonances and e) pions from direct ρ.*

The dependence of R_{long} on m_t (Figure 4.4 and Table 4.5) is not as strong as the one for $R_{t,out}$ (Figure 4.2 and Table 4.3), with the values being similar for all the samples of particles. However R_{long} is the most consistently decreasing component. One observes a rather steep slope for $R_{t,out}$ basically due to the boost influence and a weaker one for R_{long} (see Eq. 3.34). The scatter of the values obtained from different samples illustrates that the

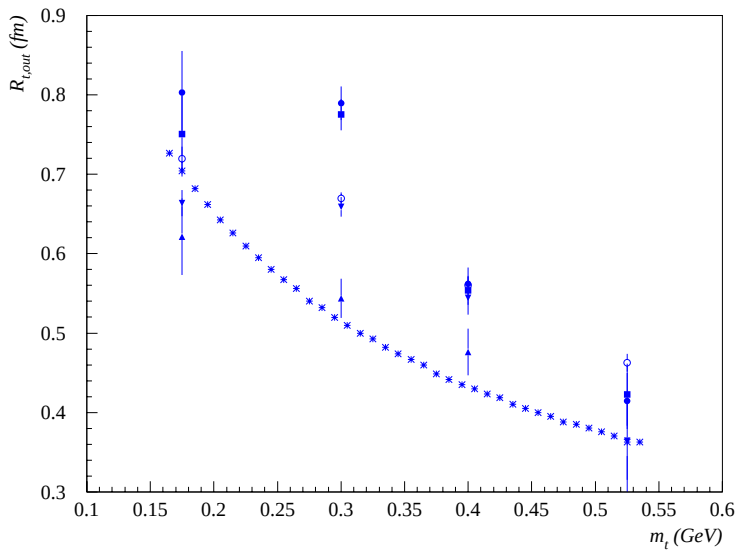

Figure 4.2: *m_t dependence of $R_{t,out}$. One represents with • the results for all charged particles, with ■ the ones for all pions, for direct pions using ▲, for pions coming from all the resonances decay with ▼ and for pions coming from the decays of direct ρ with ○. On the same graph is represented, as reference, $1/\gamma$ (*).*

m_t (GeV)	a)	b)	c)	d)	e)
0.19	0.532±0.031	0.554±0.032	0.538±0.033	0.618±0.012	0.661±0.011
0.30	0.535±0.016	0.517±0.015	0.490±0.021	0.508±0.010	0.538±0.007
0.38	0.460±0.023	0.473±0.017	0.457±0.021	0.443±0.021	0.460±0.008
0.52	0.398±0.023	0.443±0.040	0.430±0.043	0.404±0.038	0.424±0.011

Table 4.5: *Values of R_{long} for : a) all particles, b) all pions, c) direct pions, d) pions from all resonances and e) pions from direct ρ.*

BEC radius components depend on the origin of the particles implied in the analysis. Starting from this observation, it was decided to study how the one-dimensional BEC function integrated over m_t will look like, in case of different origin of the particles that are involved in BEC.

The correlation function (3.27), obtained using the JETSET generated

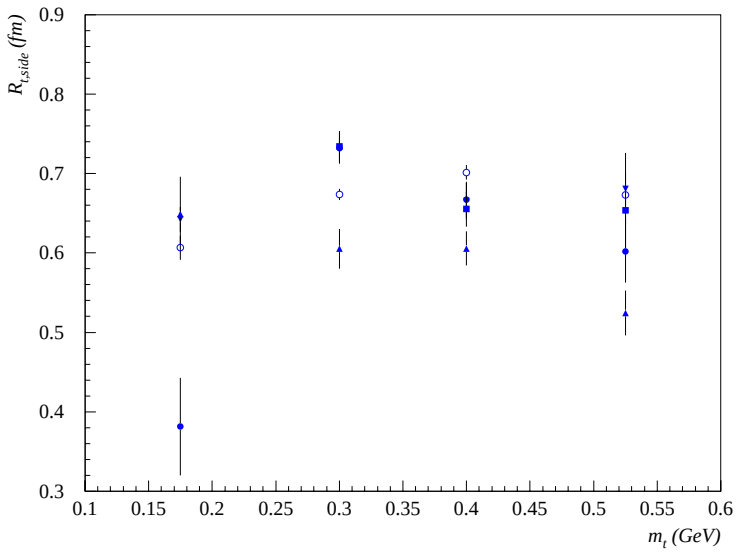

Figure 4.3: *m_t dependence of $R_{t,side}$. One represents with • the results for all charged particles, with ■ the ones for all pions, for direct pions using ▲, for pions coming from all the resonances decay with ▼ and for pions coming from the decays of direct ρ with ○.*

events, was fitted in the range of 0.05 GeV $< Q <$ 1.5 GeV, using Eq. (3.12) in order to find its parameters for different sample composition (See Appendix A). The study showed that the simulated correlation functions are not well described by a Gaussian (see Figure 4.5) and that the output values of parameters are quite different not only from the input values, but also from case to case (as it was pointed out earlier, for example, in the article of Fiałkowski and Wit [36]). Fitted values of the radii 3.23, which are 20% to 40% higher than the input are obtained. The shape of the resulting correlation function is not particularly close to a Gaussian for all the studied cases (see Figure 4.5), even if the input correlation function was Gaussian, hence the values of the fitted parameters are not very well determined and should be discussed with great care. This is a consequence of the LUBOEI algorithm, as will be explained below.

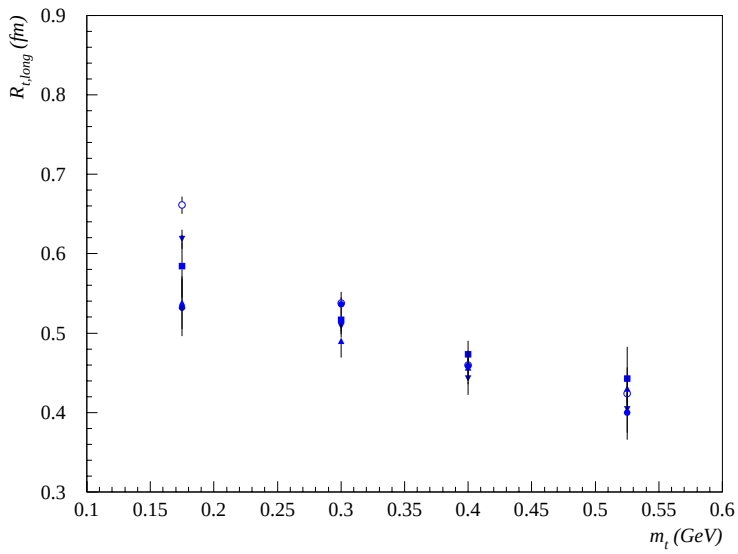

Figure 4.4: *m_t dependence of R_{long}. One represents with • the results for all charged particles, with ■ the ones for all pions, for direct pions using ▲, for pions coming from all the resonances decay with ▼ and for pions coming from the decays of direct ρ with ○.*

4.3 The dependence on input radius

One of the most puzzling inconsistencies in the JETSET simulation of BEC is that the input parameters of (3.23) cannot be obtained with the same parameters by fitting the resulting measured $C_2(Q)$ with formula (3.23). This is mostly due to the improper phase space approximation in Eq.(3.23). However, this approximation can still be valid for certain input boson source size R_{inp}. To find out whether it is true, the $C_2(Q)$ for different input values of R_{inp} in formula (3.23) was studied. Only JETSET samples of pions coming from the direct ρ decays were used since this sample is relatively pure, reproduces satisfactorily the input λ (see Appendix A) and the multiplicity is higher than for direct pions. We observed (see Appendix A) that when the input radius decreases, the shape of the output function is more and more different from the shape of the input function. Figure 4.6 represents the radii R_o obtained through the fit by the Eq. (3.23), as a function of the input radii R_{inp} for JETSET. One can observe that for the values of

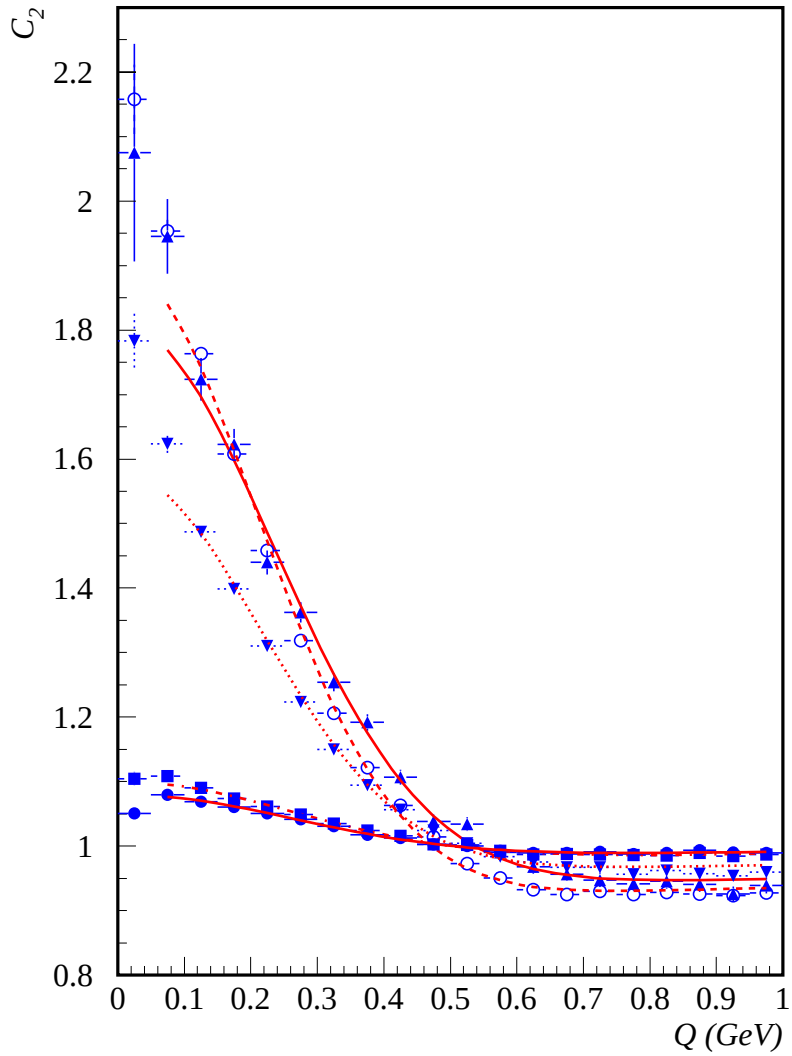

Figure 4.5: *The shape of the correlation function in different cases: all charged particles (•), pions (■), direct pions (blacktriangle), pions coming from all the resonances decay (▼), pions from direct ρ (○).*

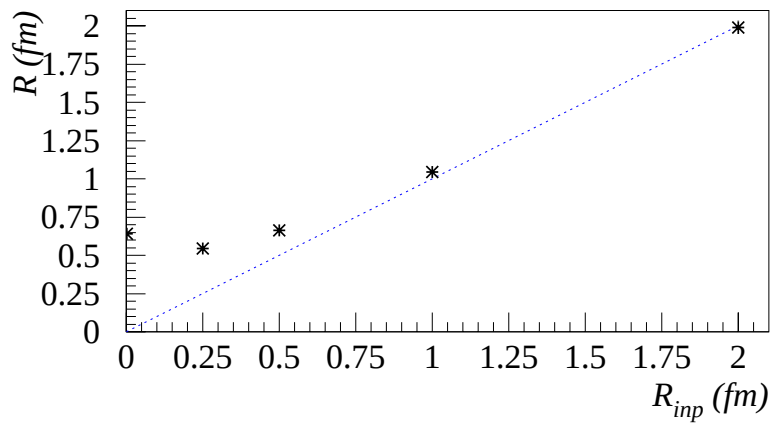

Figure 4.6: *Fitted values of output radii R_o for different input radii R_{inp}.*

input radii less than 0.5 fm, the output fitted radii were found to be almost constant around 0.6 fm. For input R_{inp} values bigger than 1 fm, the points are lying very close to the diagonal, showing a good agreement between input and output radii.

We observe the appearance of an artificial length scale of the resulting radius, $R_o \sim 0.6$ fm, which is independent of input radius R_{inp}, for the region $0 < R_{inp} \leq 0.6$ fm. This new scale is connected to the peak value of the inclusive Q distribution. In the studied algorithm, Q is shifted to a lower value Q' to give an enhancement when we take the ratio of the Q' distribution to the Q distribution. This works only for a monotonically increasing function, like the spherical phase space distribution. The true Q distribution, however, exhibits a peak around 0.5 GeV. For $R_{inp} \leq 0.6$ fm, the shift of Q to a lower Q' implies a depletion, not an enhancement in the region to the right of the peak ($Q > 0.5\ GeV$), see Fig 4.7, possibly giving a $C_2 < 1$ for this region. For the Q distribution, the peak position constitutes a limitation of the correlation width and gives rise to an artificial length scale.

One of the reasons of this inconsistency is the inaccurate approximation of Q spectrum by phase space. Distortions introduced by using a spherical

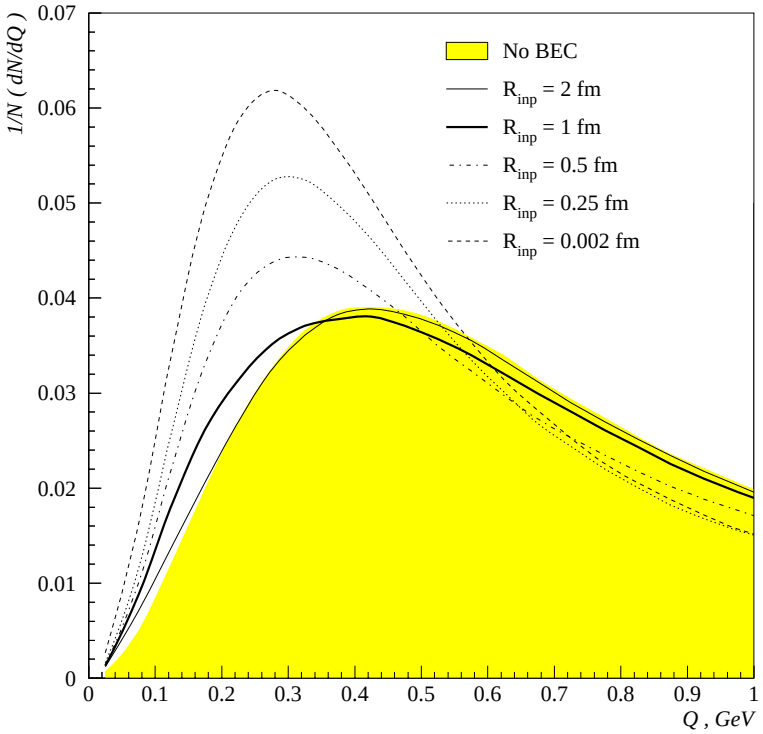

Figure 4.7: *Distribution of Q as a function of the input source radii R_{inp}. The shaded area shows this distribution in absence of BEC.*

Experiment	λ	R(fm)
OPAL	$0.866 \pm 0.032 \pm 0.140$	$0.928 \pm 0.019 \pm 0.150$
ALEPH	$0.510 \pm 0.040 \pm 0.110$	$0.650 \pm 0.040 \pm 0.160$
DELPHI	$0.400 \pm 0.030 \pm 0.050$	$0.620 \pm 0.040 \pm 0.200$
L3	$0.252 \pm 0.006 \pm 0.044$	$0.764 \pm 0.024 \pm 0.153$

Table 4.6: *The values obtained by fitting the Bose-Einstein distributions obtained by the four LEP1 experiment to eq. 3.23. The first errors are the statistic ones and the second are the systematic ones.*

shape of the source are negligible for sources large enough but are clearly present for small sources.

Since the method used in JETSET is the only method extensively used to compare the Monte Carlo results with data and since the values obtained for the BEC function parameters at LEP are mainly in this particular range (see Table 4.6 and [22]), further developments of it or of other approaches are necessary.

One might hope that modifying the spherical shape of the source to more complicated ones, introducing different source shapes and sizes for direct pions and pions from resonance decay products, one will improve the agreement with data as well as the agreement between the input and output values. So far the attempts to improve JETSET results by modifying the spherical shape of the source have been unsuccessful [36, 37].

Knowing that JETSET does not distinguish between components of the invariant momentum difference Q, we should expect similar behaviour of radius parameters of two-, Eq. (3.35), and three-dimensional correlation functions, Eq. (3.33). As one can see from Figure 4.8 and Figure 4.6, transverse radii follow the same pattern as the radius of the one-dimensional correlation function, being almost constant for values of Q less than 0.5 fm, and then increasing with R_{inp}, while the longitudinal radius tends to reproduce the input value of R_{inp} not being affected by the artificial length scale mechanism.

As it was showed above, the position of the peak in the non-correlated dN/dQ distribution constitutes the limitation of the measured correlation width R and can be interpreted as a new length scale. This conclusion is also valid for $dN/dQ_{\perp}$ and the transverse correlation radii, $R_{\perp}$ (see Figure 4.9). In the longitudinal direction, $dN/dQ_{||}$ peaks at a very small $Q_{||}$ value due to the LCMS properties, and thus the longitudinal component, $R_{||}$, is virtually insensitive to the mentioned length scale.

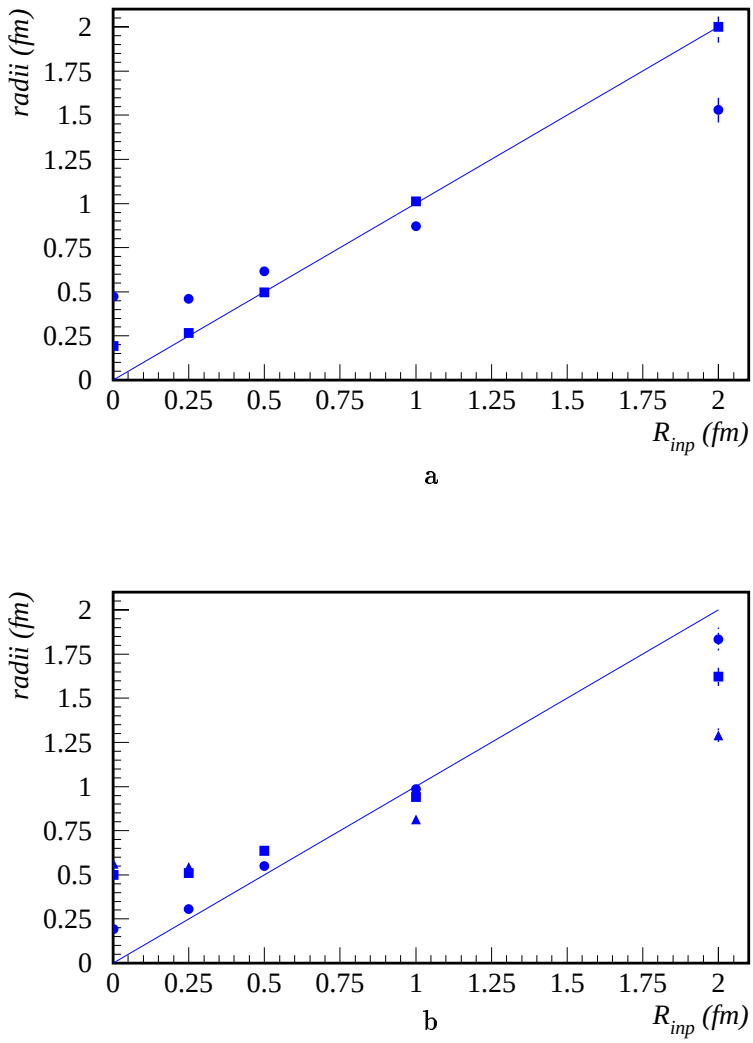

Figure 4.8: *Components of the correlation width as a function of the input source radii R_{inp} : a) $R_{||}$ (■), $R_{\perp}$ (•) and b) $R_{t,out}$ (▲), $R_{t,side}$ (■), R_{long} (•).*

R_{inp}, fm	$R_{\perp}, fm$	$R_{\parallel}, fm$	$R_{t,out}, fm$	$R_{t,side}, fm$	R_{long}, fm
0.002	0.472 ± 0.002	0.193 ± 0.001	0.562 ± 0.005	0.499 ± 0.004	0.193 ± 0.002
0.250	0.459 ± 0.003	0.266 ± 0.002	0.544 ± 0.004	0.511 ± 0.004	0.307 ± 0.003
0.500	0.616 ± 0.005	0.497 ± 0.005	0.637 ± 0.005	0.636 ± 0.005	0.549 ± 0.004
1.000	0.873 ± 0.015	1.013 ± 0.021	0.814 ± 0.011	0.940 ± 0.012	0.986 ± 0.013
2.000	1.530 ± 0.070	2.000 ± 0.090	1.291 ± 0.039	1.622 ± 0.051	1.835 ± 0.065

Table 4.7: *Components of the correlation width as a function of the input source radii R_{inp} : a) $R_{\parallel}$, $R_{\perp}$ and b) $R_{t,out}$, $R_{t,side}$, R_{long}.*

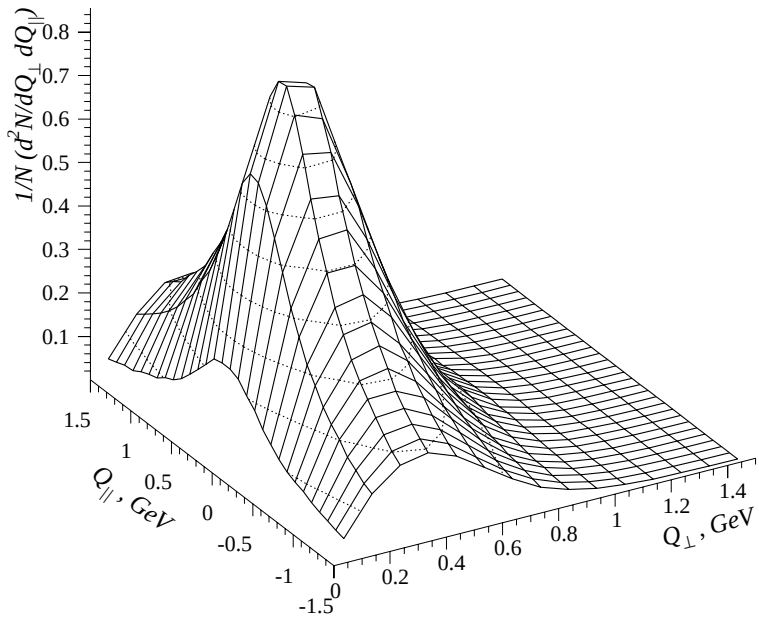

Figure 4.9: *Two-dimensional distribution $d^2N/dQ_{\perp}\,dQ_{\parallel}$ in absence of BEC.*

Since the m_t dependence was observed in the region where the secondary effects given by the length scale are strong, we study how this tendency is varying with the input JETSET radius. $R_{t,out}$ has a similar dependence on

m_t (GeV)	$R_{inp} = 0.25$ fm	$R_{inp} = 0.5$ fm	$R_{inp} = 1$ fm	$R_{inp} = 2$ fm
$0.1 \leq m_t < 0.25$	0.616±0.020	0.720±0.015	0.896±0.029	1.391±0.089
$0.25 \leq m_t < 0.35$	0.647±0.010	0.669±0.008	0.807±0.021	1.121±0.074
$0.35 \leq m_t < 0.45$	0.637±0.008	0.560±0.011	0.740±0.024	0.986±0.079
$0.45 \leq m_t < 0.60$	0.542±0.014	0.463±0.011	0.560±0.030	0.585±0.073

Table 4.8: *Values of $R_{t,out}$ for different input radii.*

m_t (Figure 4.10 a and Table 4.8) for all the input radii, with the dependence becoming weaker at small input values of radius. The dependence of $R_{t,out}$ on the input radius for different m_t ranges, is very weak, $R_{t,out}$ slowly increasing with the input radius in all the m_t ranges.(Figure 4.10b).

$R_{t,side}$, as function of m_t, is constant for all the input radii (Figure 4.11a and Table 4.9). The dependence on the input radii in different m_t ranges (Figure 4.11b) is following the same pattern as the one already seen for the radius of the one-dimensional distribution (Figure 4.6), being almost constant up to 0.5 fm and then increasing with the increase of the the input radii.

m_t (GeV)	$R_{inp} = 0.25$ fm	$R_{inp} = 0.5$ fm	$R_{inp} = 1$ fm	$R_{inp} = 2$ fm
$0.1 \leq m_t < 0.25$	0.602±0.019	0.607±0.015	0.906±0.029	1.492±0.101
$0.25 \leq m_t < 0.35$	0.667±0.010	0.674±0.007	0.952±0.024	1.338±0.135
$0.35 \leq m_t < 0.45$	0.674±0.017	0.701±0.009	0.966±0.033	1.662±0.172
$0.45 \leq m_t < 0.60$	0.607±0.049	0.673±0.013	0.969±0.063	1.575±0.165

Table 4.9: *Values of $R_{t,side}$ for different input radii.*

R_{long} is slowly decreasing with m_t for all the input radii. The dependence is stronger for larger input radii. R_{long} as a function of R_{inp} in different m_t is increasing with the input radii increasing.

m_t (GeV)	$R_{inp} = 0.25$ fm	$R_{inp} = 0.5$ fm	$R_{inp} = 1$ fm	$R_{inp} = 2$ fm
$0.1 \leq m_t < 0.25$	0.640±0.019	0.661±0.011	0.990±0.028	1.751±0.110
$0.25 \leq m_t < 0.35$	0.540±0.010	0.538±0.007	0.916±0.026	1.650±0.125
$0.35 \leq m_t < 0.45$	0.735±0.010	0.460±0.008	0.878±0.035	1.477±0.078
$0.45 \leq m_t < 0.6$	0.607±0.013	0.424±0.011	0.734±0.044	1.066±0.171

Table 4.10: *Values of R_{long} for different input radii.*

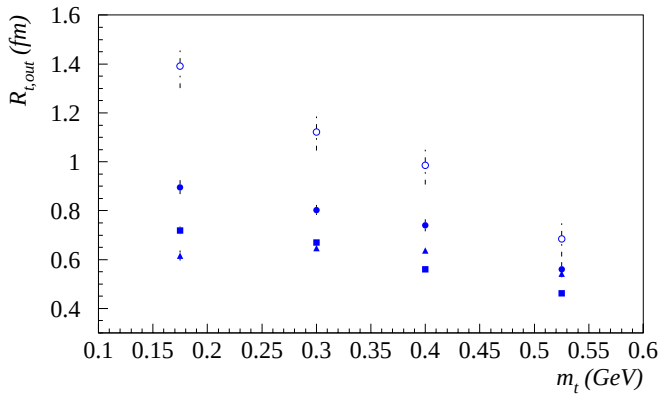

a)

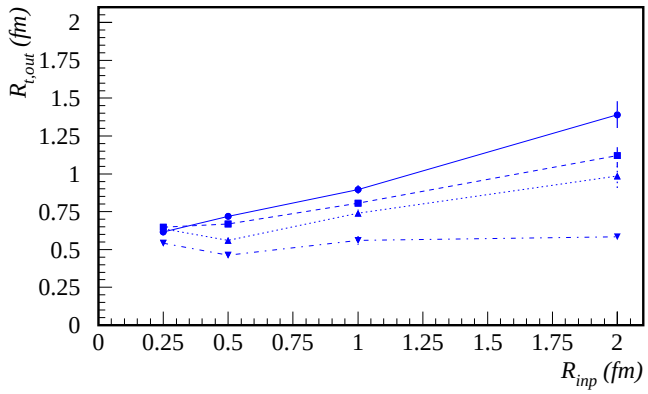

b)

Figure 4.10: *$R_{t,out}$ dependence a) on m_t for different input radii: R_{inp} =2 fm (circ), $R_{inp} = 1fm$ (•), $R_{inp} = 0.5fm$ (■), $R_{inp} = 0.25fm$ (▲); b) on the input radius and different ranges for m_t: $0.1\ GeV < m_t < 0.25\ GeV$ (•), $0.25\ GeV < m_t < 0.35\ GeV$ (■), $0.35\ GeV < m_t < 0.45\ GeV$ (▲), $0.45\ GeV < m_t < 0.6\ GeV$ (▼).*

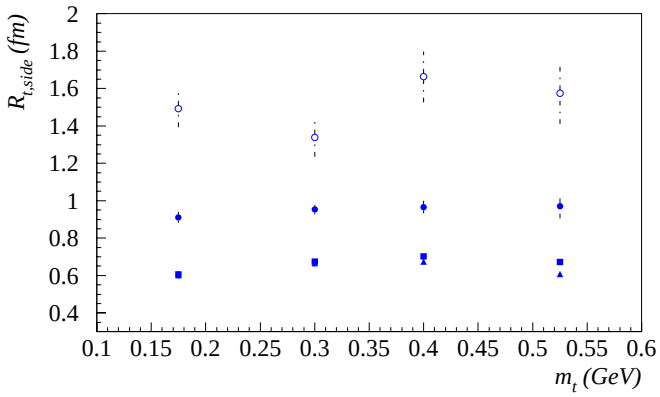

a)

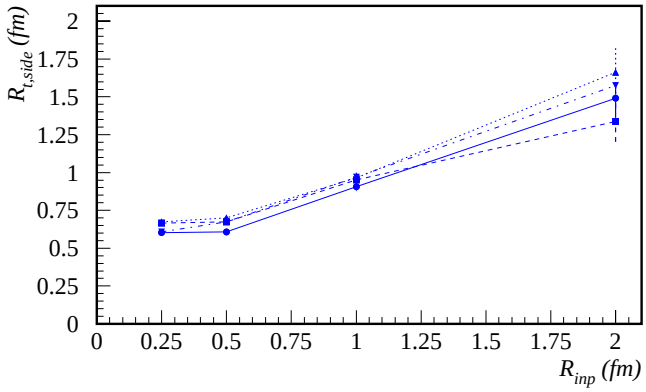

b)

Figure 4.11: *$R_{t,side}$ dependence a) on m_t for different input radii: R_{inp} =2 fm (•), R_{inp} = 1fm (○), R_{inp} = 0.5fm (■), R_{inp} = 0.25fm (▲); b) on the input radius and different ranges for m_t: 0.1 GeV < m_t < 0.25 GeV (•), 0.25 GeV < m_t < 0.35 GeV (■), 0.35 GeV < m_t < 0.45 GeV (▲), 0.45 GeV < m_t < 0.6 GeV (▼).*

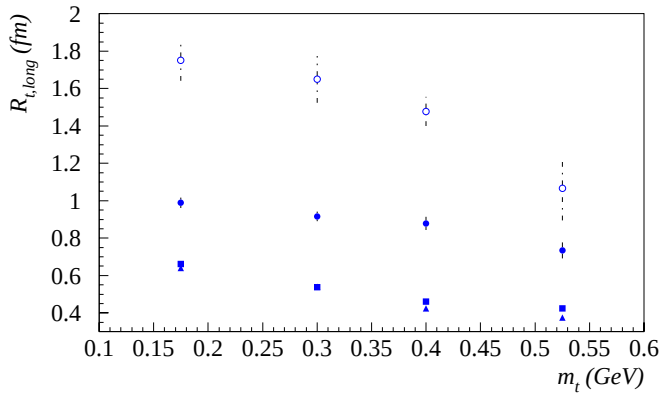

a)

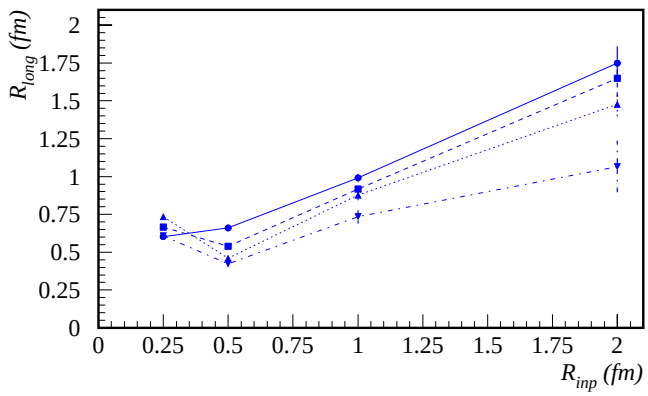

b)

Figure 4.12: *R_{long} dependence a) on m_t for different input radii: R_{inp} =2 fm (○), $R_{inp} = 1fm$ (•), $R_{inp} = 0.5fm$ (■), $R_{inp} = 0.25fm$ (▲); b) on the input radius and different ranges for m_t: $0.1\ GeV < m_t < 0.25\ GeV$ (•), $0.25\ GeV < m_t < 0.35\ GeV$ (■), $0.35\ GeV < m_t < 0.45\ GeV$ (▲), $0.45\ GeV < m_t < 0.6\ GeV$ (▼).*

The decrease of R_{long}, best seen for large input values of radius, cannot be given by the artificial length scale effect but by some intrinsic properties of the string model in the way it is implemented in the JETSET generator.

4.4 Discussion

Using the specific correlation function parameterization in the Longitudinal Center-of-Mass System it was shown that two-jet JETSET generated events exhibit a similar behaviour to that indicated previously by experimental DELPHI data (see Section 3.7). This similarity suggested that the observed phenomenon can be explained in the framework of the string model, and that JETSET generator provided sufficient information for corresponding studies.

A detailed analysis of the Bose-Einstein correlation, implemented in the JETSET particle generator, has been performed. Our main result is that an artificial new length scale is introduced due to the way the generator is working. This scale is given by the peak position of the Q distribution. Appearance of this artificial scale causes the previously unexplained phenomenon, namely, the fact that JETSET, while reproducing well experimental data, is self-inconsistent and fails to reproduce its own built-in Bose-Einstein correlation function for input radii of around 0.5 fm. The radius is reproduced for big sources, while for the small ones, the output value is almost constant irrespective to the input radius. It should be stressed that the Bose-Einstein parameters in JETSET for radius less than 1 fm should not be taken as physically meaningful parameters.

As a result, we should state that the built-in JETSET model for simulating BEC is fully applicable only for sufficiently big sizes of boson source. At the same time, experimental data indicate that this size is around 0.5 fm (see Table 4.6). This means that this kind of model has no predictive power in this range. One should be very careful when using JETSET with this model for calculation of detector corrections, because it can not produce an adequate unfolding matrix.

The study of the m_t dependence of the BEC function for samples of particles of different origin showed that the λ dependence on m_t is given by the mixture of particles with different origin. The dependence of the three components of the radius on m_t cannot be explained as an effect given by the mixture of particle, resonance production or artificial length scale. Yet this effect is reproduced by JETSET without any explicit input of the transverse mass dependence (save the dependence of $R_{t,out}$ that is partially

given by boost). The results presented in this chapter are pointing to a mechanism in the main JETSET block, in the string fragmentation implementation, LUBOEI not introducing the m_t dependence, only preserving some fragmentation features. We are currently working on this problem looking, together with theorists, for new observables.

It has to be mentioned that nowadays some other models for simulation of BEC are being developed [26, 12]. They use direct implementation of the Bose-Einstein interference into the string model, being theoretically accurate in this sense. At the moment they spend too much computing resources to be used by high-energy physics experiments, but they do have predictive power. One of the most interesting predictions is that the transverse component of the boson source size, $R_\perp$, must be significantly smaller then the longitudinal one, $R_{||}$, a subject that will be presented in the next chapter. This must encourage further work towards developing and implementing advanced models for the BEC simulation in particle generators.

Chapter 5

BEC at DELPHI

During LEP first running period (LEP1), 1989 - 1995, Z^0 bosons were produced in abundance. LEP turned out to be a very good environment for QCD studies of the fragmentation and hadronization of quarks and gluons.

Using the 1992 - 1995 data, the study of BEC function for identical particles can be performed with a high precision due to the big amount of the data accumulated[1]. This study is important since the process of hadron production, or fragmentation, in high energy physics is poorly comprehended and the space-time characteristics of a hadron source give important information about the hadronization process as a whole and make possible tests of fragmentation models.

Detailed studies of the two-particle BEC in Z^0 hadronic decays in e^+e^- annihilation allow the determination of the dimension and shape of the source of bosons, making possible the comparison between the transverse and longitudinal radii of the BEC (with respect to the initial parton direction of motion). This allows to test the string model prediction [26] that the transverse correlation length is considerably smaller than the longitudinal one.

5.1 Data selection

Data collected by the DELPHI detector [13, 14] in 1992-1995 at centre-of-mass energies around $\sqrt{s} = 91.2$ GeV were used. Only charged particles in hadronic events were considered in the analysis [14].

The following selection criteria were applied to select the charged tracks: the tracks were taken into account if their impact parameter was below

[1] Above five millions hadronic events

1 cm in the transverse plane and below 5 cm along the beam axis; the measured track length was above 50 cm; the momentum p was in the range of 0.1 GeV/c < p <50 GeV/c and the polar angle between 25° and 155°. All the charged particles were assumed to be pions. This assumption is not affecting in a significant way the result of the analysis [22].

Hadronic events were selected by requiring that: (a) they contained at least 5 charged particles with momentum above 0.2 GeV/c; (b) the total energy of all charged particles exceeded 15 GeV; (c) each hemisphere with respect to the sphericity axis[2] contained a total energy of charged particles larger than 3 GeV; (d) the polar angle of the sphericity axis was between 40° and 140°, so that the events are well contained inside the TPC.

In this analysis two-jet events were selected in order to compare the result with the theoretical prediction [26]. These events are also convenient because the procedures of preparing the reference sample and the definition of LCMS (presented in Section 3.6) are easier to apply and to understand in this case. Since the thrust axis of the two-jet events is well aligned with the direction of motion of the initial partons, its direction can be selected as the physical axis of the hadronization process, and the possible influence of hard gluon radiation can be neglected. The two-jet event selection was done using the LUCLUS [21] clustering algorithm (with parameter d_{join} = 8 GeV/c), requiring the thrust value to be more than 0.95, and, the jet acollinearity should not exceed 5°. A total of about 810 000 events satisfied these criteria.

To purify the reference sample and to reduce the background, additional selection criteria were applied for each pair of particles. To stay away from the two-particle phase-space limits, where kinematic correlations are significant, a pair of tracks was selected for the analysis, if both particles had momenta below 5 GeV/c. To exclude partially overlapping tracks which can be poorly reconstructed, the angle between tracks (θ) was required to exceed 2°. To reduce the correlations caused by the local transverse momentum compensation, pairs were rejected if the angle between tracks in a

[2]The sphericity tensor is defined as:

$$S^{\alpha\beta} = \frac{\sum_i p_i^\alpha p_i^\beta}{\sum_i |p_i|^2},$$

where $\alpha, \beta = 1, 2, 3$ corresponds to x, y, z components. By standard diagonalisation of $S^{\alpha\beta}$ one may find three eigenvalues $\lambda_1 \geq \lambda_2 \geq \lambda_3$ with $\lambda_1 + \lambda_2 + \lambda_3 = 1$. The sphericity of the event is then defined as:

$$S = \frac{3}{2}(\lambda_2 + \lambda_3).$$

Sphericity is a measure of the summed p_t with respect to the event axis. A two-jet event corresponds to $S \sim 0$ and an isotropic one to $S \sim 1$.

plane, transverse to the thrust axis, (θ_{trans}), was more than 120°. In addition, to reduce the contribution from resonance decays and to eliminate the region where the Coulomb correction is substantial, pairs were rejected if Q was less than 0.06 GeV (as you shall see further, removal of this cut is not affecting noticeable our results).

5.2 Correction procedure

Data used in the BEC analysis were corrected for detector effects. Since the detector was modified during the years (see chapter 2), the distribution were corrected year by year. The weighted mean of the obtained corrected distributions was used in the analysis. Events generated with the JETSET 7.3 PS model with DELPHI tuning [41] were used to estimate the acceptance corrections and to account for effects arising from the limited detector resolution. The selected events were passed through the DELSIM [43] detector simulation and the same selection criteria were used as for real data. Correction coefficients $c(Q)$ were calculated as the ratios of distributions at the generation level (JETSET only) to those at the reconstruction level (JETSET+DELSIM):

$$c(Q) = \frac{(\frac{dN^{\pm\pm}}{dQ})_{gen}}{(\frac{dN^{\pm\pm}}{dQ})_{rec}} , \tag{5.1}$$

where indices *"gen"* and *"rec"* refer to the generation and reconstruction level respectively. Looking to Figure 5.1b one can see that the correction coefficient is almost constant, being close to unity.

The mixed reference sample is prepared using the same set of hadronic events as for the real data and a mixing procedure analogous with the one presented previously. Within the applied selection criteria, the mixed sample does not contain BEC and satisfies most of the basic requirements for the reference sample (see Section 3.4).

To correct for the effects introduced by the mixing procedure, the measured two-particle correlation function $C_2(Q)$ is calculated as a double-ratio (see Section 3.4):

$$C_2(Q) = \frac{r_{data}(Q)}{r_{noBE}(Q)} , \tag{5.2}$$

where

$$r_{data}(Q) = \frac{(\frac{dN^{\pm\pm}}{dQ})_{data}}{(\frac{dN^{\pm\pm}}{dQ})_{data,mix}} \quad and \quad r_{noBE}(Q) = \frac{(\frac{dN^{\pm\pm}}{dQ})_{noBE}}{(\frac{dN^{\pm\pm}}{dQ})_{noBE,mix}} . \tag{5.3}$$

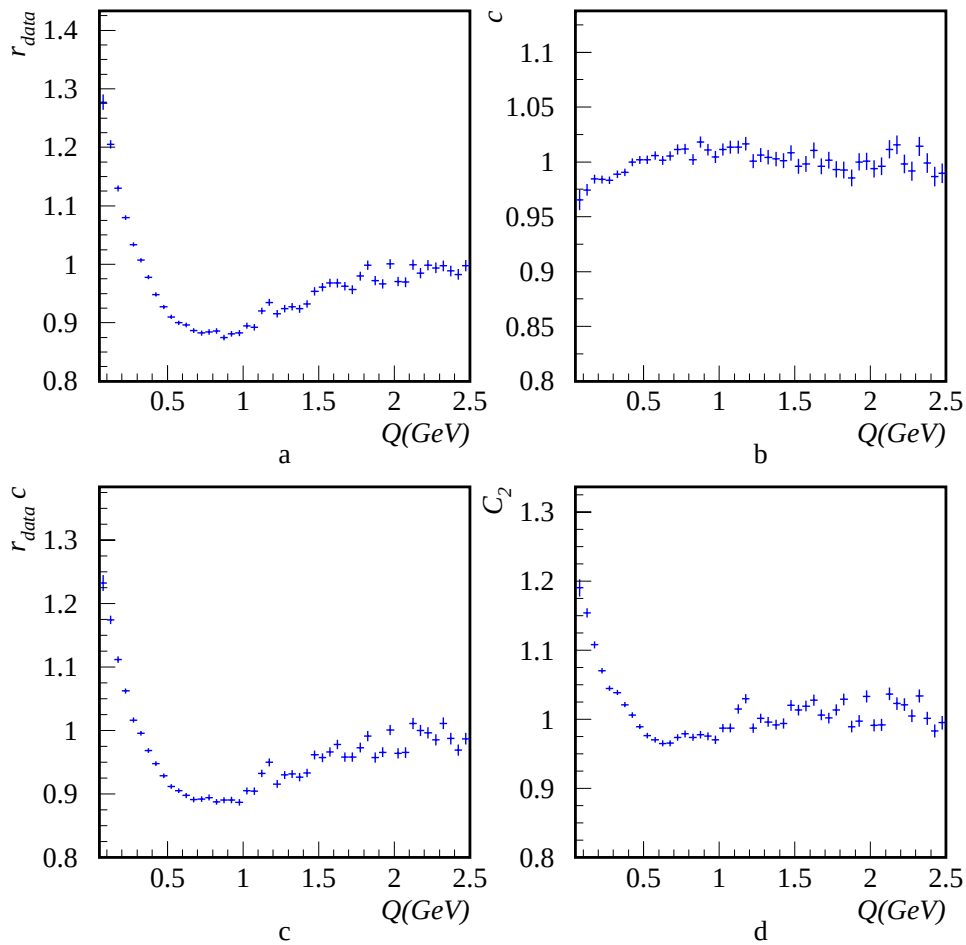

Figure 5.1: *a) correlation function not corrected for detector effects and effects introduced by the mixing procedure, r_{data}; b) correction coefficient, c; c) correlation function corrected for detector effects, $r_{data} \cdot c$; d) correlation function corrected for the detector effects and effects introduced by the mixing procedure, C_2. The distributions are constructed using the 1995 data. For simplicity, in this figure, we present the results only for the one-dimensional distribution*

Here $(dN^{\pm\pm}/dQ)_{data}$ is the Q-distribution of the pion pairs with the same charge in real data, while the subscript *"data,mix"* denotes the same quantity but for pairs from the reference sample. The indices *"noBE"* and *"noBE,mix"* refer to analogous quantities in absence of BEC obtained from

the JETSET sample without BEC. The procedure, step by step, is presented in Figure 5.1.

The reference sample $(dN^{\pm\pm}/dQ)_{data,mix}$ is corrected for the detector effects using a correction coefficient similar to (5.1):

$$c_{mix}(Q) = \frac{(\frac{dN^{\pm\pm}}{dQ})_{gen,mix}}{(\frac{dN^{\pm\pm}}{dQ})_{rec,mix}} , \tag{5.4}$$

where *"mix"* denotes the mixed samples. The final, corrected, correlation function is then evaluated from Eq.(5.2) as:

$$C_2(Q) = \frac{r_{data}(Q)}{r_{noBE}(Q)} \frac{c(Q)}{c_{mix}(Q)} . \tag{5.5}$$

5.3 Two-dimensional BEC – systematic errors

The measurement of the correlation function in the two-dimensional LCMS, requires accumulation of double-differential distributions $d^2N^{\pm\pm}/dQ_\perp dQ_{||}$, where $N^{\pm\pm}$ is the number of like-sign pairs and $Q_\perp$, $Q_{||}$ are defined as in Section 3.6. The distributions are corrected for detector effects and for the effects introduced by the mixing procedure

The correlation function (5.5) as measured from the DELPHI data is shown in Figure 5.2. The quantitative evaluation of the two-dimensional correlation function parameters was made by fitting the parameterization (3.35) to the measured correlation function $C_2(Q_\perp, Q_{||})$. The fit has been performed in the enhancement region of 0 GeV $< Q_\perp <$ 0.6 GeV and $|Q_{||}|$ <0.8 GeV.

The following values were obtained for the correlation function parameters:

$$\begin{aligned} \lambda &= 0.261 \pm 0.007, \\ R_\perp &= 0.530 \pm 0.020 \text{ fm}, \\ R_{||} &= 0.850 \pm 0.020 \text{ fm}. \end{aligned} \tag{5.6}$$

The correlation strength is slightly correlated (about 30%) with the radii. The ratio of the transverse and longitudinal radii is $R_\perp/R_{||} = 0.62 \pm 0.02$.

To study the systematic uncertainty of the analysis we varied the selected fit region, the maximal value of $|Q_{||}|$ in the range 0.6 GeV to 1.1 GeV, and the one of $Q_\perp$ from 0.6 GeV to 1 GeV, see for results Table 5.1.

Another source of systematic errors are the selection criteria: the two-jet selection and the selection of pairs of tracks used for the BEC analysis. To

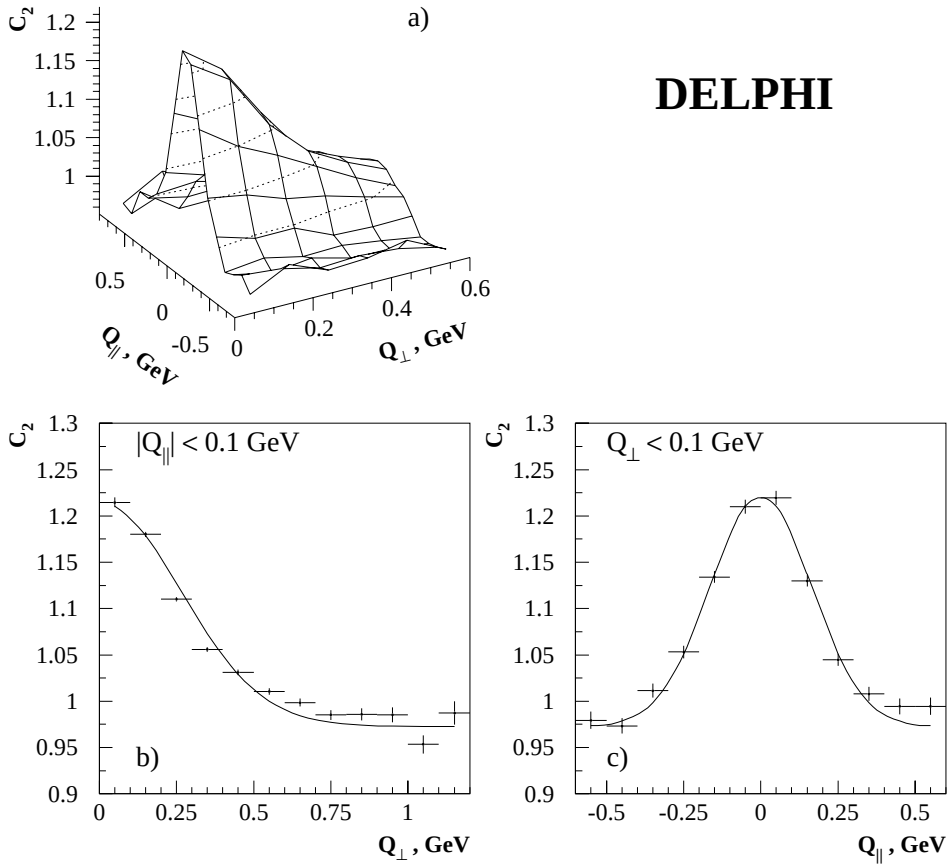

Figure 5.2: *Two-dimensional correlation function, $C_2(Q_{||}, Q_{\perp})$ (a), as measured by DELPHI in hadronic decays of Z^0. Its transverse (b) and longitudinal (c) slices at the correlation function peak are shown together with the fit to the Eq.(3.35).*

estimate the variation of the BEC parameters when modifying the selection criteria, first we performed a fast estimation, using only the sample of 1995 data, after, for the selection criteria that proved interesting for our analysis,

	error for $R_\perp$ (fm)	error for $R_\parallel$ (fm)	error for $R_\perp/R_\parallel$
$\lvert Q_\parallel^{max}\rvert \in$ [0.5,1.0] GeV $Q_\perp^{max} \in$ [0.5,1.0] GeV	± 0.03	± 0.03	± 0.04

Table 5.1: *Contribution of the selected fit region to the systematic uncertainty. The maximal value of $|Q_\parallel|$ was varied in the range 0.6 GeV to 1.1 GeV, and the one of $Q_\perp$ from 0.6 GeV to 1 GeV.*

we calculate the systematic uncertainty using the full sample 1992-1995. The study of the two-jet selection criteria proved to be very interesting from the theoretical point of view, since modifying the two-jet structure of the sample, the shape of the source would be also changed. The results of this study are presented in Table 5.2.

cut	$R_\perp(fm)$	$R_\parallel(fm)$	$R_\perp/R_\parallel$
d_{join}=6 GeV/c	0.58±0.05	0.80±0.07	0.72±0.07
d_{join}=10 GeV/c	0.44±0.03	0.78±0.04	0.57±0.04
no LUCLUS, T >0.95	0.42±0.02	0.76±0.04	0.55±0.03
Nr jets > 2	0.76±0.04	1.04±0.05	0.72±0.04
No T cut	0.63±0.04	0.87±0.06	0.71±0.06
T >0.89	0.64±0.05	0.76±0.07	0.84±0.08
T >0.91	0.65±0.05	0.79±0.07	0.83±0.08
T >0.93	0.58±0.04	0.88±0.06	0.67±0.06
T >0.97	0.39±0.04	0.69±0.05	0.56±0.06
$acol < 7^\circ$	0.52±0.03	0.82±0.05	0.63±0.05
$acol < 3^\circ$	0.46±0.04	0.72±0.06	0.64±0.07
no 2-jet selection	0.48±0.01	0.77±0.02	0.62±0.02
reference values	0.53±0.02	0.85±0.02	0.62±0.02

Table 5.2: *Study of the systematic variation of results estimated in case of the variation of the two-jet selection criteria; T stays for thrust, acol for acollinearity. Only the 1995 data were used here.*

The way in which the choice of d_{join} is influencing the shape of the source is not straightforward to understand since the criteria used to select two-jet events are strongly correlated. To justify this affirmation, in Figure 5.3 are represented, in the upper row of histograms, the distributions of the number

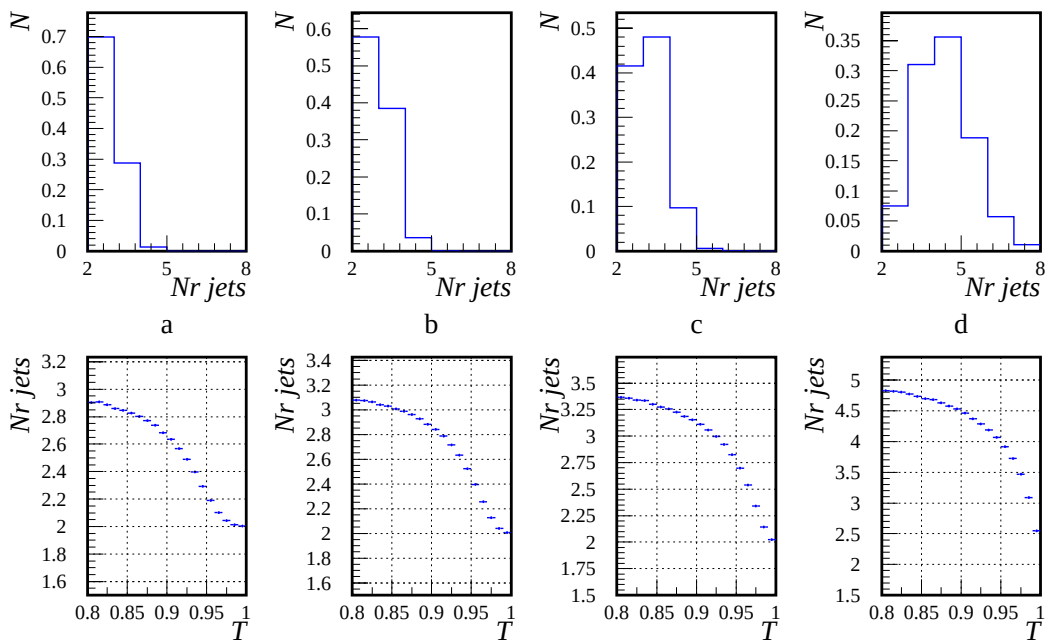

Figure 5.3: *The way in which the two-jet selection criteria interplay. The upper histograms represents the distribution of the number of jets for a) djoin = 10, b) djoin = 8, c) djoin = 6, d)djoin = 2.7 and the lower one the average of number of jets per event as a function of thrust. The distribution are constructed using* JETSET+*DELSIM simulated data*

of jets for different d_{join} values and in the lower one the average number of jets as a function of thrust. It is easy to observe that if the value of d_{join} is large, almost all the events are considered two-jet events and the cut, requiring the number of jets reported by LUCLUS procedure to be equal with two, will not give a pure sample of two-jet events. The main role in providing a good two-jet sample is played in this case by the minimal thrust cut. At large values of d_{join}, we arrive to some kind of saturation, the value of the ratio of radii being almost constant for a given value of the minimal thrust cut, if d_{join} is varying. In the same way for small values of d_{join}, the cut on the number of jets is mainly doing the selection of the two-jet events, the thrust cut playing almost no role. In this region the choice of d_{join} is strongly affecting our results and the variation of thrust cut is almost not modifying them. The decrease of d_{joint} to 2.7[3] gave a severe restriction of the statistics. The variation of the acollinearity cut is affecting very little our results.

However since in this analysis we are interested only in the two-jet events, to estimate the systematic uncertainty, $d_{joint} = 8$ was fixed and the minimal thrust value was varied in the range from 0.93 and 0.97. The whole data samples was used, 1992-1995 statistics. The results are presented in Fig 5.4. As one can see, the source is getting less elongated if the purity of the two-jet events is decreasing. The three-jet events in the sample are affecting the longitudinal appearance of the source.

cut	$R_\perp$	$R_{\|\|}$	$R_\perp/R_{\|\|}$
no Q cut	0.48±0.04	0.79±0.06	0.61±0.05
$\theta_{trans} > 130°$	0.48±0.04	0.77±0.05	0.62±0.05
$\theta_{trans} > 110°$	0.47±0.04	0.76±0.06	0.62±0.05
no θ_{trans} cut	0.49±0.03	0.71±0.05	0.68±0.05
$\Delta\theta > 1°$	0.47±0.04	0.75±0.06	0.63±0.06
$\Delta\theta > 3°$	0.47±0.03	0.74±0.05	0.64±0.05
reference values	0.53±0.02	0.85±0.02	0.62±0.02

Table 5.3: *BEC analysis with different pair selection criteria. Only the 1995 data were used here to estimate systematic uncertainty.*

In Table 5.3 the radius components values obtained when varying the pair selection criteria are listed. The contribution to the systematic uncer-

[3] 2.7 GeV/c, is a standard DELPHI cut to select two- or three-jet events for QCD studies (e.g for α_s calculation).

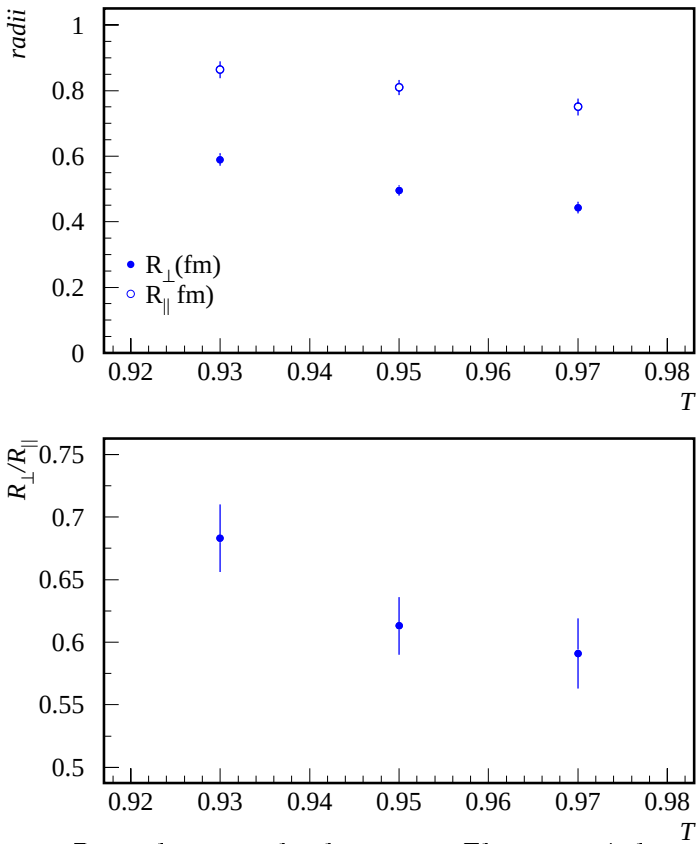

Figure 5.4: *Dependence on the thrust-cut. The source is less elongated if the purity of the two-jet sample is decreasing. Whole data sample, 1992-1995, is used.*

tainty is low for cut values around the basic ones. We also studied the way in which the removal of the 120° cut for the transverse angle between tracks is influencing the result, see Figure 5.5 and Table 5.3. When removing this cut the transverse radius increases with 0.01 fm and the longitudinal one decreases with 0.07 fm, see Table 5.3, confirming the appearance of an additional correlation, not of BEC type. Since the removal of 120° cut introduces additional correlations that affects the structure of the analysed event, it was not used in estimating the final value of the systematic uncertainty.

The total systematic error was evaluated by adding all the contributions in quadrature. The following values for the correlation radius components

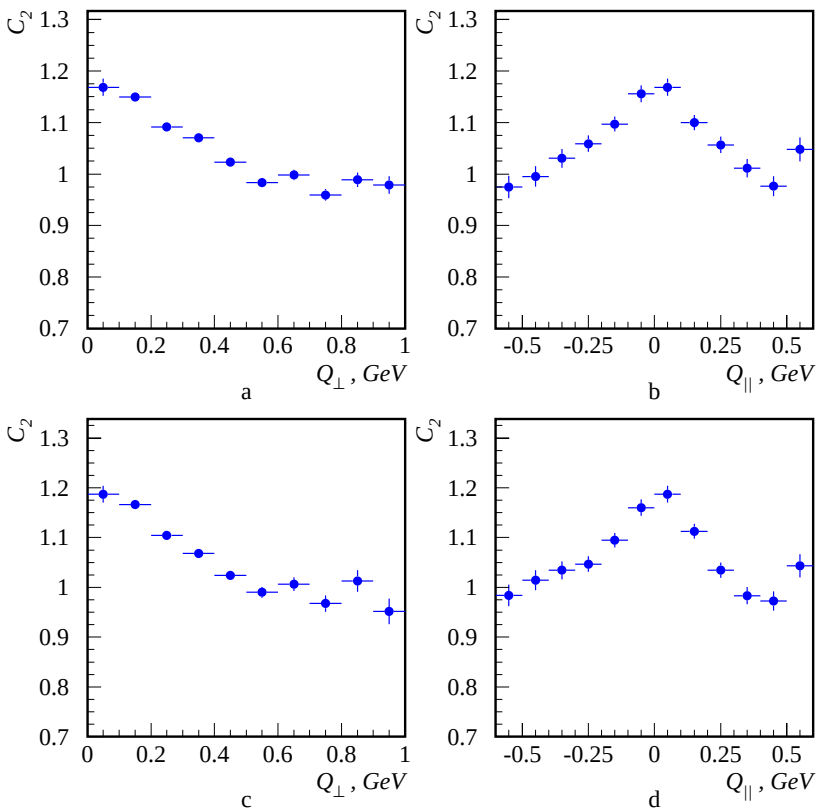

Figure 5.5: *Transverse and longitudinal slices at the correlation function peak: a) and b) in the absence of the transverse angle cut; c) and d) with the transverse angle cut. It is easy to observe the background, at the distribution tails. Also the peak is narrower for c) and d) projections.*

were obtained:

$$\begin{aligned} \lambda &= 0.261 \pm 0.007 \pm 0.010 \ , \\ R_\perp &= 0.530 \pm 0.020 \pm 0.070 \text{ fm} \ , \\ R_{||} &= 0.850 \pm 0.020 \pm 0.070 \text{ fm} \ , \\ \frac{R_\perp}{R_{||}} &= 0.620 \pm 0.020 \pm 0.050 \ , \end{aligned} \tag{5.7}$$

where the first error is statistical, and the second is the systematic uncertainty. The values obtained are in qualitative agreement with the theoretical prediction of [26], according to which the longitudinal correlation length in $Z^0 \to q\bar{q}$ hadronic decay has to be larger than the transverse one, if the string fragmentation model is used.

In the JETSET generator, see Section 3.3, BEC is simulated by changing the final state particle momenta so that the Gaussian distribution of Eq.(3.23) is reproduced. The procedure is performed in terms of Q, not resolving it into components, hence $R_\perp$ and $R_{||}$ are expected to be similar when taking into account only the description of the LUBOEI procedure. In the previous chapter it was shown that, since the artificial scale effect is affecting in a different way the components of radius, this is not true in our region of interest. The two-dimensional fit to the correlation function evaluated from the JETSET generated decays of Z^0 gives a ratio of $R_\perp/R_{||}$ between 0.9 and 1.2, for input values close to DELPHI tuning [4]. This is very different from the ratio of (5.7) and reflects the fact that the BEC implementation in JETSET is not appropriate for the multidimensional description of the correlation.

5.4 Three-dimensional analysis

Three-dimensional DELPHI analysis of 1992-1995 data (preliminary) was performed by fitting the correlation function, obtained in the same way as in the two-dimensional case, to the parameterization:

$$C_2(Q_{t,out}, Q_{t,side}, Q_{long}) = N(1 + \lambda e^{-Q^2_{t,out}R^2_{t,out} - Q^2_{t,side}R^2_{t,side} - Q^2_{long}R^2_{long}}) \tag{5.8}$$

The advantage of LCMS is that it allows the measurement of the two transverse radius components, $R_{t,out}$ and $R_{t,side}$, the former receiving contribution from the difference in the emission time of bosons, and the latter being the "true" transverse correlation length (see Section 3.6). The three-dimensional analysis of the BEC using the fit of the formula (5.8) to the corresponding correlation function, evaluated analogously to the two-dimensional case, gives the following results:

$$\begin{aligned} \lambda &= 0.25 \pm 0.01 \pm 0.01 \ , \\ R_{t,out} &= 0.57 \pm 0.01 \pm 0.08 \text{ fm} \ , \\ R_{t,side} &= 0.46 \pm 0.01 \pm 0.05 \text{ fm} \ , \end{aligned}$$

[4] For all the main JETSET parameters.

$$\begin{aligned} R_{long} &= 0.80 \pm 0.01 \pm 0.06 \text{ fm} , \\ R_{t,out}/R_{long} &= 0.71 \pm 0.01 \pm 0.07 , \\ R_{t,side}/R_{long} &= 0.57 \pm 0.01 \pm 0.04 . \end{aligned} \tag{5.9}$$

This fit has been performed in the region of $|Q_{t,out}|$ <0.6 GeV, $|Q_{t,side}|$ <0.6 GeV and $|Q_{long}|$ <0.8 GeV. Ratios $R_{t,out}/R_{long}$ and $R_{t,side}/R_{long}$ were obtained by fitting the distribution, using them as parameters. The value of $R_{t,side}/R_{long}$ is smaller than that of $R_{\perp}/R_{||}$ in Eq.(5.7), and its uncertainty is somewhat lower, indicating that $R_{t,side}$ is a better estimator of the transverse correlation length. Since the temporal "size" of the source contributes only to $R_{t,out}$, $R_{t,side}$ radius is smaller. The source is even more elongated if we take into account just the "true" transverse size, $R_{t,side}$.

5.5 LEP1 results comparison

An elongation of the pion source was also observed by the L3 [27] and OPAL [29] collaborations at LEP1.

The L3 collaboration used all the hadronic events in their analysis, without applying additional selection criteria neither for two-jet events, nor for pairs of tracks. As you have seen in section 5.3, if the selection of the two-jet events is less tight, one also gets contribution from the correlations between particles produced in gluon jets. The presence of this contribution is expected to lead to a more spherical source shape and to a bigger value of the ratio of the transverse to longitudinal radius components, closer to unity. This contribution together with the fact that the additional transverse correlations are not eliminated in the L3 analysis can account for the difference between DELPHI result and L3 one. The reported L3 result, obtained from the three dimensional fit is:

$$\frac{R_{t,side}}{R_{long}} = 0.81 \pm 0.02^{+0.03}_{-0.19} . \tag{5.10}$$

The two-dimensional result, reported by L3, confirmed the elongation observed in the three-dimensional fits. The difference between the R_{long} values reported by DELPHI and L3 can be a consequence of the θ_{trans} <120° cut in DELPHI data.

The OPAL Collaboration used the unlike-charge reference sample in their analysis of two-jet events. The selection of the two-jet events is done using a different clustering algorithm and a different sample of particles is used to determine the thrust axis direction. The correction procedure of the data

	Reference sample	$R_{t,out}$(fm)	$R_{t,side}$(fm)	R_{long}(fm)
DELPHI	mixing	0.57±0.01	0.46±0.01	0.80±0.01
	unlike-charge	0.55±0.02	0.70±0.02	0.87±0.02
L3	mixing	0.53±0.02	0.59±0.01	0.74±0.02
OPAL	unlike	0.53±0.06	0.78±0.06	1.02±0.09

Table 5.4: *The results obtained by the three LEP experiments. Only the statistical errors are listed.*

sample is also different and the additional transverse correlations are not eliminated. All these reasons make the comparison of the results difficult. The reported result is:

$$\frac{R_{long}}{R_{t,side}} = 1.222 \pm 0.027^{+0.075}_{-0.012} \quad . \tag{5.11}$$

That corresponds to $\frac{R_{t,side}}{R_{long}} = 0.820 \pm 0.040^{+0.018}_{-0.111}$. Even if the result obtained for the ratio is close to the L3 results (astonishing if taking into account the fact that OPAL used for analysis only two-jet events) the value obtained for $R_{t,side}$ and R_{long} are different for OPAL and L3, see Table 5.4.

The values obtained by DELPHI using unlike-charge reference sample, as OPAL does, are close to their results pointing to the conclusion that the difference in the radius component values is mainly given by the use of different reference sample. This can be understood taking into account the systematic uncertainties introduced by the use of unlike-charge reference sample. To sustain the last affirmation we present in Table 5.5 the results obtained by the LEP experiments analysing the one-dimensional correlation function [22, 44]: As you can see there is a systematic difference between the

Experiment	Unlike-charge R, fm	Mixing R, fm
ALEPH	0.81 ± 0.04	0.51 ± 0.02
DELPHI	0.83 ± 0.03	0.47 ± 0.03
L3	0.94 ± 0.04	0.58 ± 0.05
OPAL	0.93 ± 0.02	

Table 5.5: *Results obtained by fitting the one dimensional correlation function*

results obtained using the mixing procedure and the results obtained using

the unlike-charge reference sample (the radius is bigger in case of unlike-charge reference sample). The mixed reference sample gives more uniform results being less affected by systematic uncertainty.

5.6 Discussion

This two-dimensional analysis of the Bose-Einstein effect using the 1992–1995 DELPHI data confirms the prediction that the longitudinal correlation length, $R_{||}$, in $Z^0 \to q\bar{q}$ decay is bigger than the transverse one, $R_{\perp}$, in agreement with the picture that the bosons produced in the string fragmentation are subject to Bose-Einstein correlations during the hadronization process. The measured values are:

$$R_{\perp} = 0.53 \pm 0.08 \text{ fm} \ , \ R_{||} = 0.85 \pm 0.08 \text{ fm} \ .$$

The measured ratio of the radii components is $R_{\perp}/R_{||} = 0.62 \pm 0.06$, which is consistent with qualitative predictions [26]. A cleaner measurement can be made using $R_{t,side}$ as an estimator of the transverse correlation length, giving the ratio $R_{t,side}/R_{long} = 0.57 \pm 0.04$. These results cannot be reproduced by the JETSET generator.

The analysis presented here reproduced to a large extent the conditions presented in the theoretical work, by performing a good selection of the two-jet events, eliminating the additional correlations and using a cleaner reference sample.

The measurement of the shape of the BEC presented here makes use of the LCMS system to obtain a clear interpretation of the observed difference between transverse and longitudinal correlation radii. Together with analogous measurements done by other LEP experiments, it represents an improvement in BEC studies compared to previous studies at lower energies [25], which used the laboratory system. While the TASSO and MARK-II collaborations barely hinted at the possibility of the pion source in the process $e^+e^- \to hadrons$ being elliptical, this new result provides clear evidence for the elongation of the source. The results have implications for the modelling of hadronic final states performed by event generators.

Summary

A new interest for the study of Bose-Einstein correlation (BEC) in e^+e^- annihilation at the Z^0 peak arose recently due to a theoretical work which suggested a significant influence of BEC in W mass determination [10]. Estimations of the strength of this effect are strongly affected by the model used for simulation and by a set of model parameters conventionally optimised at the Z^0 peak. The interest for studies of the event generators and their BEC simulation appeared in the same context.

A detailed analysis of the BEC implemented in JETSET particle generator is presented in this thesis. The main result is that an artificial length scale is introduced due to the way the generator is working. This length scale is given by the position of the peak of the invariant four-momentum difference distribution. The radius, used as input of JETSET, is reproduced for large sources, while for small ones, the output value for the radius is almost constant irrespective of the input one.

Study of the transverse-mass (m_t) dependence of the three-dimensional BEC function parameters showed that the λ parameter dependence on m_t is given by the mixture of particles of different origin while the radius components dependence is pointing to a mechanism in the main JETSET block in the string fragmentation.

Some other models for BEC simulation have been developed using direct implementation of BEC in the string model. They spend too much computing resources to be used by high-energy physics experiments, but they do have predictive power. The two-dimensional analysis of BEC using DELPHI data confirmed one of these predictions, namely that the longitudinal correlation length in the $Z^0 \longrightarrow q\bar{q}$ decay is bigger than the transverse one, if the bosons produced in the string fragmentation are subject to BEC during the hadronization process.

The studies presented here contribute to a better understanding of BEC and give some hints about the requirements to the next generation of particle generators.

Acknowledgements

I would like to express my gratitude to all the staff of Particle Physics Department in Lund University, especially to Professor Bengt Lörstad and Professor Göran Jarlskog who shared the supervision and to Dr. Oxana Smirnova, who helped me a lot. I am also grateful to Professor Torbjörn Sjöstrand and Professor Bo Andersson, from the Theory Department in Lund, for valuable discussions and suggestions.

This work could not have begun without the financial support from Swedish Institute and I would like to thank the people that offered me this opportunity.

All my good thoughts to the Department of Nuclear and Particle Physics in Bucharest University especially to Professor Tatiana Angelescu and to everybody who taught me something there.

There are lots of other people that helped me, taught me and supported me during my education, in Dubna: Professor Gennadii Ososkov and Dr. Yuri Panebratsev's group, and in Bucharest: Dr. Mircea Penţia and all the people from IFIN-HH that helped me along the years. I would like to thank all of them.

To everybody who supported me and believed in me along the last years, a huge "Thank you!".

Last but not the least I would like to thank to Kristina Gunne who helped me with the printing of the thesis.

Bibliography

[1] B.R. Martin, G. Shaw, **"Particle Physics"**, 1992, ISBN 0-471-92359-1.

[2] S.Y. Lee **"Accelerator Physics"**, *World Scientific Pub Co*; ISBN: 981023709X.

[3] S. Myers, **"The LEP collider from design to approval and commissioning"**, *Proceedings of CERN Accelerator School*, CERN yellow report 91-08.

[4] S. Glashow, *Nucl. Phys.* B 22(1961) 579;
A. Salam, **"Elementary Particle Theory"**, ed N. Svartholm, Almquist and Forlag, Stockholm(1968);
S. Weinberg, *Phys.Rev.Lett.* 19 (1967) 1264.

[5] R.K. Ellis, W.J. Stirling, B.R. Webber **"QCD and Collider Physics"**, *Cambridge Monographs on Particle Physics, Nuclear Physics and Cosmology*, ISBN 0521 58189 3.

[6] P. Darriulat **"Research at CERN to-day and to-morrow**; *Proceedings of 1994 European School of High-energy Physics Zakopane*; editors N. Ellis and M.B. Gavela, CERN, Geneva CERN yellow report 94-04 (65-76).

[7] L. Foa, **"From LEP to LHC, a review of results and a look to the future"**, *Nucl.Phys. B* (Proc suppl) 75A (1999), 28-36.

[8] G. Goldhaber et al., Phys.Rev.Lett. C3 (1959) 181; see also G. Goldhaber, **The GGLP effect from 1959 to 1984**, LBL-1947 and *Proc. First Int. Workshop on Local Equilibrium in Strong Interaction Physics*, eds. D.K. Scottand, R.M. Weiner, (*World Scientific Publishing Co.*, 1985)

[9] G. Goldhaber, S. Goldhaber, W. Lee and A. Pais, *Phys. Rev. C* 120 (1960) 300.

[10] L. Lönnblad and T. Sjöstrand, *Phys. Lett. B* 351 (1995) 293.

[11] V. Kartvelishvili, R. Kvatadze, R. Møller, *Phys. Lett. B* 408 (1997) 331.

[12] Ŝ. Todorova-Nová, J. Rameš, **" Simulation of Bose-Einstein effect using space-time aspects of Lund string fragmentation model"**, IReS 97-29, PRA-HEP 97/16.

[13] DELPHI Coll.,P. Aarnio et al., *Nucl.Instr. and Meth.* A 303(1991) 223.

[14] DELPHI Coll., P. Abreu et al., *Nucl.Instr. and Meth.* A 378 (1996), 57.

[15] R. Hanbury-Brown and R.Q. Twiss, *Phil. Mag.* 45(1954) 663; Nature 178 (1956)1046.

[16] U. Heinz, M. Jacob, **"Evidence for a New State of Matter: An Assesment of the Results from the CERN Lead Beam Programme"**, CERN Press office.

[17] NA44 Coll., H. Beker et al., *Phys. Rev. Letter*, 74 (1995) 3340.

[18] T. Csörgo, B. Lörstad, *Phys. Rev. C*, 54 (1996) 1390-1403.

[19] A. N. Mahlin and Yu.M. Sinyukov, *Z. Phys.* C39 (1988) 39.

[20] B. Lörstad, O. Smirnova **"Transverse Mass Dependence of Bose-Einstein Correlation Radii in e^+e^- Annihilation at LEP Energies"**, *Proceedings of the 7th International Workshop on Multiparticle Production 'Correlations and Fluctuations"*, June 30 to July 6, 1996, Nijmegen, The Netherlands.

[21] T. Sjöstrand, *Comp. Phys. Comm.* 28 (1983) 229;
T. Sjöstrand, **Pythia 5.6 and Jetset 7.3: Physics and Manual**, CERN-TH.6488/92 (1992).

[22] OPAL Coll., P .D. Acton et al., *Phys. Lett. B* 267 (1991) 143 ;
DELPHI Coll., P. Abreu et al., *Phys. Lett. B* 286 (1992) 201;
ALEPH Coll., D. Decamp et al., *Z. Phys.*, C 54 (1992) 75;
L3 Coll., *"Measurement of Bose-Einstein Correlations for Both Charged and Neutral Pions from Z Decays at LEP"*, L3 Note 2272 (1998), submitted to ICHEP XXIX, Vancouver, 1998.

[23] OPAL Coll., P .D. Acton et al., *Z. Phys.* C 56 (1992) 521.

[24] DELPHI Coll., P. Abreu et al., *Phys. Lett.* B 355 (1995) 415.

[25] TPC Coll.,H.Aihara et al., *Phys. Rev.* D 31 (1985) 996;
TASSO Coll., M. Althoff et al., *Z. Phys.* C 30 (1986) 35;
Mark II Coll., I. Juricic et al., *Phys. Rev.* D 39 (1989) 1.

[26] B. Andersson and M. Ringnér, *Nucl. Phys.* B 513 (1998) 627;
B. Andersson and M. Ringnér, *Phys. Lett.* B 421 (1998) 283.

[27] L3 Coll., M. Acciarri et al., *Phys. Lett.* B 458 (1999) 517 .

[28] DELPHI Coll., P. Abreu et al. *Phys. Lett.* B 471 (2000) 460-470.

[29] OPAL Coll., **"Transverse and Longitudinal Bose-Einstein Correlations in Hadronic Z^0 Decays"**, CERN-EP-2000-004.

[30] B. Lörstad, *Int. J. Mod. Phys. A* ,vol 4, No. 12 (1989) 2861-2896.

[31] B. Andersson , G. Gustafson, G. Ingelman and T. Sjöstrand, **"Parton fragmentation and string dynamics"** *Physics reports (review Section of physics Letters* 97, Nos 2 and 3 (1983) 31-145. North Holland Publishing company.
B. Andersson **"The Lund Model"**, *Cambridge monographs on Particle Physics, Nuclear Physics and Cosmology*, 1998, ISBN 0 521 42094 6.

[32] B. Andersson and W. Hofmann, *Phys.Lett.* B 169 (1986) 364.

[33] M.G. Bowler, *Phys.Lett.B* 180 (1986) 229 and 185 B (1987) 205.

[34] G. Marchesini, B. R.W eber , G. Abbiendi, G.K nowles, M.H. Seymour and L. Stanco, **"Herwig 5.9"**, *Comp.Phys. Comm* 82 (1994), 74.

[35] K. Fialkovski, R. Wit, *European Journal of Physics* C 2 (1998) 691-695.

[36] K. Fialkovski, R. Wit, *Z. Phys. C* 74 (1997) 145-149.

[37] S. Haywood **"Where are we going with Bose-Einstein - A mini review"** *RAL Report*, RAL-94-074.

[38] O. Smirnova, **"Studies of the Fragmentation Process in the Hadronic Decays of Z^0 Boson"**, *Thesis submitted for the degree of Doctor in Philosophy in Physics*, Lund University, October 1996.

[39] G. Alexander; H.J. Lipkin, *Phys.Lett.B* 456 (1999) 270-276.

[40] T. Csörgő and S. Pratt, in *"Proceedings of the Budapest Workshop on Relativistic Heavy Ion Physics at Present and Future Accelerators"*, edited by T. Csörgő et al., CRIP preprint KFKI-1991-28/A, p75, 1991.

[41] DELPHI Coll., P. Abreu et al., *Z. Phys.* C73(1996) 11.

[42] NA35 Coll., T. Alber et al., *Z. Phys.*, C66 (1995) 77.

[43] **DELSIM Reference Manual**, DELPHI Note 87-98 PROG 100 (1989), unpublished.

[44] O. Smirnova, **"Bose-Einstein correlation at Z^0 peak"**, *Proceedings of "XXVII International Symposium on Multiparticle dynamics"* World Scientific, 1998.

Appendix A

Eur. Phys. J. C 6, 629–635 (1999)
DOI 10.1007/s100529901055

THE EUROPEAN
PHYSICAL JOURNAL C
© Springer-Verlag 1999

Appearance of an artificial length scale in JETSET Bose-Einstein simulation

Raluca Mureşan[a], Oxana Smirnova[b], Bengt Lörstad

Department of Elementary Particle Physics, Lund University, Box 118, SE-22100 Lund, Sweden

Received: 13 November 1997 / Revised version: 5 September 1998 / Published online: 14 January 1999

Abstract. This work studies the algorithm which implements the Bose-Einstein correlation effect in the JETSET 7.4 event generator. This algorithm attempts to reproduce an expected correlation function with a given correlation radius and amplitude. The two-particle correlation function is studied in the generated Z^0 hadronic decays for different values of the built-in radius parameter. Samples consisting of only charged particles are used, as well as subsamples of pions, pions coming from the string decay and pions from the resonance decays. The Bose-Einstein correlation function, extracted from the generated events, is parameterized analogously to the built-in JETSET correlation function and its parameters are compared with the input ones. We found that the measured correlation function reproduces the built-in one, if the input radius parameter is larger than $1\,fm$. For lower input radii an artificial new length scale appears due to the way the Bose-Einstein correlation is implemented.

1 Introduction

The study of Bose-Einstein correlation function for identical particles is of particular interest, since the process of hadron production, or fragmentation, in high energy physics is poorly comprehended. At this moment, no appropriate theory can describe it, only phenomenological models being available for the hadronization process and the Bose-Einstein phenomenon in particular. To account for and to describe it properly in event generators, the Bose-Einstein phenomenon must be well understood, therefore, more profound studies are required. Recently it was shown that the measurement of W mass at LEP2 is likely to be affected by Bose-Einstein correlation between pions from different W's [1–3]. Consequently, a significant interest was shown for the study of Bose-Einstein correlations in e^+e^- annihilation in the last years [4–7]. Comparison of the LEP data with the analysis of the $e^+e^- \to Z^0$ events, generated with the JETSET [8] particle generator with the built-in algorithm for the Bose-Einstein correlation simulation, showed that the model reproduces experimental data very well [6, 9–11].

Since JETSET is the simulation program the most commonly used by e^+e^- annihilation experimental groups, the analysis of the built-in method of implementing the Bose-Einstein correlations[1], its performance, its drawbacks, and the possible improvements were studied in several works [12, 13]. Our aim is to clarify the dependence of the correlation function on assumed input correlation radius and the particle sample composition.

The paper is organised as follows: in Sect. 2 the theory of the Bose-Einstein correlations is presented. Section 3 is dedicated to the description of the JETSET simulation program and the way in which the Bose-Einstein algorithm is implemented. Implementation issues and practical hints for our analysis are presented in Sect. 4. In Sect. 5 the behaviour of the correlation function for particles with different origin is studied and in Sect. 6 its dependence on the input correlation radius is investigated. Finally, in Sect. 7 the reader finds the conclusions.

2 Bose-Einstein correlation

During the 50-ies, in particle physics experiments, it was discovered that the produced bosons show a tendency to have close energy-momentum characteristics [14]. This phenomenon of increasing probability for emission of identical bosons from close regions of space and time is called Bose-Einstein correlation (we will not discuss correlations between fermions in this paper).

The Bose-Einstein effect originates in the quantum mechanical interference of the boson wave functions. It is a consequence of their symmetry under particle exchange, that influences the wave functions to yield an effective

[a] On leave from the National Institute for Research and Development in Nuclear Physics and Engineering "Horia Hulubei" (IFIN-HH) RO-76 900 P.O. Box MG 6, Bucharest, Romania

[b] On leave from JINR, Dubna, Moscow district, 141980 Russia

[1] JETSET is so far the only e^+e^- generator that contains a built-in Bose-Einstein correlation algorithm

clustering of the particles in the phase space, which explains their preference for occupying the same quantum states. From the characteristics of the resulting interference pattern it is possible, at least in principle, to determine the space-time dimensions of the source.

The string model describes e^+e^- annihilation data with high accuracy and provides an appropriate framework in which to consider the Bose-Einstein enhancement. In spite of a few attempts to introduce the Bose-Einstein symmetrization into the string model [15,16], the only working method to introduce the interference effects in Monte Carlo generators for e^+e^- annihilation, so far, is the shifting of the final state momenta to reproduce the assumed distribution of some variables [8]. This technique is described in details in Sect. 3. It has to be stressed that such a method has nothing to do with the quantum mechanics and only simulates the expected effect.

2.1 The Bose-Einstein correlation function

Considering the production of two identical bosons with four-momenta p_1 and p_2, denoting $P(p_1, p_2)$ the probability density of two particles to be produced, and $P(p_1)$ and $P(p_2)$ as the probability densities for a single particle to be produced with momentum p_1 or p_2, the correlation function C_2 of two identical bosons is defined as [17]:

$$C_2(p_1, p_2) = \frac{P(p_1, p_2)}{P(p_1)P(p_2)} \ . \tag{1}$$

From the experimental point of view, $P(p_1, p_2)$ is a double differential cross section. In practice, it is difficult to construct the product $P(p_1)P(p_2)$ due to the phase space limitations, therefore it is often replaced by $P_0(p_1, p_2)$, which is equal to $P(p_1)P(p_2)$ in the absence of correlation. One of the major problems in these kinds of studies is how to build $P_0(p_1, p_2)$, usually called the "reference sample".

The correlation function (1) is often parameterized as [17]:

$$C_2(Q) = N(1 + \lambda e^{-Q^2R^2}) \ , \tag{2}$$

where $Q = p_1 - p_2$ is the invariant four-momenta difference, and N, λ, R are free parameters. N is a normalisation constant. The interpretation of the λ parameter is that it is related to the fraction of identical bosons which do interfere, effectively representing the correlation strength. Parameter R is usually interpreted as the geometrical radius of a presumably spherical boson emitting source, or simply as the correlation radius parameter.

Near $Q = 0$, the effect of Coulomb repulsion between two identical charged bosons will lead to the suppression of the probability of finding two like-charged particles with small relative momentum. The effect is dominant in case of pions for $Q < 10$ MeV. For $Q > 50$ MeV the Coulomb repulsion is negligible. Since it has only a small effect on the studied distributions in e^+e^- annihilation, it is not discussed in the present article.

3 JETSET and Bose-Einstein correlation

JETSET is a simulation program able to generate hard processes, in particular, the electron-positron annihilation producing a boson, which decays into a quark-antiquark pair: $e^+e^- \to \gamma^*/Z^0 \to q\bar{q}$ (here '*' is used to denote that the photon is off-mass-shell). In what follows, events of this kind will be referred to as "$q\bar{q}$ events". The quark q in the reaction may have any flavour, picked at random, according to the relative couplings evaluated at the hadronic center of mass energy.

JETSET is intimately connected with the string fragmentation model in the form of the so-called Lund model. The JETSET program has a probabilistic and iterative nature, with the fragmentation process being described in terms of one or few simple underlying branches, as, for example, $string \to hadron + remainder\ string$ and so on. At each branching probabilistic rules are given for production of new flavours and for sharing of the energy and momentum between the products.

To understand the fragmentation model, we can use as an example the simplest possible system: a 2-jet colour singlet $q\bar{q}$ event, as produced in e^+e^- annihilation, where we have a linear confinement picture. The energy stored in the colour dipole field between a charge and an anticharge increases linearly with the separation between charges, if the Coulomb term is neglected. This assumption of the linear confinement provides the starting point for the string model. As q and $\bar{q}$ partons move apart from their common production vertex, a colour flux tube or maybe a colour vortex line is considered to be stretched between the $q\bar{q}$. The potential energy stored inside the string increases and the string may break, producing a new $q'\bar{q}'$ pair, so that the system splits into two colour singlet systems $q'\bar{q}$ and $q\bar{q}'$. If the invariant mass of these pairs is large enough, further breaks may occur. The generator does not take into account either the propagation of the resonances, or the space-time picture of the particle creation. The string break-up process is assumed to proceed until only the on-mass-shell hadrons remain, each hadron corresponding to a small piece of string with a quark at one end and an antiquark at the other.

To simulate the Bose-Einstein effect, an algorithm, which does not represent a true model, is used, for which very specific assumptions and choices are made. In this scheme the fragmentation is allowed to proceed independently of Bose-Einstein effect. The four-momentum difference, Q_{ij}, associated to a pair of identical particles i, j is defined as:

$$Q_{ij} = \sqrt{(p_i + p_j)^2 - 4m^2} \ , \tag{3}$$

where m is the common particle mass and p_i, p_j are particle momenta.

A shifted smaller Q'_{ij} is then sought, such that the ratio of "shifted" to the "unshifted" Q distribution is given by the requested parameterization $C_2(Q)$. The shape can be chosen to be either exponential or Gaussian :

$$C_2(Q) = 1 + \lambda e^{-(QR)^r}, \quad r = 1 \ or \ 2 \ , \tag{4}$$

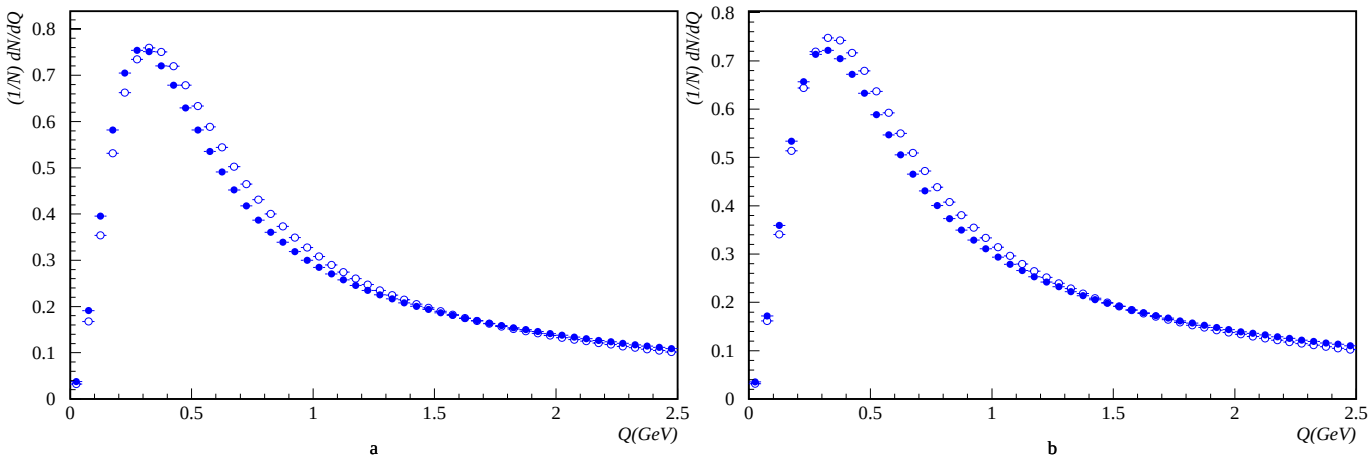

Fig. 1. The stored Q histograms (normalised to unity), for all charged particles, 2 millions JETSET events: **a** Bose-Einstein correlation effect included, but the mixing procedure not performed: closed circles, Bose-Einstein correlation effect included, and the mixing procedure performed: open circles, **b** Bose-Einstein effect not included, and the mixing procedure performed: open circles, Bose-Einstein effect not included, and the mixing procedure not performed: closed circles

where λ, R and r are input parameters of the algorithm (we have used in this work only the Gaussian form, $r = 2$).

If the inclusive distribution of the Q_{ij} is assumed to be given just by the simple, spherical phase space, Q'_{ij} can be found as a solution of the equation:

$$\int_0^{Q_{ij}} \frac{Q^2 dQ}{\sqrt{Q^2+4m^2}} = \int_0^{Q'_{ij}} C_2(Q) \frac{Q^2 dQ}{\sqrt{Q^2+4m^2}} \ . \qquad (5)$$

That gives as a new distribution Q'_{ij} – the product of the old distribution Q_{ij} and $C_2(Q)$:

$$Q'_{ij} = Q_{ij} C_2(Q) \ . \qquad (6)$$

This procedure is performed for all the pairs of identical bosons (for resonances with a width above a certain value - in our case $0.020 GeV$ - the decays are assumed to take place before the stage where Bose-Einstein effects are introduced). The new values for Q are calculated and a global shift of momenta for all the particles is performed adding all the possible pair shifts. Finally, all the momenta are rescaled by a common factor to restore the original value of the total centre of mass energy. The obtained invariant Q distribution is in this way shifted, see Fig. 1. This algorithm is implemented in the LUBOEI subroutine, a standard component of the JETSET generator. The assumption of the simple spherical phase space is valid only for the part of the true Q distribution to the left of the peak, see Fig. 1. Instead of a monotonic increase, which is given by the spherical phase space, the experimental Q distribution has a maximum around 0.5 GeV, then falls power-like for large Q. Fiałkowski and Wit [12] and Haywood [13] proposed modified procedures using approximations of the experimental Q distributions to estimate the Q shift. However, using these methods, the final shifted Q distribution did not correspond to the input values of R parameters as in (4), for $R \leq 1\, fm$.

4 Computational program: main assumptions

We used JETSET in order to generate $q\bar{q}$ events at the center of mass energy of 91.2 GeV. Due to the low efficiency of neutral particle reconstruction in e^+e^- experiments, the study of the Bose-Einstein effect was performed only for charged particles and for subsamples of charged pions, pions that were produced directly from the hadronization of quarks and gluons, pions coming from resonance decays and separately of pions that appeared in decays of ρ mesons which were in turn produced in the hadronization of the string (direct ρ's). Different values of the JETSET input radius R (see (4)) are used for studies.

4.1 The reference sample

In order to prepare the reference sample for a proper correlation function (see Sect. 2.1), we have to find a sample of particles which are not subject to Bose-Einstein correlation, but do obey the same kinematics as a regular e^+e^- event.

There are several procedures to prepare a reference sample. For this study, as, for example, in [10,11], we combined particles from different events, assuming that the selection criteria of the two-jet events provide us with a set of kinematically similar events. This so-called "mixing" procedure can be described by following steps:

– After the thrust[2] axis calculation, each event is rotated to a new coordinate system, which has the z axis along the thrust axis.

[2] The quantity thrust T is defined by:

$$T = \max_{|\mathbf{n}|=1} \frac{\sum_i |\mathbf{n}\cdot\mathbf{p}_i|}{\sum_i |\mathbf{p}_i|} \ ,$$

and the thrust axis $\mathbf{v}_1$ is given by the $\mathbf{n}$ vector for which the maximum is obtained. The allowed range is $1/2 \leq T \leq 1$, with a 2-jet event corresponding to $T \approx 1$ and an isotropic event to $T \approx 1/2$

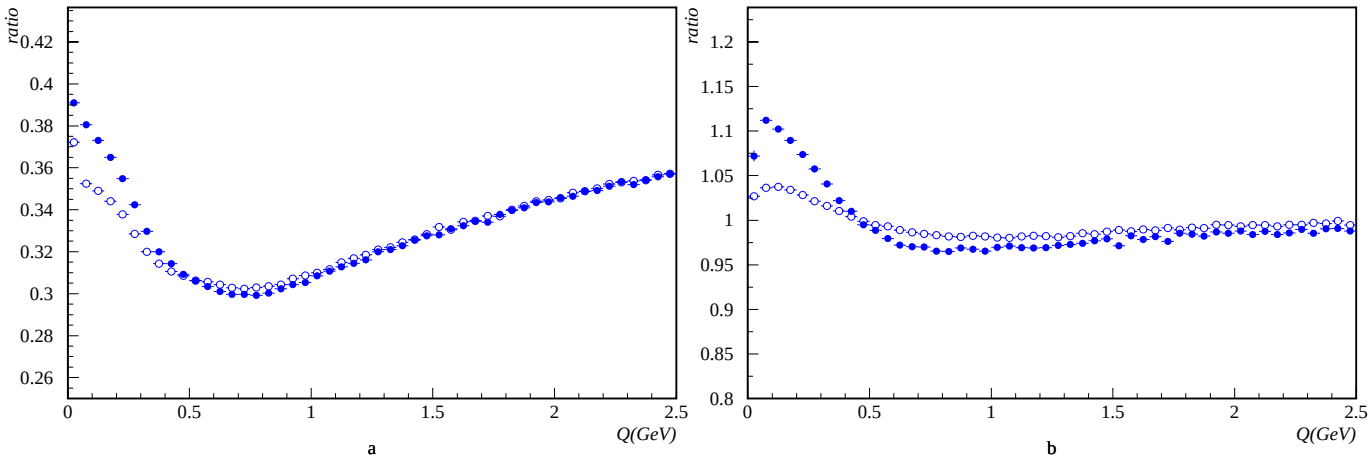

Fig. 2. **a** The ratios $N_{BEon}(Q)/N^{MIX}_{BEon}(Q)$ (closed circles) and $N_{BEoff}(Q)/N^{MIX}_{BEoff}(Q)$ (open circles), **b** The ratios $N_{BEon}(Q)/N_{BEoff}(Q)$ (closed circles) and $N^{MIX}_{BEon}(Q)/N^{MIX}_{BEoff}(Q)$ (open circles)

– Tracks from each rotated event are stored in a reference buffer. Events in the buffer are continuously updated to prevent any regularities in the particles spectra.
– The reference sample is built using randomly picked tracks from the reference buffer. First, a random event of the stored ones is selected, then a track from this event is also randomly picked out.

The mixing procedure does not conserve energy and momentum, and destroys not only the Bose-Einstein correlation but even some other kinds of correlations, making necessary some corrections.

4.2 The correction procedure

To construct properly the correlation function, eliminating side effects introduced by the mixing procedure, we accumulate four kinds of number of charge-like pairs N as a function of Q:

– Bose-Einstein correlation effect turned on, but the mixing procedure not performed: N_{BEon}, see Fig. 1a (closed circles).
– Bose-Einstein correlation effect turned on, and the mixing procedure performed: N^{MIX}_{BEon}, see Fig. 1a (open circles).
– Bose-Einstein effect turned off, and the mixing procedure performed: N^{MIX}_{BEoff}, see Fig. 1b (open circles).
– Bose-Einstein effect turned off, and the mixing procedure not performed: N_{BEoff}, see Fig. 1b (closed circles).

The corrected correlation function is given by:

$$C_2(Q) = \frac{N_{BEon}(Q)/N^{MIX}_{BEon}(Q)}{N_{BEoff}(Q)/N^{MIX}_{BEoff}(Q)} \ . \qquad (7)$$

In this way we get $C_2(Q)$ almost constant for $Q > 1$ GeV, as we show below (see Fig. 3).

Figure 2a shows that the ratios $N_{BEon}(Q)/N^{MIX}_{BEon}(Q)$ and $N_{BEoff}(Q)/N^{MIX}_{BEoff}(Q)$ are very similar in shape.

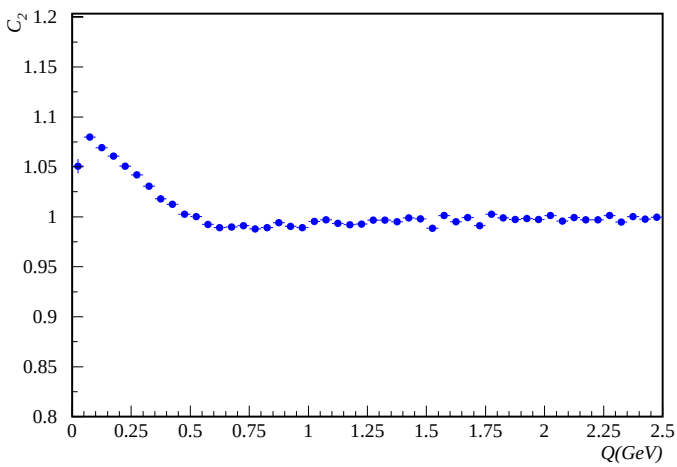

Fig. 3. The final corrected correlation function, as in (7)

Even in the $N_{BEoff}(Q)/N^{MIX}_{BEoff}(Q)$ case, a small enhancement, that has approximately the same width, appears due to the other kinds of correlation. In Fig. 2b, the ratio $N^{MIX}_{BEon}(Q)/N^{MIX}_{BEoff}(Q)$ shows that the mixing procedure does not eliminate correlations totally. This is why we have to calculate the double ratio (7) to obtain a clear Bose-Einstein effect over the $C_2(Q) = 1$ level, see Fig. 3.

4.3 Event and track selection

To be able to test the string model and to compare with the previous experimental data, we generate $q\bar{q}$ events only, requiring also the thrust value to be bigger than 0.95. In order to purify the data samples, to reduce the background and to save computing resources, the following cuts were introduced:

– The correlation function was constructed only for pairs of particles belonging to the same jet , each having momentum below 5 GeV/c to avoid the limits of phase space, where dynamical correlations are strong.

Table 1. Number of events analysed. Samples of pions coming from direct ρ were collected for five different values of input correlation function radii R

Sample composition	Number of events	Average multiplicity
Charged particles	2 000 000	14
Pions	2 000 000	12
Direct pions	5 000 000	2
Pions from all resonances	5 000 000	6
Pions from direct ρ	50 000 000	3

Table 2. Results of the one-dimensional fit of $C_2(Q)$

Sample composition	λ	R (fm)	χ^2/ndf
Charged particles	0.106±0.005	0.531±0.018	26/25
Charged pions	0.132±0.005	0.534±0.008	37/25
Direct pions	0.950±0.039	0.602±0.018	39/25
Pions from all resonances	0.656±0.010	0.651±0.008	111/25
Pions from direct ρ	1.090±0.010	0.665±0.005	160/25
Input values	1	0.5	

– To reduce correlations due to the local transverse momentum compensation, the pairs were rejected if their opening angle in transverse plane exceeded 120°. This cut was introduced for the compatibility with experimental data and reduces slightly the background at high Q values.

Since the number of pairs of particles that accomplished all our cuts is small (especially in the case of mixed samples for pions from resonances and direct pions, where the multiplicity is low) it was necessary to analyse large samples (see Table 1).

5 The dependence on the particle origin

The correlation function (7), obtained with the help of JETSET, was fitted in the interval of 0.05 GeV $< Q <$ 1.5 GeV, using formula (2) in order to find its parameters. These output fit parameters, λ and R, are given in Table 2 for different sample composition.

Table 2 shows that the simulated correlation functions are not always well described by a Gaussian. The output values of parameters are quite different not only from the input values, but also from case to case.

The λ parameter represents a measure of the fraction of particles sensitive to the effect. In our case it is easy to understand that for charged particles and for pions, where the particles have different origins, λ has low values. The value of this parameter in the case of pions coming from all resonances is also far from the input value, even if it is considerably higher compared to the one for charged particles and charged pions. This is due to the fact that there are some pions coming from long-lived resonances and thus are not subject to Bose-Einstein symmetrization.

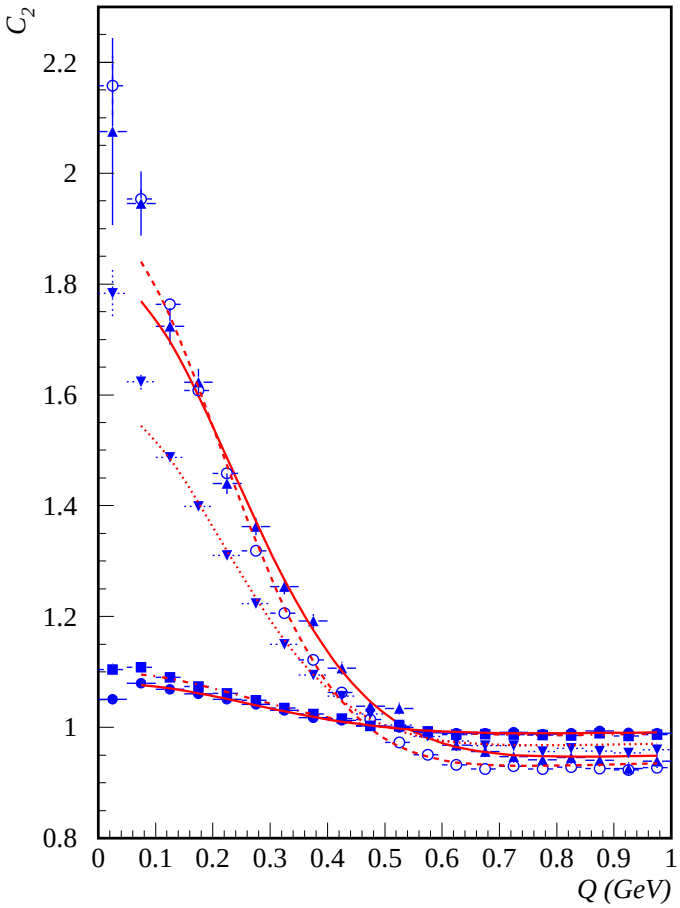

Fig. 4. The shape of the correlation function in different cases: all charged particles (closed circles), pions (squares), direct pions (up triangles), pions coming from all the resonances decay (down triangles), pions from direct ρ (open circles)

In JETSET a corresponding mechanism is implemented that allow to ignore them. In case of direct pions and pions coming from ρ decay, where the pion source has a high purity, the fitted values of λ are close to the input value $\lambda = 1$. For the radii, we obtained fitted values which are 20% to 40% higher than the input.

The correlation function $C_2(Q)$ at $Q > 0.5\,GeV$ eventually becomes smaller than one. The shape of the resulting correlation function is not particularly close to a Gaussian at very low Q, (see Fig. 4).

6 The dependence on input radius

Following the study of Fiałkowski and Wit [12], we studied how the correlation changes with the input JETSET radius. The shape of the functions changes from the input Gaussian due to the global shift of the momenta, the adding of all the pair shifts and the poor approximation of the phase space for input radius of $\sim 0.5 fm$.

For this study we used only samples of pions coming from the direct ρ decays, since this sample is relatively pure and the multiplicity is higher than for direct pions. It is easy to observe, Fig. 5, that when the input radius

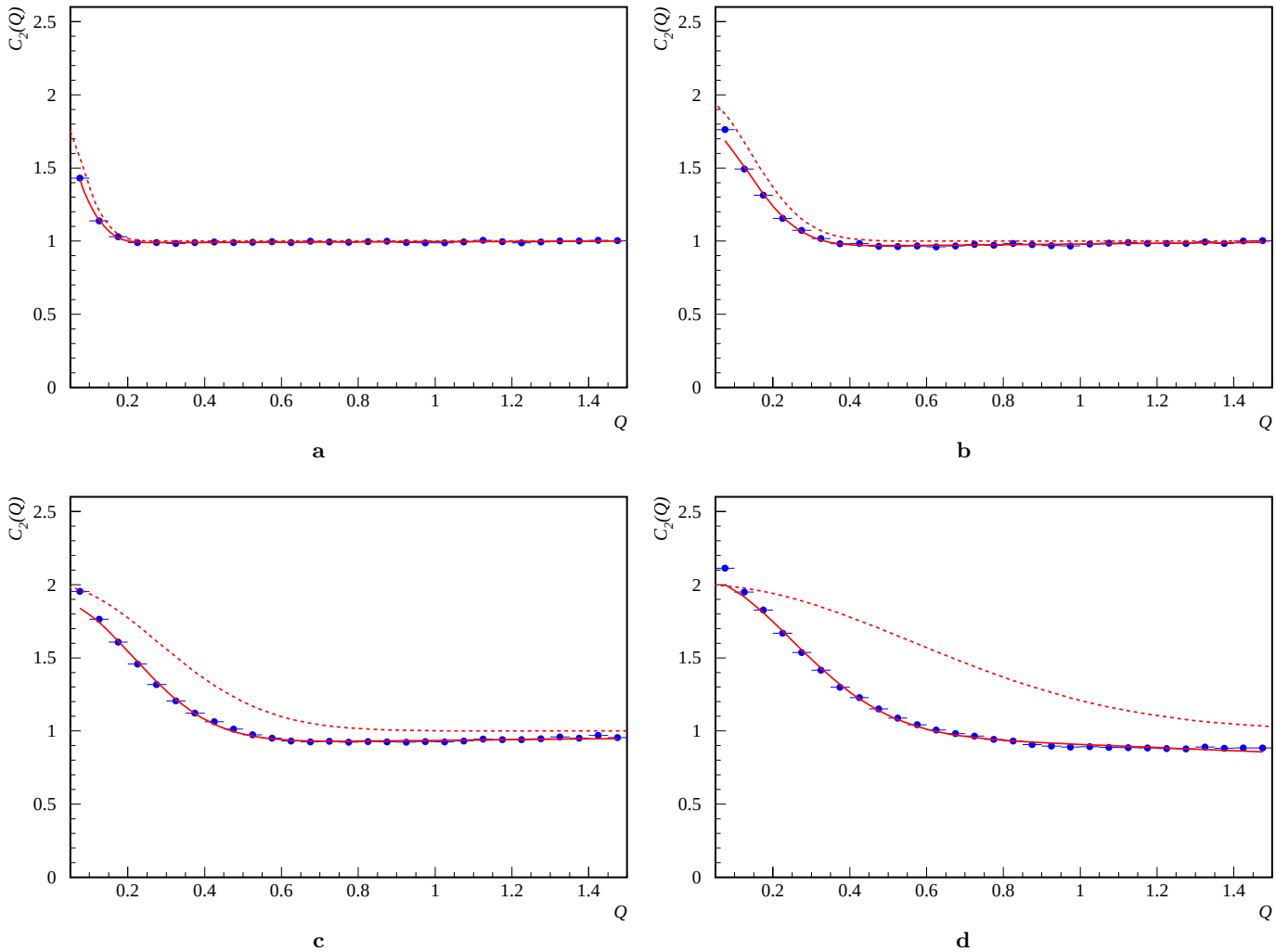

Fig. 5. The shapes of the output correlation function (full curve) and the input correlation function (dashed curve) for different input radii: **a** R_{in} =2 fm, **b** R_{in} =1 fm, **c** R_{in} =0.5 fm, **d** R_{in} =0.25 fm

decreases, the shape of the output function (full curve) is more and more different from the shape of the input function (dashed curve).

Figure 6 represents the radii R_o obtained through the fit by (2), as a function of the input radii R_{in} for JETSET. One can observe that for the values of input radii less than 0.5 fm, almost constant values of the output fitted radii were found, around 0.6 fm. For input R_{in} values bigger than 1 fm, the points are lying very close to the diagonal, showing a good agreement between input and output radii.

We observe the appearance of a new length scale of the resulting radius, $R_o \sim 0.6\,fm$, which is independent of the input radius R_{in}, for the region $0 < R_{in} \leq 0.6\,fm$. This new scale is connected to the peak value of the inclusive Q distribution. In the studied algorithm, Q is shifted to a lower value Q' to give an enhancement when we take the ratio of the Q' distribution to the Q distribution. This works only for a monotonically increasing function, such as the spherical phase space distribution. The true Q distribution, however, exhibits a peak around 0.5 GeV (which

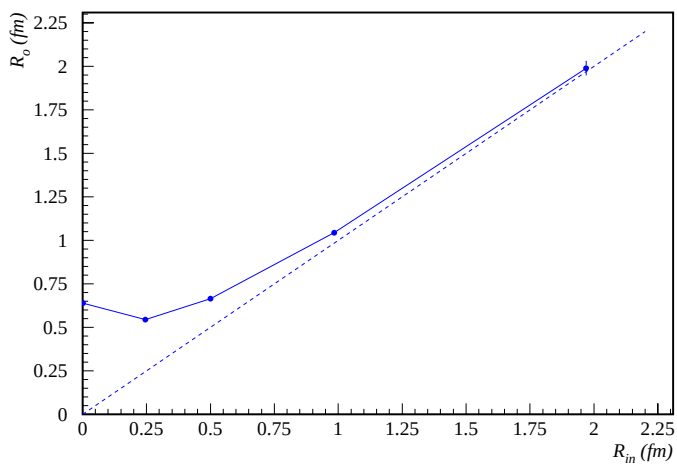

Fig. 6. Fitted values of output radii R_o for different input radii R_{in}

corresponds to $2.5\,fm$). For $R_{in} \leq 0.6\,fm$, the shift of Q to a lower Q' implies a depletion, not an enhancement in

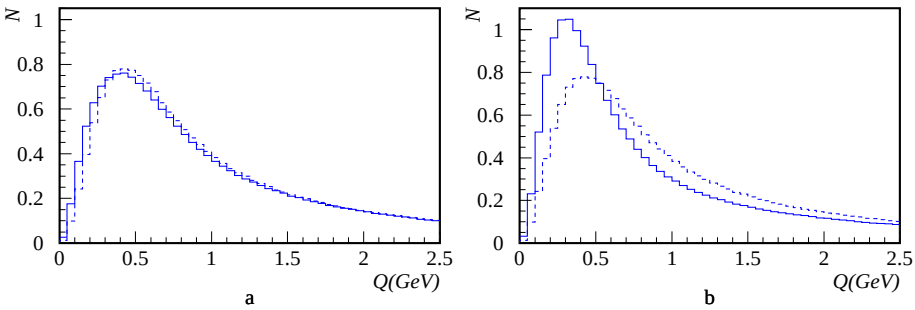

Fig. 7. The Q distribution with Bose-Einstein simulation (full line), and without it (dashed line) for **a** $R_{in} = 1fm$, **b** $R_{in} = 0.25fm$. All the distributions are normalised to the total number of pairs

the region to the right of the peak ($Q > 0.5\ GeV$), see Fig. 7, possibly giving a $C_2 < 1$ for this region, as seen in Fig. 5c and Fig. 5d. For the Q distribution, the peak position constitutes a limitation of the correlation width and gives rise to an artificial length scale.

To summarise, for the input radius values higher than $1\,fm$, the input correlation function seems to be well reproduced by the constructed output correlations. For lower input radii secondary effects, due to the way in which the Bose-Einstein correlation is introduced, are important. This is consistent with earlier results from other studies [12,13]. It is worth noting that experimental data seems to be reproduced by this secondary effects simulation using $R_{in} = 0.5\,fm$ [6,9–11].

7 Conclusions

An analysis of the Bose-Einstein correlation, implemented in the JETSET particle generator, has been performed. Our main result is that an artificial new length scale is introduced due to the way the generator is working. This scale is given by the peak position of the Q distribution. Appearance of this artificial scale causes the previously unexplained phenomenon; namely, the fact that JETSET, while reproducing well experimental data, is self-inconsistent and fails to reproduce its own built-in Bose-Einstein correlation function for input radii of around 0.5 fm. For radii larger than 1 fm we have not seen any strong artificial scale effects.

Acknowledgements. We are grateful to T. Sjöstrand for valuable discussions and suggestions.

References

1. L. Lönnblad, T. Sjöstrand, Phys. Lett. B **351**, 293 (1995)
2. P. Abreu et al., DELPHI Coll., Phys. Lett. B **401**, 181 (1997)
3. V. Kartvelishvili, R. Kvatadze, R. Møller, *Estimating the effects of Bose-Einstein correlations on the W mass measurement at LEP2*, University of Manchester preprint MC-TH-97/04, MAN/HEP/97/1
4. D. Decamp et al., ALEPH Coll., Z. Phys. C **54**, 75 (1992)
5. P. Abreu et al., DELPHI Coll., Phys. Lett. B **286**, 201 (1992)
6. P. Abreu et al., DELPHI Coll., Z. Phys. C **63**, 17 (1994)
7. A. Engler, H. R. Hoorani, *Measurement of Bose-Einstein correlations between charged pions using the LEP1 data*, L3 Note 2139 (submitted to Int. Europhysics Conference on High Energy Physics, Jerusalem 97)
8. T. Sjöstrand, Comp. Phys. Comm. **82**, 74 (1994); T. Sjöstrand, PYTHIA *5.6 and* JETSET *7.3*, CERN-TH.6488/92, 1992
9. P. Abreu et al., DELPHI Coll., Phys. Lett. B **355**, 415 (1995)
10. O. Smirnova, *Studies of the Fragmentation Process in Hadronic Decays of Z^0 Boson*, Thesis for the degree of Doctor of Philosophy in Physics, Lund University, 1996, LUNFD6/(NFFL-7127)1996
11. B. Lörstad, O. Smirnova, *Transverse Mass Dependence of Bose-Einstein Correlation Radii in e^+e^- Annihilation at LEP Energies*, in *Proceedings of the 7th International Workshop on Multiparticle Production 'Correlations and Fluctuations', Nijmegen, 1996*, edited by R.C. Hwa et al. (World Scientific, Singapore, 1997)
12. K. Fiałkowski, R. Wit, Z. Phys. C **74**, 145 (1997)
13. S. Haywood, *Where are we going with Bose-Einstein – a mini review*, RAL Report RAL-94-074
14. G. Goldhaber et al., Phys. Rev. Lett C **3**, 181 (1959)
15. B. Andersson, M. Ringnér, Phys. Lett. B **421**, 283 (1998)
16. Ŝ. Todorova-Nová, J. Rameš, *Simulation of bose-Einstein effect using space-time aspects of Lund string fragmentation model*, IReS 97-29, PRA-HEP 97/16
17. B. Lörstad, Int. J. Mod. Phys. A**4**(12), 2861 (1989)

Appendix B

Tests of the JETSET Bose-Einstein correlation model in the e^+e^- annihilation process

O.Smirnova, B.Lörstad, R.Mureşan
Department of Physics, Elementary Particle Physics,
Box 118, 221 00 Lund, Sweden
E-mail: oxana@quark.lu.se

Studies of implementation of the simulation of the Bose-Einstein correlation effects in the JETSET particle generator are performed. Analysis of dependance of the one-dimensional correlation function parameters on the presumed boson source size reveals appearance of the effective new length scale, which limits applicability of the simple momentum-shifting mechanism, employed by JETSET to simulate the Bose-Einstein correlation. Two- and three-dimensional correlation functions are analysed as well and compared to the DELPHI data.

1 Introduction

Recent interest in profound studies of the Bose-Einstein correlations (BEC in what follows) was sparked by reports on possible influence of this phenomenon on the measured value of the W boson mass in e^+e^- annihilation [1,2]. Estimations of the strength of this influence were done using the Monte Carlo particle generator JETSET[3], which includes a phenomenological model for two-particle BEC simulation. JETSET (together with PYTHIA [3]) is so far the only e^+e^- annihilation event generator which accounts for BEC. It is known to reproduce well majority of experimental data, including some basic features connected to BEC. However, more sophisticated studies reveal not only certain discrepancies between experimental and model results, but also self-inconsistencies in the model itself [4,5]. Therefore, it is of particular importance to establish the extent of applicability of this model and to have a full understanding of its advantages and drawbacks.

This work is devoted to studies of the built-in JETSET algorithm which is used to simulate BEC in hadronic decays of Z boson. The following section describes the physical process and corresponding observables. Overview of the studied model is presented in the next section. The last section contains results and discussion.

2 Scope of the study and definitions

The goal of this analysis is to study methods and consequences of implementing Bose-Einstein correlation models in the JETSET event generator, and to find

out eventually how can it affect data analysis. To accomplish this goal, Bose-Einstein correlations between pions produced in hadronic decays of the Z boson are investigated. These decays are generated by the JETSET event generator, which uses the so-called Lund string model to simulate electron-positron annihilation events at a given center of mass energy, in our case $E_{cm} = 91.2\ GeV$.

Only the correlations between pairs of particles are studied, whith the two-particle correlation function is defined as

$$C_2(p_1, p_2) = \frac{P(p_1, p_2)}{P(p_1)P(p_2)} \ , \tag{1}$$

where p_1 and p_2 are four-momenta of two particles, $P(p_1, p_2)$ – two-particle probability density, and $P(p_1)$ and $P(p_2)$ denotes single-particle probability densities.

Defined as above C_2 is parameterized in terms of the invariant four-momenta difference $Q = \sqrt{(\vec{p}_1 - \vec{p}_2)^2 - (E_1 - E_2)^2}$ as

$$C_2(Q) = N(1 + \lambda e^{-R^2 Q^2}) \ . \tag{2}$$

This parameterization is one of the most commonly used[6], with the parameter R giving the width (or source size) and λ – the strength of the correlation.

In order to be able to compare our results with experimental data, only charged pions were used in the analysis. Although prompt pions produced in the string decay are the most clean sample, we selected only pions produced in decays of prompt ρ mesons, due to the following advantages :

– high sample uniformity: no admixture of particles which are not subject to Bose-Einstein correlations;

– sufficient average multiplicity of the sample: more pions are produced in decays of ρ mesons then promptly from the string.

Studies were performed not only for the one-dimensional correlation function $C_2(Q)$, but also for two- and three-dimensional cases. To facilitate calculations, the Longitudinal Centre-of-Mass System [7,8] (LCMS) was used to measure four-momentum difference. This is the system in which the sum of the two particles momenta is perpendicular to the jet axis, hence only two-jet $q\overline{q}$ events were generated for further simplicity. In LCMS, Q is resolved into Q_{long}, parallel to the jet axis, $Q_{t,out}$, collinear with the pair momentum sum, and complementary $Q_{t,side}$, perpendicular to both Q_{long} and $Q_{t,out}$. It is more convenient in some cases to use only two-dimensional picture with longitudinal $Q_{\parallel} \equiv Q_{long}$ and perpendicular $Q_{\perp} = \sqrt{Q_{t,out}^2 + Q_{t,side}^2}$. Parameterization of C_2 for these two- and three-dimensional cases was chosen correspondingly as

$$C_2(Q_{\perp}, Q_{\parallel}) = N(1 + \lambda e^{-Q_{\perp}^2 R_{\perp}^2 - Q_{\parallel}^2 R_{\parallel}^2}) \ , \tag{3}$$

$$C_2(Q_{t,out}, Q_{t,side}, Q_{long}) = N(1 + \lambda e^{-Q^2_{t,out}R^2_{t,out} - Q^2_{t,side}R^2_{t,side} - Q^2_{long}R^2_{long}}) \ . \tag{4}$$

In high-energy physics experiments involving detectors, it is difficult to construct the product $P(p_1)P(p_2)$ from Eq.(1) due to the phase space limitations. Therefore it is often replaced by $P_0(p_1, p_2)$, which is equal to $P(p_1)P(p_2)$ in a hypothetical case of absence of all the correlations. To make our results comparable with experiment, we must construct a reference sample corresponding to $P_0(p_1, p_2)$. Therefore, the measured two-particle correlation function is calculated as the double-ratio, using the event mixing technique [8] :

$$r_{BE}(Q) = \frac{N^{\pm\pm}_{BE}(Q)}{N^{\pm\pm}_{BE,mix}(Q)} \ , \ r_{noBE}(Q) = \frac{N^{\pm\pm}_{noBE}(Q)}{N^{\pm\pm}_{noBE,mix}(Q)} \ , \ C_2(Q) = \frac{r_{BE}(Q)}{r_{noBE}(Q)} \tag{5}$$

Here $N^{\pm\pm}_{BE}(Q)$ is number of like charged pions as a function of the four-momenta difference Q in presence of Bose-Einstein correlations. Subscript "BE, mix" denotes same quantity but with pairs of pions picked from different events. Indices "$noBE$" and "$noBE, mix$" correspond to analogous quantities in absence of BEC (i.e., the simulation of BEC is not included into the event generation).

3 Model description

As it was already mentioned, JETSET is the only particle generator which allows and actually includes an algorithm emulating Bose-Einstein correlations. Recall that BEC is the quantum mechanical phenomenon, which has to appear during the fragmentation stage. However, in the standard implementation of BEC in JETSET, the fragmentation and decays of the short-lived particles like ρ are allowed to proceed independently of the Bose-Einstein effect. The BEC simulation algorithm is applied to the final state particles, for which the four-momenta difference $Q_{i,j}$ is being calculated for each pair of identical bosons i, j. A shifted smaller $Q'_{i,j}$ is then to be found, such that the ratio $C_2(Q)$ of "shifted" to the original Q distribution is given by the requested parameterization (Gaussian or exponential). In our case, the Gaussian parameterization identical to the form (2) was used :

$$C_2(Q) = 1 + \lambda e^{-R^2_{inp}Q^2} \ , \tag{6}$$

where λ and R_{inp} are input parameters of the model. The input value of λ is often set to 1, as it was done in this analysis too. Values of R_{inp} usually are chosen to fit experimental results.

Further, under assumption of a spherical phase space, Q' is the solution

of the equation :

$$\int_0^{Q_{i,j}} \frac{Q^2 dQ}{\sqrt{Q^2+4m^2}} = \int_0^{Q'_{i,j}} C_2(Q) \frac{Q^2 dQ}{\sqrt{Q^2+4m^2}} \ . \tag{7}$$

After applying corresponding four-momentum shift to each pair of considered bosons, all particle momenta are re-weighted to satisfy the energy-momentum conservation. This built-in JETSET algorithm works only in terms of the invariant four-momenta difference Q, i.e., it does not distinguish between different Q components. This is yet another ambiguous assumption of the model. Also, it does not include particle correlations of higher orders.

Evidently, this algorithm is absolutely phenomenological and is not based on any fundamental theory. It solely changes the final state particles momenta in order to resemble presence of the Bose-Einstein correlations. Moreover, presumption of the spherical shape for the phase space in Eq.(7) is correct only for the case of very low Q (see the following discussion).

In spite of all the ambiguities, JETSET reproduces fairly well experimental data, such as shift of the ρ mass and observed Bose-Einstein correlations in terms of Q. It is widely used to calculate acceptance corrections for detectors and for various estimations, like the W mass shift mentioned in the Introduction. To our mind, this peculiarity is worth investigating, if not in order to get better understanding of the BEC influence in experimental data, then at least in order to establish limits of applicability of such a simulation model.

4 Analysis and discussion

One of the most puzzling inconsistencies in the JETSET simulation of BEC is that the input shape of (6) can not be obtained with the same parameters by fitting the resulting measured $C_2(Q)$ with formula (2) (see, for example, article by Fiałkowski and Wit [5]). This is mostly due to the improper phase space approximation in Eq.(7). However, this approximation can still be valid for certain input boson source size R_{inp}. To find out whether it is true, we studied $C_2(Q)$ for different input values of R_{inp} in formula (6).

Measured as the double-ratio (5) two-particle correlation function generated with different input source size R_{inp} was fitted by the form (2). The λ parameter always was reproduced at values close to 1, due to the high purity of the sample. The output source size R, however, behaved differently, see Fig. 1 and the corresponding table. Preliminary DELPHI results measured in 1991-1995 on all the charged particles are shown in the same table for comparison.

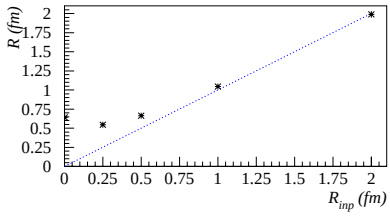

Figure 1: Width R of the measured in JETSET generated events correlation function $C_2(Q)$ as a function of the input source radii R_{inp}. Line represents the expected dependence.

R_{inp}, fm	R, fm
0.002	0.640 ± 0.005
0.250	0.545 ± 0.006
0.500	0.663 ± 0.005
1.000	1.046 ± 0.010
2.000	1.990 ± 0.042
DELPHI	0.489 ± 0.010

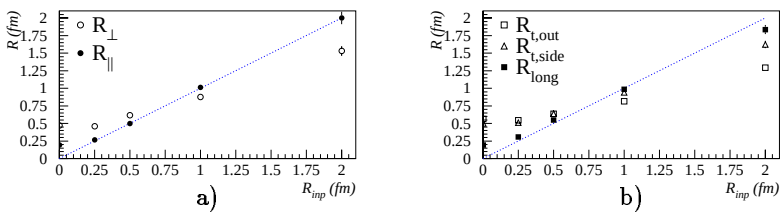

Figure 2: Components of the correlation width as a function of the input source radii R_{inp} : a) $R_{\|}$, $R_{\perp}$ and b) $R_{t,out}$, $R_{t,side}$, R_{long}.

R_{inp}, fm	$R_{\perp}, fm$	$R_{\|}, fm$	$R_{t,out}, fm$	$R_{t,side}, fm$	R_{long}, fm
0.002	0.472 ± 0.002	0.193 ± 0.001	0.562 ± 0.005	0.499 ± 0.004	0.193 ± 0.002
0.250	0.459 ± 0.003	0.266 ± 0.002	0.544 ± 0.004	0.511 ± 0.004	0.307 ± 0.003
0.500	0.616 ± 0.005	0.497 ± 0.005	0.637 ± 0.005	0.636 ± 0.005	0.549 ± 0.004
1.000	0.873 ± 0.015	1.013 ± 0.021	0.814 ± 0.011	0.940 ± 0.012	0.986 ± 0.013
2.000	1.530 ± 0.070	2.000 ± 0.090	1.291 ± 0.039	1.622 ± 0.051	1.835 ± 0.065
DELPHI	0.300 ± 0.040	0.640 ± 0.020	0.364 ± 0.009	0.173 ± 0.019	0.628 ± 0.008

It is clearly seen that the measured R does not depend on the input R_{inp} when the latter is below $\approx 0.6\, fm$. For the higher values of R_{inp} JETSET basically reproduces the demanded correlation function.

Knowing that JETSET does not distinguish between components of invariant momentum difference Q, we should expect similar behaviour of radius parameters of two- and three-dimensional correlation functions. Parameterization of these functions is performed in a form of a multi-dimensional Gaussians (3) and (4) correspondingly.

As one can see from Fig. 2 and in the corresponding table, transverse radii follow the same pattern as the R, while the longitudinal radius tends to

reproduce the input value of R_{inp}.

All these results show that there is a certain mechanism in the model, which imposes lower limit of around $0.6\,fm$ onto measured R and its transverse components, and almost does not affect the longitudinal radius. The explanation of this phenomenon is illustrated at Fig. 3 for the one-dimensional case. It shows evolution of the dN/dQ distribution with input source radius R_{inp} in comparison with the original non-correlated distribution. It is clearly seen that the expected Bose-Einstein enhancement appears only to the left of the non-correlated distribution peak, $Q < 0.3\,GeV$. Since the model conserves multiplicity, and because the assumption of the spherical phase space in Eq.(7) is valid only for this region of the linearly increasing dN/dQ, a depletion appears for $Q > 0.3\,GeV$, which results in a non-Gaussian output correlation function.

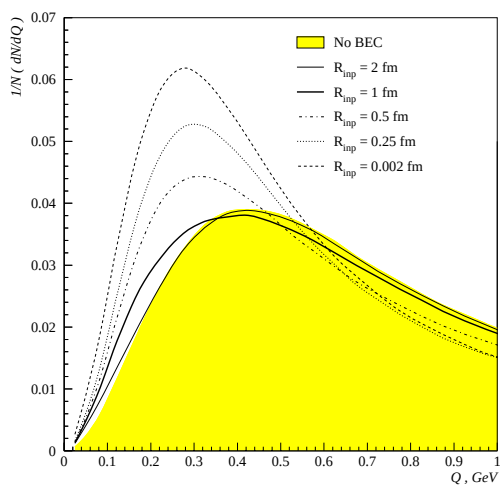

Figure 3: Distribution of Q as a function of the input source radii R_{inp}. Shaded area shows this distribution in absence of BEC.

Therefore, the position of the peak in the non-correlated dN/dQ distribution constitutes the limitation of the measured correlation width R and can be interpreted as a new length scale. This conclusion is also valid for transverse correlation radii (see Fig. 4). In the longitudinal direction, $dN/dQ_{\|}$ has less rapid falloff and peaks at a very small $Q_{\|}$ value due to the LCMS properties, and thus is virtually insensitive to the mentioned length scale.

As a result, one should state that the built-in JETSET model for simulating BEC is fully applicable only for sufficiently big sizes of boson source :

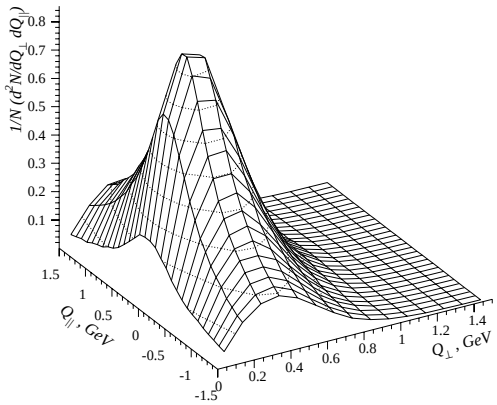

Figure 4: Two-dimensional distribution $d^2N/dQ_\perp dQ_\parallel$ in absence of BEC.

above $1\,fm$. At the same time, experimental data indicate that this size is around $0.5\,fm$ at the Z peak [9]. This means that, at first, this kind of model has no predictive power. At second, one should be very careful when using JETSET with this model for calculation of detector corrections, because it can not produce an adequate unfolding matrix.

It has to be mentioned that nowadays some other models for simulation of BEC are being developed [10,11]. They use direct implementation of the Bose-Einstein interference into the string model, being theoretically accurate in this sense. At the moment they take too much computing resources to be used by high-energy physics experiments, but they do have predictive power. One of the most interesting predictions is that the transverse component of the boson source size, $R_\perp$, must be significantly smaller then the longitudinal one, $R_\parallel$. As one can see, it is being confirmed by the preliminary DELPHI results, but it is not the case for the present JETSET version. This must encourage further works towards developing and implementing advanced models for the BEC simulation in particle generators.

Acknowledgments

We would like to thank T. Sjöstrand for valuable help during this analysis. Some of us (O. S. and B. L.) are grateful to the organisers of the "Correlations and Fluctuations 98" workshop for their hospitality and for creating an outstanding working environment.

References

1. L. Lönnblad and T. Sjöstrand, *Phys. Lett.* B **351**, 293 (1995).
2. V. Kartvelishvili, R. Kvatadze, R. Møller, "Estimating the effects of Bose-Einstein correlations on the W mass measurement at LEP2", University of Manchester preprint MC-TH-97/04, MAN/HEP/97/1
3. T. Sjöstrand, *Comp. Phys. Comm.* **28**, 229 (1983);
   T. Sjöstrand, PYTHIA *5.6 and* JETSET *7.3*, CERN-TH.6488/92 (1992).
4. S. Haywood, "Where Are We Going With Bose-Einstein – a Mini Review", RAL Report RAL-94-074
5. K. Fiałkowski and R. Wit, *Z. Phys.* C **74**, 145 (1997).
6. B. Lörstad, *Int. J. Mod. Phys.* A4 **12**, 2861 (1989).
7. T. Csörgő and S. Pratt, in "Proceedings of the Workshop on Relativistic Heavy Ion Physics", KFKI-1991-28/A, p75.
8. B. Lörstad, O. Smirnova: "Transverse Mass Dependence of Bose-Einstein Correlation Radii in e^+e^- Annihilation at LEP Energies": Proceedings of the 7th International Workshop on Multiparticle Production 'Correlations and Fluctuations', June 30 to July 6, 1996, Nijmegen, The Netherlands.
9. OPAL Coll., P .D. Acton et al., *Phys. Lett.* B **267**, 143 (1991);
   DELPHI Coll., P. Abreu et al., *Phys. Lett.* B **286**, 201 (1992);
   ALEPH Coll., D. Decamp et al., *Z. Phys.* C **54**, 75 (1992).
10. B. Andersson and M. Ringnér, *Nucl. Phys.* B **513**, 627 (1998);
    B. Andersson and M. Ringnér, *Phys. Lett.* B **421**, 283 (1998).
11. Ŝ. Todorova-Nová, J. Rameš, " Simulation of Bose-Einstein effect using space-time aspects of Lund string fragmentation model", IReS 97-29, PRA-HEP 97/16.

Appendix C

ELSEVIER

6 January 2000

PHYSICS LETTERS B

Physics Letters B 471 (2000) 460–470

Two-dimensional analysis of the Bose-Einstein correlations in e^+e^- annihilation at the Z^0 peak

DELPHI Collaboration

P. Abreu [u], W. Adam [ay], T. Adye [ak], P. Adzic [k], Z. Albrecht [q], T. Alderweireld [b], G.D. Alekseev [p], R. Alemany [ax], T. Allmendinger [q], P.P. Allport [v], S. Almehed [x], U. Amaldi [i,ab], N. Amapane [at], S. Amato [av], E.G. Anassontzis [c], P. Andersson [as], A. Andreazza [i], S. Andringa [u], P. Antilogus [y], W-D. Apel [q], Y. Arnoud [i], B. Åsman [as], J-E. Augustin [y], A. Augustinus [i], P. Baillon [i], P. Bambade [s], F. Barao [u], G. Barbiellini [au], R. Barbier [y], D.Y. Bardin [p], G. Barker [q], A. Baroncelli [am], M. Battaglia [o], M. Baubillier [w], K-H. Becks [ba], M. Begalli [f], A. Behrmann [ba], P. Beilliere [h], Yu. Belokopytov [i], K. Belous [aq], N.C. Benekos [af], A.C. Benvenuti [e], C. Berat [n], M. Berggren [w], D. Bertrand [b], M. Besancon [an], M. Bigi [at], M.S. Bilenky [p], M-A. Bizouard [s], D. Bloch [j], H.M. Blom [ae], M. Bonesini [ab], M. Boonekamp [an], P.S.L. Booth [v], A.W. Borgland [d], G. Borisov [s], C. Bosio [ap], O. Botner [aw], E. Boudinov [ae], B. Bouquet [s], C. Bourdarios [s], T.J.V. Bowcock [v], I. Boyko [p], I. Bozovic [k], M. Bozzo [m], M. Bracko [ar], P. Branchini [am], R.A. Brenner [aw], P. Bruckman [i], J-M. Brunet [h], L. Bugge [ag], T. Buran [ag], B. Buschbeck [ay], P. Buschmann [ba], S. Cabrera [ax], M. Caccia [aa], M. Calvi [ab], T. Camporesi [i], V. Canale [al], F. Carena [i], L. Carroll [v], C. Caso [m], M.V. Castillo Gimenez [ax], A. Cattai [i], F.R. Cavallo [e], V. Chabaud [i], M. Chapkin [aq], Ph. Charpentier [i], P. Checchia [aj], G.A. Chelkov [p], R. Chierici [at], P. Chliapnikov [i,aq], P. Chochula [g], V. Chorowicz [y], J. Chudoba [ad], K. Cieslik [r], P. Collins [i], R. Contri [m], E. Cortina [ax], G. Cosme [s], F. Cossutti [i], H.B. Crawley [a], D. Crennell [ak], S. Crepe [n], G. Crosetti [m], J. Cuevas Maestro [ah], S. Czellar [o], M. Davenport [i], W. Da Silva [w], G. Della Ricca [au], P. Delpierre [z], N. Demaria [i], A. De Angelis [au], W. De Boer [q], C. De Clercq [b], B. De Lotto [au], A. De Min [aj], L. De Paula [av], H. Dijkstra [i], L. Di Ciaccio [i,al], J. Dolbeau [h], K. Doroba [az], M. Dracos [j], J. Drees [ba], M. Dris [af], A. Duperrin [y], J-D. Durand [i], G. Eigen [d], T. Ekelof [aw], G. Ekspong [as], M. Ellert [aw], M. Elsing [i], J-P. Engel [j], M. Espirito Santo [i], G. Fanourakis [k],

0370-2693/00/$ - see front matter © 2000 Published by Elsevier Science B.V. All rights reserved.
PII: S0370-2693(99)01391-X

D. Fassouliotis [k], J. Fayot [w], M. Feindt [q], A. Ferrer [ax], E. Ferrer-Ribas [s], F. Ferro [m], S. Fichet [w], A. Firestone [a], U. Flagmeyer [ba], H. Foeth [i], E. Fokitis [af], F. Fontanelli [m], B. Franek [ak], A.G. Frodesen [d], R. Fruhwirth [ay], F. Fulda-Quenzer [s], J. Fuster [ax], A. Galloni [v], D. Gamba [at], S. Gamblin [s], M. Gandelman [av], C. Garcia [ax], C. Gaspar [i], M. Gaspar [av], U. Gasparini [aj], Ph. Gavillet [i], E.N. Gazis [af], D. Gele [j], T. Geralis [k], N. Ghodbane [y], I. Gil [ax], F. Glege [ba], R. Gokieli [i,az], B. Golob [i,ar], G. Gomez-Ceballos [ao], P. Goncalves [u], I. Gonzalez Caballero [ao], G. Gopal [ak], L. Gorn [a], Yu. Gouz [aq], V. Gracco [m], J. Grahl [a], E. Graziani [am], P. Gris [an], G. Grosdidier [s], K. Grzelak [az], J. Guy [ak], C. Haag [q], F. Hahn [i], S. Hahn [ba], S. Haider [i], A. Hallgren [aw], K. Hamacher [ba], J. Hansen [ag], F.J. Harris [ai], V. Hedberg [i,x], S. Heising [q], J.J. Hernandez [ax], P. Herquet [b], H. Herr [i], T.L. Hessing [ai], J.-M. Heuser [ba], E. Higon [ax], S-O. Holmgren [as], P.J. Holt [ai], S. Hoorelbeke [b], M. Houlden [v], J. Hrubec [ay], M. Huber [q], K. Huet [b], G.J. Hughes [v], K. Hultqvist [i,as], J.N. Jackson [v], R. Jacobsson [i], P. Jalocha [r], R. Janik [g], Ch. Jarlskog [x], G. Jarlskog [x], P. Jarry [an], B. Jean-Marie [s], D. Jeans [ai], E.K. Johansson [as], P. Jonsson [y], C. Joram [i], P. Juillot [j], L. Jungermann [q], F. Kapusta [w], K. Karafasoulis [k], S. Katsanevas [y], E.C. Katsoufis [af], R. Keranen [q], G. Kernel [ar], B.P. Kersevan [ar], B.A. Khomenko [p], N.N. Khovanski [p], A. Kiiskinen [o], B. King [v], A. Kinvig [v], N.J. Kjaer [i], O. Klapp [ba], H. Klein [i], P. Kluit [ae], P. Kokkinias [k], V. Kostioukhine [aq], C. Kourkoumelis [c], O. Kouznetsov [p], M. Krammer [ay], E. Kriznic [ar], Z. Krumstein [p], P. Kubinec [g], J. Kurowska [az], K. Kurvinen [o], J.W. Lamsa [a], D.W. Lane [a], V. Lapin [aq], J-P. Laugier [an], R. Lauhakangas [o], G. Leder [ay], F. Ledroit [n], V. Lefebure [b], L. Leinonen [as], A. Leisos [k], R. Leitner [ad], J. Lemonne [b], G. Lenzen [ba], V. Lepeltier [s], T. Lesiak [r], M. Lethuillier [an], J. Libby [ai], W. Liebig [ba], D. Liko [i], A. Lipniacka [i,as], I. Lippi [aj], B. Loerstad [x], J.G. Loken [ai], J.H. Lopes [av], J.M. Lopez [ao], R. Lopez-Fernandez [n], D. Loukas [k], P. Lutz [an], L. Lyons [ai], J. MacNaughton [ay], J.R. Mahon [f], A. Maio [u], A. Malek [ba], T.G.M. Malmgren [as], S. Maltezos [af], V. Malychev [p], F. Mandl [ay], J. Marco [ao], R. Marco [ao], B. Marechal [av], M. Margoni [aj], J-C. Marin [i], C. Mariotti [i], A. Markou [k], C. Martinez-Rivero [s], F. Martinez-Vidal [ax], S. Marti i Garcia [i], J. Masik [l], N. Mastroyiannopoulos [k], F. Matorras [ao], C. Matteuzzi [ab], G. Matthiae [al], F. Mazzucato [aj], M. Mazzucato [aj], M. Mc Cubbin [v], R. Mc Kay [a], R. Mc Nulty [v], G. Mc Pherson [v], C. Meroni [aa], W.T. Meyer [a], E. Migliore [i], L. Mirabito [y], W.A. Mitaroff [ay], U. Mjoernmark [x], T. Moa [as], M. Moch [q], R. Moeller [ac], K. Moenig [i,1], M.R. Monge [m], D. Moraes [av], X. Moreau [w],

[1] Now at DESY-Zeuthen, Platanenallee 6, D-15735 Zeuthen, Germany.

P. Morettini [m], G. Morton [ai], U. Mueller [ba], K. Muenich [ba], M. Mulders [ae], C. Mulet-Marquis [n], R. Muresan [x], W.J. Murray [ak], B. Muryn [r], G. Myatt [ai], T. Myklebust [ag], F. Naraghi [n], M. Nassiakou [k], F.L. Navarria [e], S. Navas [ax], K. Nawrocki [az], P. Negri [ab], N. Neufeld [i], R. Nicolaidou [an], B.S. Nielsen [ac], P. Niezurawski [az], M. Nikolenko [j,p], V. Nomokonov [o], A. Nygren [x], V. Obraztsov [aq], A.G. Olshevski [p], A. Onofre [u], R. Orava [o], G. Orazi [j], K. Osterberg [o], A. Ouraou [an], M. Paganoni [ab], S. Paiano [e], R. Pain [w], R. Paiva [u], J. Palacios [ai], H. Palka [r], Th.D. Papadopoulou [i,af], L. Pape [i], C. Parkes [i], F. Parodi [m], U. Parzefall [v], A. Passeri [am], O. Passon [ba], T. Pavel [x], M. Pegoraro [aj], L. Peralta [u], M. Pernicka [ay], A. Perrotta [e], C. Petridou [au], A. Petrolini [m], H.T. Phillips [ak], F. Pierre [an], M. Pimenta [u], E. Piotto [aa], T. Podobnik [ar], M.E. Pol [f], G. Polok [r], P. Poropat [au], V. Pozdniakov [p], P. Privitera [al], N. Pukhaeva [p], A. Pullia [ab], D. Radojicic [ai], S. Ragazzi [ab], H. Rahmani [af], J. Rames [l], P.N. Ratoff [t], A.L. Read [ag], P. Rebecchi [i], N.G. Redaelli [ab], M. Regler [ay], J. Rehn [q], D. Reid [ae], R. Reinhardt [ba], P.B. Renton [ai], L.K. Resvanis [c], F. Richard [s], J. Ridky [l], G. Rinaudo [at], I. Ripp-Baudot [j], O. Rohne [ag], A. Romero [at], P. Ronchese [aj], E.I. Rosenberg [a], P. Rosinsky [g], P. Roudeau [s], T. Rovelli [e], Ch. Royon [an], V. Ruhlmann-Kleider [an], A. Ruiz [ao], H. Saarikko [o], Y. Sacquin [an], A. Sadovsky [p], G. Sajot [n], J. Salt [ax], D. Sampsonidis [k], M. Sannino [m], Ph. Schwemling [w],B. Schwering [ba], U. Schwickerath [q], F. Scuri [au], P. Seager [t], Y. Sedykh [p], A.M. Segar [ai], N. Seibert [q], R. Sekulin [ak], R.C. Shellard [f], M. Siebel [ba], L. Simard [an], F. Simonetto [aj], A.N. Sisakian [p], G. Smadja [y], O. Smirnova [x], G.R. Smith [ak], A. Sokolov [aq], O. Solovianov [aq], A. Sopczak [q], R. Sosnowski [az], T. Spassov [u], E. Spiriti [am], S. Squarcia [m], C. Stanescu [am], S. Stanic [ar], M. Stanitzki [q], K. Stevenson [ai], A. Stocchi [s], J. Strauss [ay], R. Strub [j], B. Stugu [d], M. Szczekowski [az], M. Szeptycka [az], T. Tabarelli [ab], A. Taffard [v], F. Tegenfeldt [aw], F. Terranova [ab], J. Thomas [ai], J. Timmermans [ae], N. Tinti [e], L.G. Tkatchev [p], M. Tobin [v], S. Todorova [i], A. Tomaradze [b], B. Tome [u], A. Tonazzo [i], L. Tortora [am], P. Tortosa [ax], G. Transtromer [x], D. Treille [i], G. Tristram [h], M. Trochimczuk [az], C. Troncon [aa], M-L. Turluer [an], I.A. Tyapkin [p], P. Tyapkin [x], S. Tzamarias [k], O. Ullaland [i], V. Uvarov [aq], G. Valenti [i,e], E. Vallazza [au], C. Vander Velde [b], P. Van Dam [ae], W. Van den Boeck [b], W.K. Van Doninck [b], J. Van Eldik [i,ae], A. Van Lysebetten [b], N. van Remortel [b], I. Van Vulpen [ae], G. Vegni [aa], L. Ventura [aj], W. Venus [ak,i], F. Verbeure [b], P. Verdier [y], M. Verlato [aj], L.S. Vertogradov [p], V. Verzi [aa], D. Vilanova [an], L. Vitale [au], E. Vlasov [aq], A.S. Vodopyanov [p], G. Voulgaris [c], V. Vrba [l], H. Wahlen [ba], C. Walck [as], A.J. Washbrook [v], C. Weiser [i], D. Wicke [ba], J.H. Wickens [b], G.R. Wilkinson [ai], M. Winter [j], M. Witek [r], G. Wolf [i], J. Yi [a], O. Yushchenko [aq], A. Zaitsev [aq], A. Zalewska [r], P. Zalewski [az], D. Zavrtanik [ar],

E. Zevgolatakos [k], N.I. Zimin [p,x], A. Zintchenko [p], Ph. Zoller [j], G.C. Zucchelli [as], G. Zumerle [aj]

[a] Department of Physics and Astronomy, Iowa State University, Ames, IA 50011-3160, USA
[b] Physics Department, Universitaire Instelling Antwerpen, Universiteitsplein 1, B-2610 Antwerpen, Belgium, and IIHE, ULB-VUB, Pleinlaan 2, B-1050 Brussels, Belgium, and Faculté des Sciences, Université de l'Etat Mons, Av. Maistriau 19, B-7000 Mons, Belgium
[c] Physics Laboratory, University of Athens, Solonos Str. 104, GR-10680 Athens, Greece
[d] Department of Physics, University of Bergen, Allégaten 55, NO-5007 Bergen, Norway
[e] Dipartimento di Fisica, Università di Bologna and INFN, Via Irnerio 46, IT-40126 Bologna, Italy
[f] Centro Brasileiro de Pesquisas Físicas, rua Xavier Sigaud 150, BR-22290 Rio de Janeiro, Brazil, and Departamento de Física, Pontifícia Universidade Católica, C.P. 38071 BR-22453 Rio de Janeiro, Brazil, and Instituto de Física, Universidade Estadual do Rio de Janeiro, rua São Francisco Xavier 524, Rio de Janeiro, Brazil
[g] Comenius University, Faculty of Mathematics and Physics, Mlynska Dolina, SK-84215 Bratislava, Slovakia
[h] Collège de France, Laboratoire de Physique Corpusculaire, IN2P3-CNRS, FR-75231 Paris Cedex 05, France
[i] CERN, CH-1211 Geneva 23, Switzerland
[j] Institut de Recherches Subatomiques, IN2P3 - CNRS / ULP - BP20, FR-67037 Strasbourg Cedex, France
[k] Institute of Nuclear Physics, N.C.S.R. Demokritos, P.O. Box 60228, GR-15310 Athens, Greece
[l] FZU, Institute of Physics of the C.A.S. High Energy Physics Division, Na Slovance 2, CZ-180 40 Praha 8, Czech Republic
[m] Dipartimento di Fisica, Università di Genova and INFN, Via Dodecaneso 33, IT-16146 Genova, Italy
[n] Institut des Sciences Nucléaires, IN2P3-CNRS, Université de Grenoble 1, FR-38026 Grenoble Cedex, France
[o] Helsinki Institute of Physics, HIP, P.O. Box 9, FI-00014 Helsinki, Finland
[p] Joint Institute for Nuclear Research, Dubna, Head Post Office, P.O. Box 79, RU-101 000 Moscow, Russian Federation
[q] Institut für Experimentelle Kernphysik, Universität Karlsruhe, Postfach 6980, DE-76128 Karlsruhe, Germany
[r] Institute of Nuclear Physics and University of Mining and Metalurgy, Ul. Kawiory 26a, PL-30055 Krakow, Poland
[s] Université de Paris-Sud, Laboratoire de l'Accélérateur Linéaire, IN2P3-CNRS, Bât. 200, FR-91405 Orsay Cedex, France
[t] School of Physics and Chemistry, University of Lancaster, Lancaster LA1 4YB, UK
[u] LIP, IST, FCUL - Av. Elias Garcia, 14-1°, PT-1000 Lisboa Codex, Portugal
[v] Department of Physics, University of Liverpool, P.O. Box 147, Liverpool L69 3BX, UK
[w] LPNHE, IN2P3-CNRS, Université de Paris VI et VII, Tour 33 (RdC), 4 place Jussieu, FR-75252 Paris Cedex 05, France
[x] Department of Physics, University of Lund, Sölvegatan 14, SE-223 63 Lund, Sweden
[y] Université Claude Bernard de Lyon, IPNL, IN2P3-CNRS, FR-69622 Villeurbanne Cedex, France
[z] Université d'Aix - Marseille II - CPP, IN2P3-CNRS, FR-13288 Marseille Cedex 09, France
[aa] Dipartimento di Fisica, Università di Milano and INFN-MILANO, Via Celoria 16, IT-20133 Milan, Italy
[ab] Dipartimento di Fisica, Università di Milano-Bicocca and INFN-MILANO, Piazza delle Scienze 2, IT-20126 Milan, Italy
[ac] Niels Bohr Institute, Blegdamsvej 17, DK-2100 Copenhagen Ø, Denmark
[ad] IPNP of MFF, Charles University, Areal MFF, V Holesovickach 2, CZ-180 00, Praha 8, Czech Republic
[ae] NIKHEF, Postbus 41882, NL-1009 DB Amsterdam, The Netherlands
[af] National Technical University, Physics Department, Zografou Campus, GR-15773 Athens, Greece
[ag] Physics Department, University of Oslo, Blindern, NO-1000 Oslo 3, Norway
[ah] Departamento de Fisica, Universidad Oviedo, Avda. Calvo Sotelo s / n, ES-33007 Oviedo, Spain
[ai] Department of Physics, University of Oxford, Keble Road, Oxford OX1 3RH, UK
[aj] Dipartimento di Fisica, Università di Padova and INFN, Via Marzolo 8, IT-35131 Padua, Italy
[ak] Rutherford Appleton Laboratory, Chilton, Didcot OX11 OQX, UK
[al] Dipartimento di Fisica, Università di Roma II and INFN, Tor Vergata, IT-00173 Rome, Italy
[am] Dipartimento di Fisica, Università di Roma III and INFN, Via della Vasca Navale 84, IT-00146 Rome, Italy
[an] DAPNIA / Service de Physique des Particules, CEA-Saclay, FR-91191 Gif-sur-Yvette Cedex, France
[ao] Instituto de Fisica de Cantabria (CSIC-UC), Avda. los Castros s / n, ES-39006 Santander, Spain
[ap] Dipartimento di Fisica, Università degli Studi di Roma La Sapienza, Piazzale Aldo Moro 2, IT-00185 Rome, Italy
[aq] Institute for High Energy Physics, Serpukov P.O. Box 35, Protvino (Moscow Region), Russian Federation
[ar] J. Stefan Institute, Jamova 39, SI-1000 Ljubljana, Slovenia and Laboratory for Astroparticle Physics, Nova Gorica Polytechnic, Kostanjeviska 16a, SI-5000 Nova Gorica, Slovenia, and Department of Physics, University of Ljubljana, SI-1000 Ljubljana, Slovenia
[as] Fysikum, Stockholm University, Box 6730, SE-113 85 Stockholm, Sweden
[at] Dipartimento di Fisica Sperimentale, Università di Torino and INFN, Via P. Giuria 1, IT-10125 Turin, Italy
[au] Dipartimento di Fisica, Università di Trieste and INFN, Via A. Valerio 2, IT-34127 Trieste, Italy, and Istituto di Fisica, Università di Udine, IT-33100 Udine, Italy
[av] Universidade Federal do Rio de Janeiro, C.P. 68528 Cidade Universitária, Ilha do Fundão BR-21945-970 Rio de Janeiro, Brazil

[aw] Department of Radiation Sciences, University of Uppsala, P.O. Box 535, SE-751 21 Uppsala, Sweden
[ax] IFIC, Valencia-CSIC, and D.F.A.M.N., Universidad de Valencia, Avda. Dr. Moliner 50, ES-46100 Burjassot (Valencia), Spain
[ay] Institut für Hochenergiephysik, Österreichische Akademie der Wissenschaften, Nikolsdorfergasse 18, AT-1050 Vienna, Austria
[az] Institute for Nuclear Studies and University of Warsaw, Ul. Hoza 69, PL-00681 Warsaw, Poland
[ba] Fachbereich Physik, University of Wuppertal, Postfach 100 127, DE-42097 Wuppertal, Germany

Received 26 November 1999; received in revised form 29 November 1999; accepted 29 November 1999
Editor: L. Montanet

Abstract

The study of the directional dependence of two-particle correlations in the hadronic decays of the Z^0 boson is performed using the data collected by the DELPHI experiment in the 1992–1995 running periods. The comparison between the transverse, $R_\perp$, and longitudinal, $R_\parallel$, correlation radii confirms the string model prediction that the transverse correlation length is smaller than the longitudinal one, with the measured values of $R_\perp = 0.53 \pm 0.08$ fm and $R_\parallel = 0.85 \pm 0.08$ fm, for selected $Z^0 \to q\bar{q}$ events. © 2000 Published by Elsevier Science B.V. All rights reserved.

1. Introduction

Detailed studies of the two-particle Bose-Einstein correlations (BEC) in Z^0 hadronic decays in e^+e^- annihilation allow the determination of the shape of the source of bosons, which gives the possibility to analyse the spatial and temporal characteristics of the hadronisation region. These studies are of considerable interest mainly due to the recent predictions of possible influence of BEC on the measured value of the W boson mass in e^+e^- annihilation [1,2]. Estimates of the strength of this effect have been made using the Monte Carlo particle generator JETSET [3], involving a simple algorithm for the two-particle BEC simulation which uses a correlation function in terms of the invariant four-momentum difference of identical partons, Q. This algorithm is known to reproduce well basic features of BEC in experimental data, like the shape of the correlation function in terms of Q [4] and the shift of the ρ^0 mass [5], but it does not describe other related effects, like the higher order correlations [6], neither it reproduces its own input parameters in a wide range [7]. More detailed tests are necessary in order to establish the extent of applicability of the mentioned algorithm and the reliability of its predictions.

In the two-jet hadronic decays $Z^0 \to q\bar{q}$, the comparison between the transverse and longitudinal radii of the BEC (with respect to the initial parton direction of motion) can test the string model prediction [8] that the transverse correlation length is considerably smaller than the longitudinal one.

Until recently, studies of the identical-boson correlations in e^+e^- annihilation process at LEP energies have concentrated on the shape of the two-particle correlation function in terms of Q [4]. At lower energies, several collaborations have studied Bose-Einstein correlations using two-dimensional distributions of components of Q [9]. Multidimensional analyses of the BEC are now being made by the LEP experiments as well. Studies performed by the L3 [10] experiment and preliminary results by DELPHI [11] and OPAL [12] at LEP1 energies indicate that the transverse size of the boson source in e^+e^- annihilation is smaller than the longitudinal one.

Here, the two-dimensional analysis of BEC in Z^0 hadronic decays is presented, using DELPHI data collected in the 1992–1995 running periods. Two-particle correlations are studied in terms of different components of the four-momentum difference. Results are compared to those obtained from the analysis of events generated by JETSET.

2. Correlation function definition

The correlation function, C_2, of two identical bosons is defined as [13]

$$C_2(p_1,p_2) = \frac{P(p_1,p_2)}{P(p_1)P(p_2)}, \tag{1}$$

where p_1 and p_2 are the four-momenta of the two particles, $P(p_1,p_2)$ is the two-particle probability

density and $P(p_1)$ and $P(p_2)$ represent single-particle probability densities. The invariant four-momentum difference Q is defined as

$$Q = \sqrt{(E_1 - E_2)^2 - (\boldsymbol{p}_1 - \boldsymbol{p}_2)^2}\,, \tag{2}$$

where $\boldsymbol{p}_1$ and $\boldsymbol{p}_2$ are the momenta of the two particles, and E_1, E_2 are their energies. As long as bosons, which are subject to BEC, have similar momenta, one would expect to observe an enhanced production of pairs with low values of Q as compared to the non-correlated case.

The most commonly used [13] parametrization of C_2 is:

$$C_2(Q) = n\left(1 + \lambda e^{-R^2 Q^2}\right), \tag{3}$$

where the parameter λ is interpreted as the strength of the correlation, and R as the size of the source of bosons, or the correlation radius. n is the overall normalisation.

In expression (3), R corresponds to an average over the spatial and temporal source dimensions. To probe the actual shape of a boson source, Bose-Einstein correlations must be studied in terms of the various components of the three-momentum difference $\boldsymbol{Q} = \boldsymbol{p_1} - \boldsymbol{p_2}$ in a chosen coordinate system.

For this purpose, the Longitudinal Centre-of-Mass System [8,14] (LCMS) is often used. The LCMS is defined for each pair of particles as the system in which the sum of the two particles' momenta is perpendicular to a selected reference axis (see Fig. 1). The reference axis has to be a physical axis of the process: for example, in e^+e^- annihilation it can be the direction of a primary parton, or of the corresponding jet. In this analysis, the thrust axis was chosen as the reference (see Section 4). In such a system, $\boldsymbol{Q}$ is decomposed into the following components: Q_{long}, parallel to the thrust axis; $Q_{t,\text{out}}$, collinear with the sum of the two particles' momenta, and the complementary $Q_{t,\text{side}}$, perpendicular to both Q_{long} and $Q_{t,\text{out}}$. This system is convenient for calculations and interpretations. The projection of the momentum sum of the two particles is non-zero only in the 't,out' direction. The spatial dimensions of the source effect all components of Q. However the energy difference and hence the temporal dimension of the source, couples only to the $Q_{t,\text{out}}$ component. If the string model is considered, the longitudinal direction of the LCMS has to be aligned with the direction of motion of the initial partons, so that the system itself will be the local rest frame of a string.

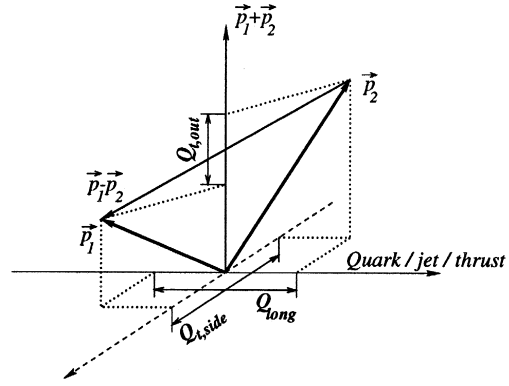

Fig. 1. The Longitudinal Centre-of-Mass System is defined, for each pair of particles, as the system in which the sum of the two particles' momenta is perpendicular to a selected reference axis. The reference axis has to be a physical axis of the process.

By analogy with Eq. (3), the three-dimensional correlation function in LCMS can be parametrized as:

$$C_2\left(Q_{t,\text{out}}, Q_{t,\text{side}}, Q_{\text{long}}\right) = n\left(1 + \lambda e^{-Q^2_{t,\text{out}} R^2_{t,\text{out}} - Q^2_{t,\text{side}} R^2_{t,\text{side}} - Q^2_{\text{long}} R^2_{\text{long}}}\right). \tag{4}$$

In this analysis, the two-dimensional projection of the LCMS is used, with longitudinal component $Q_\parallel \equiv Q_{\text{long}}$ and perpendicular component $Q_\perp = \sqrt{Q^2_{t,\text{out}} + Q^2_{t,\text{side}}}$. The parametrization of C_2 in the two-dimensional case is chosen here as:

$$C_2(Q_\perp, Q_\parallel) = n\left(1 + \lambda e^{-Q^2_\perp R^2_\perp - Q^2_\parallel R^2_\parallel}\right). \tag{5}$$

3. Data selection

Data collected by the DELPHI detector [15] in 1992–1995 at centre-of-mass energies around $\sqrt{s} = 91.2$ GeV were used.

Only charged particles in hadronic events were considered in the analysis [15]. The tracks were taken into account if their impact parameter was below 1 cm in the transverse plane and below 5 cm along the beam axis (to reduce contributions from

long-living resonance decays), the measured track length was above 50 cm, the momentum p was in the range of 0.1 GeV$/c < p <$ 50 GeV$/c$ and the polar angle between 25° and 155°. All particles were assumed to be pions.

Hadronic events were selected by requiring that: (a) they contained at least 5 charged particles with momentum above 0.2 GeV$/c$; (b) the total energy of all charged particles exceeded 15 GeV; (c) each hemisphere with respect to the sphericity axis contained a total energy of charged particles larger than 3 GeV; (d) the polar angle of the sphericity axis was between 40° and 140°, so that the events are well contained inside the TPC.

In this analysis two-jet events were selected in order to compare the result with the theoretical prediction [8]. These events are also convenient because the procedures of preparing the reference sample (see Section 4) and the definition of LCMS are easier to apply and to understand in this case. Since the thrust axis of the two-jet events is well aligned with the direction of motion of the initial partons, its direction can be selected as the physical axis of the hadronization process, and the possible influence of hard gluon radiation can be neglected. The two-jet event selection was done using the LUCLUS [3] clustering algorithm (with parameter $d_{\mathrm{join}} = 8$ GeV$/c$), requiring that the thrust value be more than 0.95, and, that the jet acollinearity shall not exceed 5°. A total of about 810 000 events satisfied these criteria.

To purify the reference sample and to reduce the background, additional selection criteria were applied for each pair of particles. To stay away from the two-particle phase-space limits, where kinematic correlations are significant, a pair of tracks was selected for the analysis, if both particles had momenta below 5 GeV$/c$. To exclude the partially overlapping tracks which can be poorly reconstructed, the angle between tracks was required to exceed 2°. To reduce the correlations caused by the local transverse momentum compensation, pairs were rejected if the angle between tracks in a plane, transverse to the thrust axis, was more than 120°. In addition, to reduce the contribution from resonance decays and to eliminate the region where the Coulomb correction is substantial, pairs were rejected if their Q was less than 0.06 GeV.

4. Correlation function measurement

The measurement of the correlation function (1) in the two-dimensional LCMS requires accumulation of the double-differential distributions $d^2N^{\pm\pm}/dQ_\perp\, dQ_\parallel$, where $N^{\pm\pm}$ is the number of like-sign pairs. All the data were corrected for detector effects. Events generated with the JETSET 7.3 PS model with DELPHI tuning [16] were used to estimate the acceptance corrections and to account for effects arising from the limited detector resolution. The selected events were passed through the DELSIM [17] detector simulation and the same selection criteria were used as for real data. Correction coefficients $c(Q_\perp, Q_\parallel)$ were calculated as the ratios of distributions at the generation level (JETSET only) to those at the reconstruction level (JETSET + DELSIM):

$$c(Q_\perp, Q_\parallel) = \frac{\left(\dfrac{d^2N^{\pm\pm}}{dQ_\perp\, dQ_\parallel}\right)_{\mathrm{gen}}}{\left(\dfrac{d^2N^{\pm\pm}}{dQ_\perp\, dQ_\parallel}\right)_{\mathrm{rec}}}, \tag{6}$$

where indices ‘gen’ and ‘rec’ refer to the generation and reconstruction level respectively.

The two-particle correlation function definition in Eq. (1) requires the knowledge of the product of the single-particle probability densities, $P(p_1)P(p_2)$. Due to the phase space limitations, it is difficult to construct this product. Therefore it is often replaced by $P_0(p_1, p_2)$, which is equal to $P(p_1)P(p_2)$ in a hypothetical case of no correlations. Technically this means that one has to construct an artificial reference sample of particles which are not subject to Bose-Einstein correlations, but obey the same kinematics as a regular event. Several techniques for obtaining a reference sample can be considered, like using the unlike-sign particle combinations, Monte Carlo simulated events without the BEC effect, or the event-mixing technique. It has been established [9] that the latter is the most reliable method. To construct the mixed reference sample, all events are rotated to a new coordinate system, which has the z axis along the thrust axis. The sample is then obtained by combining a particle from one event randomly with a like-charge particle from another.

The mixed reference sample is prepared using the same set of hadronic events as for the real data. Within the applied selection criteria, the mixed sample does not contain BEC and satisfies most of the basic requirements for the reference sample [9]. It has no additional dynamical correlations, like those coming from the K^0 and ρ^0 decays in the case of unlike-charge reference sample. Since only two-jet events are used, and the detector corrections are applied, the mixed sample contains the correlation due to the jet structure of events. Correlations due to energy-momentum conservation are also included, since the pairs close to the phase-space limits are removed (see Section 3). However, the mixing procedure does not conserve energy and momentum in general, affects the normalisation, and destroys not only the Bose-Einstein correlation but some other kinds of correlations, like those coming from the local transverse momentum compensation. Fig. 2 shows the effect of the mixing on the original Q distributions in detector-corrected DELPHI data, which contain physical BEC, and JETSET generated events without BEC simulation. Enhancement with respect to the reference distribution in the region of $Q < 0.25$ GeV is readily seen in data, manifesting the presence of BEC. In the case of the BEC-free Monte Carlo events (Fig. 2(b)), no such enhancement can be observed, with the original and the reference distributions being identical at small Q values. This illustrates the reliability of the mixing technique.

From Fig. 2(b) one can see the unwanted feature of the mixing procedure at $Q > 0.25$ GeV: the reference sample distribution deviates from the original one. This difference however is not essential for the analysis, since the region of genuine two-particle BEC lies below that value [4]. To correct for this effect, the measured two-particle correlation function $C_2(Q)$ is calculated as the double-ratio:

$$C_2(Q_\perp, Q_\parallel) = \frac{r_{\mathrm{data}}(Q_\perp, Q_\parallel)}{r_{\mathrm{noBE}}(Q_\perp, Q_\parallel)}, \tag{7}$$

where

$$r_{\mathrm{data}}(Q_\perp, Q_\parallel) = \frac{\left(\dfrac{d^2N^{\pm\pm}}{dQ_\perp\, dQ_\parallel}\right)_{\mathrm{data}}}{\left(\dfrac{d^2N^{\pm\pm}}{dQ_\perp\, dQ_\parallel}\right)_{\mathrm{data,mix}}}$$

and

$$r_{\mathrm{noBE}}(Q_\perp, Q_\parallel) = \frac{\left(\dfrac{d^2N^{\pm\pm}}{dQ_\perp\, dQ_\parallel}\right)_{\mathrm{noBE}}}{\left(\dfrac{d^2N^{\pm\pm}}{dQ_\perp\, dQ_\parallel}\right)_{\mathrm{noBE,mix}}}. \tag{8}$$

Here $(d^2N^{\pm\pm}/dQ_\perp\, dQ_\parallel)_{\mathrm{data}}$ is the Q-distribution of the pion pairs with the same charge in real data, while the subscript 'data, mix' denotes the same quantity but for pairs from the reference sample. The indices 'noBE' and 'noBE, mix' refer to analogous

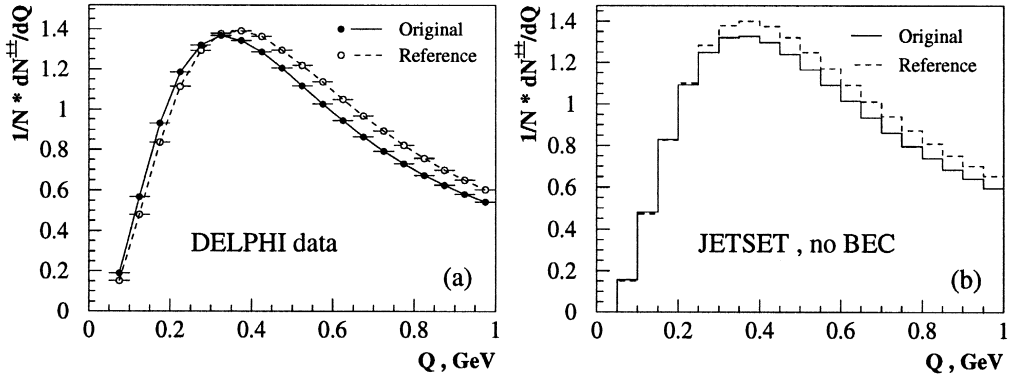

Fig. 2. Comparison of the original Q distributions of like-charge particle pairs, and the reference ones obtained by the mixing procedure: (a) in DELPHI data (data points are connected with lines for clarity) and (b) in JETSET generated events without BEC. All distributions are normalized by the total number of selected events, N.

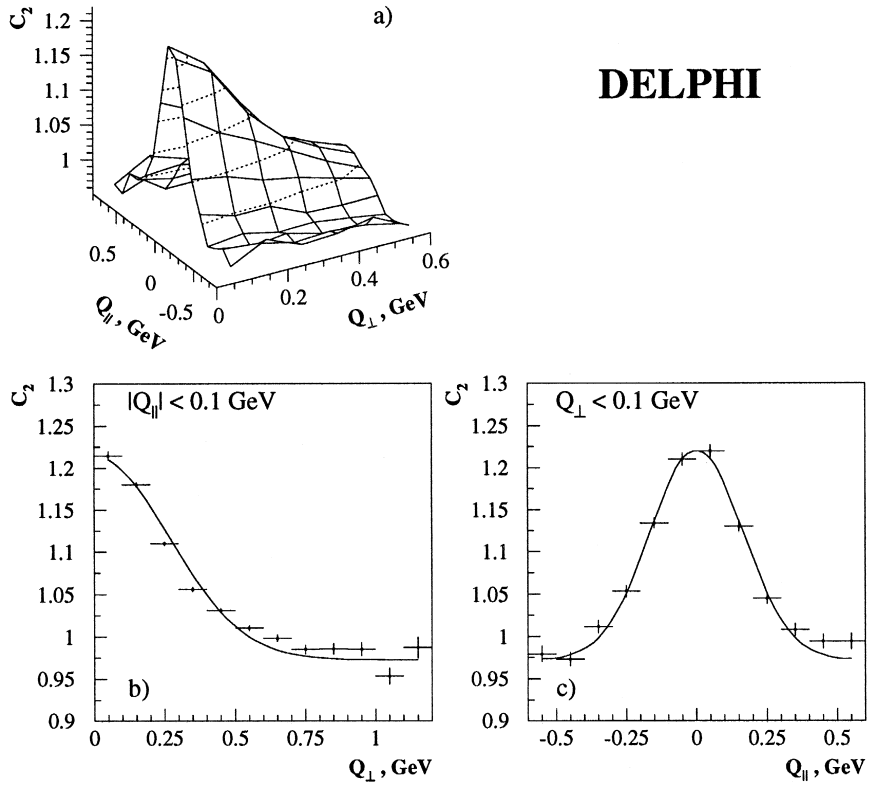

Fig. 3. Two-dimensional correlation function, $C_2(Q_\parallel, Q_\perp)$ (a), as measured by DELPHI in hadronic decays of Z^0. Its transverse (b) and longitudinal (c) slices at the peak are shown together with the fit to the Eq. (5).

quantities in absence of BEC obtained from the JETSET sample without BEC.

The reference sample $(d^2N^{\pm\pm}/dQ)_{\text{data,mix}}$ is corrected for the detector effects using a correction coefficient similar to (6):

$$c_{\text{mix}}(Q_\perp, Q_\parallel) = \frac{\left(\dfrac{d^2N^{\pm\pm}}{dQ_\perp\, dQ_\parallel}\right)_{\text{gen,mix}}}{\left(\dfrac{d^2N^{\pm\pm}}{dQ_\perp\, dQ_\parallel}\right)_{\text{rec,mix}}}, \tag{9}$$

where 'mix' denotes the mixed samples. The final, corrected, correlation function is then evaluated from Eq. (7) as:

$$C_2(Q_\perp, Q_\parallel) = \frac{r_{\text{data}}(Q_\perp, Q_\parallel)}{r_{\text{noBE}}(Q_\perp, Q_\parallel)} \frac{c(Q_\perp, Q_\parallel)}{c_{\text{mix}}(Q_\perp, Q_\parallel)}. \tag{10}$$

5. Results and discussion

The correlation function (10) as measured from the DELPHI data is shown in Fig. 3. BEC manifest themselves as the enhancement of $C_2(Q_\perp, Q_\parallel)$ at low values of the Q components.

The quantitative evaluation of the two-dimensional correlation function parameters was made by fitting the parametrization (5) to the measured correlation function $C_2(Q_\perp, Q_\parallel)$. The fit has been performed in the enhancement region of $|Q_\parallel| < 0.8$ GeV and 0 GeV $< Q_\perp <$ 0.6 GeV. Variation of the fit parameters as a function of the selected fit region contributes to the systematic uncertainty of the analysis. To estimate this contribution, the maximal value of $|Q_\parallel|$ was varied in the range from 0.6 GeV to 1.1 GeV, and the one of $Q_\perp$ – from 0.6 GeV to 1 GeV. Other sources of systematic uncertainties were evaluated varying the selection criteria. The biggest uncer-

tainty comes from varying the minimal thrust value requirement in the range between 0.93 and 0.97. The total systematic error was evaluated by adding all the contributions in quadrature.

The following values for the correlation radius components were obtained:

$$R_\perp = 0.53 \pm 0.02 \pm 0.07\,\text{fm},$$
$$R_\parallel = 0.85 \pm 0.02 \pm 0.07\,\text{fm}, \qquad (11)$$

where the first error is statistical, and the second is the systematic uncertainty. The correlation strength is found to be $\lambda = 0.261 \pm 0.007 \pm 0.010$, and it is slightly correlated (about 30%) with the radii. The χ^2 of the fit is 96 for 92 degrees of freedom. The ratio of the transverse and longitudinal radii from Eq. (11) is $R_\perp/R_\parallel = 0.62 \pm 0.10$. This ratio can be obtained as the result of a direct fit, using $R_\perp/R_\parallel$ as a parameter, and $R_\parallel$ as the complementary one. The correlation between the radii proves to be small (around 10%), and the fit leads to the value of $R_\parallel$ identical with that of (11), and for the ratio

$$R_\perp/R_\parallel = 0.62 \pm 0.02 \pm 0.05. \qquad (12)$$

The values obtained are in qualitative agreement with the theoretical prediction of [8], according to which the longitudinal correlation length in $Z^0 \to q\bar{q}$ hadronic decay has to be larger than the transverse one, if the string fragmentation model is used.

In the JETSET generator, BEC is simulated by changing the final state particle momenta so that the Gaussian distribution of Eq. (3) is reproduced [3]. The procedure is performed in terms of Q, not resolving it into components, hence $R_\perp$ and $R_\parallel$ ought to be similar in the JETSET generated events. Indeed, the two-dimensional fit to the correlation function evaluated from the JETSET generated decays of Z^0 gives a ratio of $R_\perp/R_\parallel$ between 0.9 and 1.1, depending on the generator tuning. This is very different from the ratio of (12) and reflects the fact that the BEC implementation in JETSET is not appropriate for the multidimensional description of the correlation.

An elongation of the pion source was also observed by the L3 [10] and OPAL [12] collaborations at LEP1. L3 collaboration used all the hadronic events in the analysis, without applying additional selection criteria neither for two-jet events, nor for pairs of tracks. The contribution from the correlations between particles produced in gluon jets and possibly between the two strings is expected to lead to a more spherical source shape and to a bigger value of the ratio of the radii, close to unity. The ratio measured by L3 $R_{t,\text{side}}/R_{\text{long}} = 0.81 \pm 0.02^{+0.03}_{-0.19}$ is bigger then the $R_\perp/R_\parallel$ reported in this work, which confirms these expectations. The OPAL Collaboration used the unlike-charge reference sample in their analysis of two-jet events, obtaining the ratio of radii $R_\perp/R_\parallel = 0.77 \pm 0.02 \pm 0.07$.

The measurement of the shape of the BEC presented here makes use of the LCMS system to obtain a clear interpretation of the observed difference between transverse and longitudinal correlation radii. Together with analogous measurements done by other LEP experiments, it represents an improvement in BEC studies compared to previous studies at lower energies [9], which used the laboratory system. While, the TASSO and MARK-II collaborations, barely hinted at the possibility of the pion source in the process $e^+e^- \to$ hadrons being elliptical, this new result provides clear evidence for the elongation of the source. The results have implications for the modelling of hadronic final states performed by event generators.

6. Summary

Two-dimensional analysis of the Bose-Einstein effect using the 1992–1995 DELPHI data confirms the prediction that the longitudinal correlation length, $R_\parallel$, in $Z^0 \to q\bar{q}$ decay is bigger than the transverse one, $R_\perp$, if the bosons produced in the string fragmentation are subject to Bose-Einstein correlations during the hadronization process. The measured values are:

$$R_\perp = 0.53 \pm 0.08\,\text{fm}, \quad R_\parallel = 0.85 \pm 0.08\,\text{fm}.$$

The measured ratio of the radii components is $R_\perp/R_\parallel = 0.62 \pm 0.06$, which is consistent with qualitative predictions [8]. These results cannot be reproduced by the JETSET generator because this generator includes only a simplified algorithm for the BEC simulation, which does not distinguish be-

tween the directional components of the correlation radius.

Acknowledgements

We are greatly indebted to our technical collaborators, to the members of the CERN-SL Division for the excellent performance of the LEP collider, and to the funding agencies for their support in building and operating the DELPHI detector.

We acknowledge in particular the support of

- Austrian Federal Ministry of Science and Traffics, GZ 616.364/2-III/2a/98,
- FNRS–FWO, Belgium,
- FINEP, CNPq, CAPES, FUJB and FAPERJ, Brazil,
- Czech Ministry of Industry and Trade, GA CR 202/96/0450 and GA AVCR A1010521,
- Danish Natural Research Council,
- Commission of the European Communities (DG XII),
- Direction des Sciences de la Matière, CEA, France,
- Bundesministerium für Bildung, Wissenschaft, Forschung und Technologie, Germany,
- General Secretariat for Research and Technology, Greece,
- National Science Foundation (NWO) and Foundation for Research on Matter (FOM), The Netherlands,
- Norwegian Research Council,
- State Committee for Scientific Research, Poland, 2P03B06015, 2P03B1116 and SPUB/P03/178/98,
- JNICT–Junta Nacional de Investigação Científica e Tecnológica, Portugal,
- Vedecka grantova agentura MS SR, Slovakia, Nr. 95/5195/134,
- Ministry of Science and Technology of the Republic of Slovenia,
- CICYT, Spain, AEN96–1661 and AEN96-1681,
- The Swedish Natural Science Research Council,
- Particle Physics and Astronomy Research Council, UK,
- Department of Energy, USA, DE–FG02–94ER40817.

References

[1] L. Lönnblad, T. Sjöstrand, Phys. Lett. B 351 (1995) 293.
[2] V. Kartvelishvili, R. Kvatadze, R. Møller, Phys. Lett. B 408 (1997) 331.
[3] T. Sjöstrand, Comp. Phys. Comm. 28 (1983) 229; T. Sjöstrand, Pythia 5.6 and Jetset 7.3: Physics and Manual, CERN-TH.6488/92, 1992.
[4] OPAL Collaboration, P.D. Acton et al., Phys. Lett. B 267 (1991) 143; DELPHI Collaboration, P. Abreu et al., Phys. Lett. B 286 (1992) 201; ALEPH Collaboration, D. Decamp et al., Z. Phys. C 54 (1992) 75; L3 Collaboration, Measurement of Bose-Einstein Correlations for Both Charged and Neutral Pions from Z Decays at LEP, L3 Note 2272 (1998), submitted to ICHEP XXIX, Vancouver, 1998.
[5] OPAL Collaboration, P.D. Acton et al., Z. Phys. C 56 (1992) 521.
[6] DELPHI Collaboration, P. Abreu et al., Phys. Lett. B 355 (1995) 415.
[7] R. Mureşan, O. Smirnova, B. Lörstad, Eur. Phys. J. C 6 (1999) 629.
[8] B. Andersson, M. Ringnér, Nucl. Phys. B 513 (1998) 627; B. Andersson, M. Ringnér, Phys. Lett. B 421 (1998) 283.
[9] TPC Collaboration, H. Aihara et al., Phys. Rev. D 31 (1985) 996; TASSO Collaboration, M. Althoff et al., Z. Phys. C 30 (1986) 35; Mark II Collaboration, I. Juricic et al., Phys. Rev. D 39 (1989) 1.
[10] L3 Collaboration, M. Acciarri et al., Phys. Lett. B 458 (1999) 517.
[11] B. Lörstad, O. Smirnova, Transverse Mass Dependence of Bose-Einstein Correlation Radii in e^+e^- Annihilation at LEP Energies, in: R.C. Hwa et al. (Eds.), Proc. 7th International Workshop on Multiparticle Production'Correlations and Fluctuations', World Scientific, Singapore, vol. A 57, 1997, p. 42.
[12] OPAL Collaboration, Transverse and Longitudinal Bose-Einstein Correlations in Hadronic Z^0 Decays, OPAL Note PN387 (1999), submitted to EPS-HEP 99, Tampere, 1999.
[13] B. Lörstad, Int. J. Mod. Phys. A4 12 (1989) 2861.
[14] T. Csörgő, S. Pratt, in: T. Csörgő et al. (Eds.), Proc. Budapest Workshop on Relativistic Heavy Ion Physics at Present and Future Accelerators, CRIP preprint KFKI-1991-28/A, 1991, p. 75.
[15] DELPHI Collaboration, P. Aarnio et al., Nucl. Instrum. Methods A 303 (1991) 233; DELPHI Collaboration, P. Abreu et al., Nucl. Instrum. Methods A 378 (1996) 57.
[16] DELPHI Collaboration, P. Abreu et al., Z. Phys. C 73 (1996) 11.
[17] DELSIM Reference Manual, DELPHI Note 87-98 PROG 100 (1989), unpublished.

Appendix D

MULTIDIMENSIONAL ANALYSIS OF THE BOSE-EINSTEIN CORRELATIONS AT DELPHI

BENGT LÖRSTAD, RALUCA MUREŞAN, OXANA SMIRNOVA
Dept. of Elementary Particle Physics, Lund University, Box 118, 22100 Lund, Sweden.
E-mail: raluca@quark.lu.se

The study of the directional dependence of two-particle correlations in the hadronic decay of the Z^0 boson is performed using the data collected by DELPHI experiment in 1992-1995 running periods. The comparison between the transverse $R_\perp$ and longitudinal $R_\parallel$ correlation radii confirms the string model prediction that the transverse size of the boson source is considerably smaller that the longitudinal one with the measured values $R_\perp = 0.53 \pm 0.04$ fm and $R_\parallel = 0.85 \pm 0.04$ fm.

1 Introduction

Detailed studies of the two-particle Bose-Einstein correlations (BEC) in Z^0 hadronic decays allow analysis of the spatial and the temporal characteristics of the hadronization region. Multidimensional analysis of the BEC is applied presently by the LEP experiments. Studies performed by the L3 [1] experiment and preliminary results by DELPHI [2] and OPAL [3] confirms the string model prediction that the transverse size of the boson source in e^+e^- annihilation is smaller than the longitudinal one.

The Monte Carlo particle generator JETSET [4] includes a simplified algorithm to simulate BEC using the correlation function in terms of invariant four-momentum difference of particles, Q. This algorithm reproduces some basic features of BEC well but, given the simplicity of it, more tests are necessary in order to establish the reliability of its predictions.

Here, the two-particle correlation function is studied in terms of different Q components, using 1992-1995 DELPHI data, at $\sqrt{s} = 91.2$ GeV.

2 Implementation issues, data selection

In high-energy physics experiments the BEC function is measured as the ratio between the Q-distribution of the charged-like pairs in data and the same distribution using a "reference" sample which obeys the same kinematics as the regular e^+e^- events but which is not subject to BEC:

$$C_2(Q) = \frac{(\frac{dN}{dQ})_{data}}{(\frac{dN}{dQ})_{ref}}, \tag{1}$$

where N is the number of charged-like pairs.

There are several procedures to construct the reference sample. We have chosen the "mixing" since it was established [5] as the most reliable method. The reference sample was constructed using tracks from different events. Each event was rotated to a new coordinate system which has the z axis along the thrust axis and a number of rotated events were stored in a continuously updated buffer. The reference sample was built picking up a random event from the reference buffer and a random track from this event. The sample, built by mixing particles from different events, satisfies several requirements for a reference sample, but does not conserve energy and momentum and destroys not only the Bose-Einstein correlations but some other correlations as well. To correct for this effects we used the ratio:

$$F_{noBE}(Q) = \frac{(\frac{dN}{dQ})_{noBE}}{(\frac{dN}{dQ})_{noBE,mix}}; \tag{2}$$

where the indices "$noBE''$ and "$noBE, mix''$ refer to analogous quantities in the absence of BEC, the corresponding distributions being obtained using JETSET model without BEC included.

We performed our analysis in the Longitudinal Center of Mass System, (LCMS) [6], defined for each pair of particles as the system in which the sum of the two-particles momenta is perpendicular to the selected reference axis. For e^+e^- this can be chosen as the direction of the primary parton or the corresponding jet, see fig. 1.

This system is particularly convenient for calculations since the energy difference and the temporal dimension of the source couple only to the t, out component (along the momenta sum). If the string model is considered, the longitudinal direction of the LCMS has to be aligned with the direction of the motion of the initial partons so that the system itself will be the rest frame of the string. Selection of the two-jet events gives a clean sample to test the string model. For two-dimensional studies, the components of Q are defined as $Q_{\parallel} = Q_{long}$ and $Q_{\perp} = \sqrt{Q^2_{t,out} + Q^2_{t,side}}$, where Q_{long}, $Q_{t,side}$, $Q_{t,out}$ are Q projections on the LCMS axes. We used for our analysis charged tracks from hadronic events, selecting a sample of two-jet events requiring the thrust $T > 0.95$, jet misalignment not more than $5°$ and using the LUCLUS clustering algorithm. For a two-jet sample of events, the procedures for mixed reference sample and LCMS are easier to apply since the thrust axis is well aligned with the initial parton direction of the motion. We impose some other cuts as: $p_{track} < 5$ GeV, to eliminate the tracks that do not contribute to BEC; angle between tracks $> 2°$ (detector resolution); angle between tracks

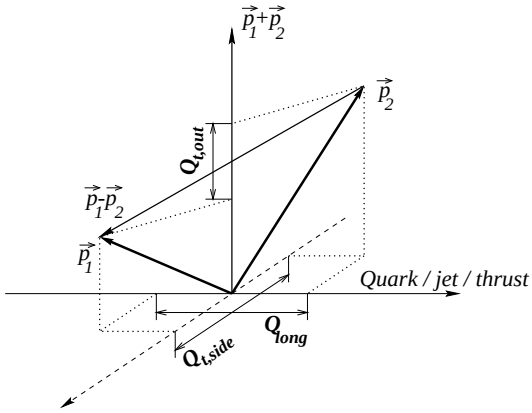

Figure 1. The LCMS

in the transverse plane $> 120°$, to reduce the contribution from the transverse momentum compensation; $Q > 0.06$ GeV to eliminate the region where the Coulomb correction is big.

To estimate the acceptance correction and to account for the effects given by the detector resolution, we used JETSET generated events with DELPHI tuning [7] and detector simulation (DELSIM) [8], the same selection as for data being applied. The correction factors,$F(Q)$ and $F_{mix}(Q)$, were calculated as:

$$F(Q) = \frac{(\frac{dN}{dQ})_{gen}}{(\frac{dN}{dQ})_{rec}}; \quad F_{mix}(Q) = \frac{(\frac{dN}{dQ})_{gen,mix}}{(\frac{dN}{dQ})_{rec,mix}}; \tag{3}$$

where indices *gen* and *rec* refer to the generation (JETSET only) and reconstruction (JETSET +DELSIM) levels. Similar correction coefficients are calculated for the two- and three-dimensional distributions respectively.

3 Study of the two-dimensional correlation function

The quantitative evaluation of the two-dimensional correlation function parameters was done by fitting the parameterization:

$$C_2(Q_\perp, Q_\parallel) = N(1 + \lambda e^{-Q_\perp^2 R_\perp^2 - Q_\parallel^2 R_\parallel^2}) \tag{4}$$

to the measured correlation function obtained using the above method. The fit was performed in the enhancement region see fig 2, $|Q_\parallel| < 0.8$ GeV and $0 < Q_\perp < 0.6$ GeV and the variation of the fit region was used to estimate the

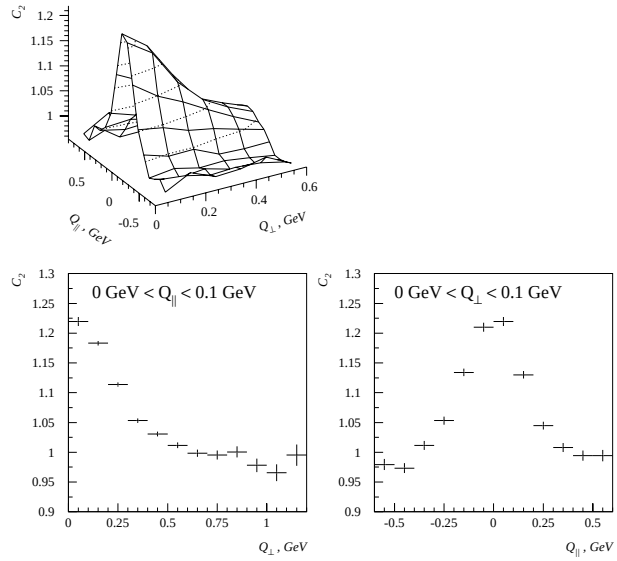

Figure 2. Two-dimensional correlation function and its projection at the peak.

systematic uncertainty of the analysis. The following values for the correlation radius components were obtained:

$$\begin{aligned} R_{\perp} &= 0.53 \pm 0.02 \pm 0.03 \text{ fm} \\ R_{\parallel} &= 0.85 \pm 0.02 \pm 0.03 \text{ fm} \end{aligned} \tag{5}$$

here the first error is statistical and the second is the estimated systematic uncertainty. We got for the ratio of the transverse and longitudinal radius components the value:

$$R_{\perp}/R_{\parallel} = 0.62 \pm 0.02 \pm 0.04 \tag{6}$$

The obtained values are in qualitative agreement with the theoretical prediction [9] according with which the longitudinal size of the boson source, Z^0, must be considerably bigger than the transverse one if the string fragmentation model is used.

The preliminary result reported by OPAL [3], using an unlike-charge reference sample, is also confirming a source elongation with $R_\perp/R_\parallel = 0.769 \pm 0.014 \pm 0.012$. The ratio decreases when OPAL uses "mixed" sample $R_\perp/R_\parallel = 0.709 \pm 0.05$ for the analysis or when the two-jet sample is more clean. L3 [1] collaboration obtained $R_\perp/R_\parallel = 0.81 \pm 0.02^{+0.03}_{-0.19}$ where no selection of two-jet events was performed. The contribution from the correlation between the particles produced in gluon jets and possibly between two strings, leads to a more symmetric source shape and to a bigger value of the ratio of the radii. L3 analysis was performed in the three-dimensional case.

BEC in JETSET is simulated by changing final state particle momenta so that the Gaussian BEC function is reproduced. Since the procedure is written in terms of Q-invariant, $R_\parallel$ and $R_\perp$ must have similar values. Indeed, the two-dimensional fit to the correlation function evaluated from the JETSET generated decays of Z^0 give a ratio of $R_\perp/R_\parallel$ between 0.9 and 1.1. reflecting the fact that BEC implementation in JETSET is not proper for multidimensional studies.

4 Further directions, preliminary results

Three-dimensional DELPHI analysis of 1992-1995 data (preliminary) was performed by fitting the correspondent correlation function to the parameterization:

$$C_2(Q_{t,out}, Q_{t,side}, Q_{long}) = N(1 + \lambda e^{-Q^2_{t,out}R^2_{t,out} - Q^2_{t,side}R^2_{t,side} - Q^2_{long}R^2_{long}}) \tag{7}$$

We obtained:

$$\begin{aligned} R_{t,out} &= 0.594 \pm 0.007 \text{ fm} \\ R_{t,side} &= 0.469 \pm 0.006 \text{ fm} \\ R_{long} &= 0.816 \pm 0.008 \text{ fm} \end{aligned} \tag{8}$$

As we were expecting, since the temporal "size" of the source contributes only to $R_{t,out}$, $R_{t,side}$ radius is smaller. The source is even more elongated if we take in to account just the "true" transverse size, $R_{t,side}$, as you can see from the ratios:

$$\begin{aligned} \frac{R_{t,out}}{R_{long}} &= 0.73 \pm 0.01 \\ \frac{R_{t,side}}{R_{long}} &= 0.58 \pm 0.01 \end{aligned} \tag{9}$$

Further studies will be performed to estimate the systematic uncertainty of these results and to investigate the dependence of the BEC function parameters on the transverse mass of the pairs.

5 Conclusion

Two-dimensional analysis of BEC, using 1992-1995 DELPHI data confirms the prediction that the longitudinal size of the boson source in Z^0 decay has to be bigger than the transverse one.

$$R_\perp = 0.53 \pm 0.04 \text{ fm}, \quad R_\parallel = 0.85 \pm 0.04 \text{ fm}$$

$$R_\perp / R_\parallel = 0.62 \pm 0.04$$

References

1. L3 Coll., M. Acciarri et al., *Phys. Lett.* B **458**, 517 (1999)
2. B. Lörstad, O. Smirnova: *"Transverse Mass Dependence of Bose-Einstein Correlation Radii in e^+e^- Annihilation at LEP Energies"*: Proceedings of the 7th International Workshop on Multiparticle Production 'Correlations and Fluctuations', edited by R.C. Hwa et al., World Scientific, Singapore A57 p.42, 1997.
3. OPAL Coll., *"Transverse and Longitudinal Bose-Einstein Correlations in Hadronic Z^0 Decays"*, OPAL Note PN387 (1999), submitted to EPS-HEP 99, Tampere, 1999.
4. T. Sjöstrand, *Comp. Phys. Comm.* **28**, 229 (1983);
   T. Sjöstrand, PYTHIA *5.6 and* JETSET *7.3 : Physics and Manual*, CERN-TH.6488/92 (1992).
5. TPC Coll.,H.Aihara et al., *Phys. Rev.* D **31**, 996 (1985);
   TASSO Coll., M. Althoff et al., *Z. Phys.* C **30**, 35 (1986);
   Mark II Coll., I. Juricic et al., *Phys. Rev.* D **39**, 1 (1989).
6. T. Csörgő and S. Pratt, in "Proceedings of the Budapest Workshop on Relativistic Heavy Ion Physics at Present and Future Accelerators", edited by T. Csörgő et al., CRIP preprint KFKI-1991-28/A, p75, 1991.
7. DELPHI Coll., P. Abreu et al., *Z. Phys.* C **73**, 11 (1996).
8. *DELSIM Reference Manual*, DELPHI Note 87-98 PROG 100 (1989), unpublished.
9. B. Andersson and M. Ringnér, *Nucl. Phys.* B **513**, 627 (1998);
   B. Andersson and M. Ringnér, *Phys. Lett.* B **421**, 283 (1998).